

การวิเคราะห์สรีรยนต์ด้วยเอทีอาร์เอฟทีไออาร์ไมโครสเปกโทรสโกปี



นางสาวพรพรรณ วัชรแสนยาก

สถาบันวิทยบริการ จุฬาลงกรณ์มหาวิทยาลัย

วิทยานิพนธ์นี้เป็นส่วนหนึ่งของการศึกษาตามหลักสูตรปริญญาวิทยาศาสตรมหาบัณฑิต

สาขาวิชาปิโตรเคมีและวิทยาศาสตร์พอลิเมอร์

คณะวิทยาศาสตร์ จุฬาลงกรณ์มหาวิทยาลัย

ปีการศึกษา 2549

ลิขสิทธิ์ของจุฬาลงกรณ์มหาวิทยาลัย

ANALYSIS OF AUTOMOTIVE PAINTS BY
ATR FT-IR MICROSPECTROSCOPY

Miss Pornpan Watcharasanyakorn



สถาบันวิทยบริการ
จุฬาลงกรณ์มหาวิทยาลัย

A Thesis Submitted in Partial Fulfillment of the Requirements
for the Degree of Master of Science Program in Petrochemistry and Polymer Science

Faculty of Science

Chulalongkorn University

Academic Year 2006

Copyright of Chulalongkorn University

Thesis Title ANALYSIS OF AUTOMOTIVE PAINTS BY ATR FT-IR
MICROSPECTROSCOPY


By Miss Pornpan Watcharasanyakorn

Field of Study Petrochemistry and Polymer Science

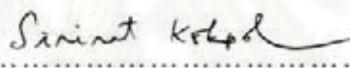
Thesis Advisor Associate Professor Supason Wanichweacharungruang, Ph.D.

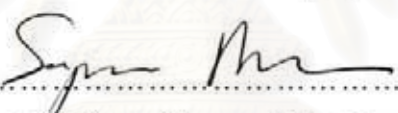
Thesis Co-advisor Police Lieutenant Montre Donfoongprai


Accepted by the Faculty of Science, Chulalongkorn University in Partial
Fulfillment of the Requirements for the Master's Degree



..... Dean of the Faculty of Science
(Professor Piamsak Menasveta, Ph.D.)

THESIS COMMITTEE


..... Chairman
(Associate Professor Sirirat Kokpol, Ph.D.)


..... Thesis Advisor
(Associate Professor Supason Wanichweacharungruang, Ph.D.)


..... Thesis Co-advisor
(Police Lieutenant Montre Donfoongprai)


..... Member
(Associate Professor Sanong Ekgasit, Ph.D.)


..... Member
(Assistant Professor Varawut Tangpasuthadol, Ph.D.)

พรพรรณ วัชรแสนยากร: การวิเคราะห์สีรถยนต์ด้วยเอทีอาร์เอฟทีไออาร์ไมโครสเปกโทรสโกปี (ANALYSIS OF AUTOMOTIVE PAINTS BY ATR FT-IR MICROSPECTROSCOPY) อ. ที่ปรึกษา: รศ. ดร. ศุภสร วณิชเวชรุ่งเรือง, อ. ที่ปรึกษาร่วม: ร้อยตำรวจโท มนตรี คอนฟูงไพโร, 104 หน้า.

เอทีอาร์เอฟทีไออาร์ไมโครสเปกโทรสโกปีสามารถใช้ตรวจสอบและพิสูจน์เอกลักษณ์ของสีรถยนต์ได้ โดยเป็นเทคนิคที่ให้ข้อมูลเชิงพื้นผิวของสาร ตัวอย่างสีรถยนต์สามชนิดได้แก่ สีรถยนต์ที่มีสีและเฉดสีแตกต่างกัน สีรถยนต์ที่มีหลายชั้น และคราบสีบางๆ สามารถตรวจสอบได้โดยใช้อุปกรณ์ไมโครสเปกโทรสโกปีแบบสไลด์ที่ใช้เพชรที่เจียรไนแล้วเป็นไออาร์อี และอุปกรณ์เจอร์มาเนียมไมโครสเปกโทรสโกปีแบบสไลด์ที่ใช้เจอร์มาเนียมรูปทรงกรวยเป็นไออาร์อี ร่วมกับกล้องจุลทรรศน์อินฟราเรด เนื่องจากอุปกรณ์ทั้งสองมีพื้นที่ในการวิเคราะห์ตัวอย่างที่เล็ก ทำให้สามารถวิเคราะห์ตัวอย่างที่มีขนาดเล็กได้ดี สเปกตรัมที่ได้จากอุปกรณ์ไมโครสเปกโทรสโกปีและเจอร์มาเนียมไมโครสเปกโทรสโกปีจะเหมือนกับสเปกตรัมที่ได้จากเทคนิคเอทีอาร์ที่ใช้กันทั่วไป จากการตรวจสอบสีรถยนต์ที่มีสีแตกต่างกัน และสีเดียวกันแต่มีเฉดสีที่ต่างกัน พบว่าสเปกตรัมที่ได้จะแตกต่างกัน เนื่องจากองค์ประกอบหลักของสี เช่น สารเชื่อมประสาน สารให้สี และสารเติมแต่งมีความแตกต่างกัน จึงสามารถแยกความแตกต่างของสีส่วนใหญ่ได้ สามารถวิเคราะห์แต่ละชั้นบนภาคตัดขวางของสีที่มีหลายชั้น โดยไม่ต้องมีการแยกชั้นสีออกจากกัน นอกจากนี้การตรวจสอบสีรถยนต์ที่มีหลายชั้นโดยการทำแผนที่พื้นผิวสามารถให้ข้อมูลขององค์ประกอบทางเคมีที่เปลี่ยนไปในแต่ละพื้นที่เล็กๆ และแยกความแตกต่างของสีที่ไม่สามารถแยกด้วยตาเปล่าได้ การตรวจวิเคราะห์คราบสีบางๆด้วยอุปกรณ์เจอร์มาเนียมไมโครสเปกโทรสโกปีแบบสไลด์สามารถทำได้โดยไม่มี การรบกวนจากสีชั้นล่าง สเปกตรัมที่ได้จะให้ข้อมูลทางเคมีของสีรถยนต์ซึ่งสามารถนำไปประยุกต์ใช้ในเชิงนิติวิทยาศาสตร์ เทคนิคนี้เป็นการวิเคราะห์ที่ไม่ทำลายตัวอย่าง ไม่ต้องเตรียมตัวอย่างในการวิเคราะห์ ใช้เวลาในการวิเคราะห์สั้น

สาขาวิชา ปิโตรเคมีและวิทยาศาสตร์พอลิเมอร์ ลายมือชื่อนิสิต..... พ. ๕๖๕๕ ๘๘ ไร่ใหม่สันเขาดง.....

ปีการศึกษา..... 2549

ลายมือชื่ออาจารย์ที่ปรึกษา.....

ลายมือชื่ออาจารย์ที่ปรึกษาร่วม.....


4872567223 : MAJOR PETROCHEMISTRY AND POLYMER SCIENCE
 KEY WORDS: AUTOMOTIVE PAINTS / FORENSIC ANALYSIS / ATR FT-IR
 MICROSPECTROSCOPY / DIAMOND μ IRE / GE μ IRE

PORNPAN WATCHARASANYAKORN: ANALYSIS OF AUTOMOTIVE
 PAINTS BY ATR FT-IR MICROSPECTROSCOPY. THESIS ADVISOR:
 ASSOC. PROF. SUPASON WANICHWEACHARUNGRUANG, PH.D.,
 THESIS CO-ADVISOR: POLICE LIEUTENANT MONTRE
 DONFOONGPRAI, 104 pp.

ATR FT-IR microspectroscopy is used to analyze and identify the automotive paints. Three types of automotive paints including paint chips of different colors and shades, multilayer automotive paints, and thin trace smear on automotive paint were characterized by ATR FT-IR microspectroscopy. Two homemade μ ATR accessories; the slide-on diamond μ IRE and the slide-on Ge μ IRE, using an infrared microscope were employed for surface characterization of automotive paints. The spectra acquired by the slide-on diamond μ IRE and the slide-on Ge μ IRE were similar to those acquired by conventional ATR technique. The spectra from different colors and shades of paint show different spectral features due to the difference in compositions such as binder, pigment, and additive. Due to small contact area of the slide-on diamond μ IRE and slide-on Ge μ IRE, an individual layer of the multilayered automotive paints can be selectively analyzed without layer separation changing in chemical composition in each small sampling position can be analyzed. In addition, paints with the same colors but different chemical composition can be identified by surface line mapping. Thin trace smear were analyzed directly without interference from paint support by the slide-on Ge μ IRE. The slide-on diamond μ IRE and the slide-on Ge μ IRE were suitable for forensic analysis of automotive paint because of their small contact area and good contact with the sample. The technique is non-destructive, has short analysis time, can be performed without a sample preparation.

Field of study. Petrochemistry and polymer science Student's signature..... 

Academic year..... 2006..... Advisor's signature..... 

Co-advisor's signature..... 

ACKNOWLEDGEMENTS

I would like to express my sincere gratitude to Associate Professor Dr. Sirirat Kokpol, and Assistant Professor Dr. Varawut Tangpasuthadol, for the insightful suggestions and contribution as thesis committee.

Gratefully thanks to Associate Professor Dr. Supason Wanichweacharungruang, my thesis advisor, Police Lieutenant Montre Donfoongprai, my thesis co-advisor, Associate Professor Chuchaat Thammacharoen, and Dr. Pimthong Thongnopkun for the invaluable guidance, comments, and suggestions.

Finally, this thesis would not have been successfully completed without the excellent advice from Associate Professor Dr. Sanong Ekgasit, who always provides me the useful guidance, suggestion, encouragement, and understanding and also patiently practices my technical skill during the whole research.

Warmest thanks to my friends and colleagues at the Sensor Research Unit, Department of Chemistry, Faculty of Science, Chulalongkorn University, for the everlasting friendship and spiritual supports throughout the time of study.

Above all, I am profoundly grateful to my wonderful parents and the endearing family for their patient love, perpetual encouragement, and overwhelming support.

สถาบันวิทยบริการ
จุฬาลงกรณ์มหาวิทยาลัย

CONTENTS

	Page
ABSTRACT IN THAI.....	iv
ABSTRACT IN ENGLISH.....	v
ACKNOWLEDGEMENTS.....	vi
LIST OF FIGURES.....	x
LIST OF TABLES.....	xv
LIST OF ABBREVIATIONS.....	xvi
LIST OF SYMBOLS.....	xvii
CHAPTER I INTRODUCTION.....	1
1.1 Automotive Paints	1
1.2 Forensic Analysis of Automotive Paints.....	4
1.2.1 Fourier Transform Infrared (FT-IR) Spectroscopy for Automotive Paint.....	6
1.2.2 ATR FT-IR Microspectroscopy for Automotive Paints.....	7
1.3 Objectives of the Research.....	8
1.4 Scope of the Research.....	8
CHAPTER II THEORETICAL BACKGROUND.....	9
2.1 Fundamentals of Infrared Spectroscopy	9
2.2 Attenuated Total Reflection Fourier Transform Infrared (ATR FT-IR) Spectroscopy.....	11
2.2.1 A Principle of Light Reflection and Refraction.....	11
2.2.2 Internal Reflection Element (IRE)	13
2.2.3 ATR Spectral Intensity.....	14
2.2.4 Penetration Depth	14
2.2.4 Limitation of ATR FT-IR Spectroscopy.....	16
2.3 ATR FT-IR Microscopy.....	16
2.3.1 The Homemade Slide-on Diamond μ IRE	18

2.3.2 The Homemade Slide-on Ge μ IRE	20
2.4 Specular Reflection.....	21
CHAPTER III EXPERIMENTAL SECTION.....	23
3.1 Materials and Equipments	23
3.1.1 Automotive Paint Samples.....	23
3.1.2 Instruments.....	24
3.1.3 Default Spectral Acquisition Parameters.....	25
3.2 Homemade μ ATR Accessories	25
3.2.1 Homemade Diamond μ ATR Accessory.....	25
3.2.2 Homemade Slide-on Diamond μ ATR Accessory	27
3.2.2 Homemade Slide-on Ge μ ATR Accessory	30
3.3 Characterization of Different Colors and Shades of Automotive Paints ...	35
3.3.1 Experimental Procedure for the Commercial ATR Accessory.....	35
3.3.2 Experimental Procedure for the Homemade μ ATR Accessories.....	36
3.4 Characterization of Multilayer Automotive Paints	36
3.4.1 Depth Profiling of Multilayer Automotive Paints	36
3.4.2 Characterization of Individual Layer on Cross-section Surface of Multilayer Automotive Paints by the Homemade μ ATR Accessories.....	37
3.4.3 Characterization of Multilayer Automotive Paints by Cross-section Surface Line Mapping	39
3.4.4 Specular Reflection of Individual Layer on Cross-section Surface of Multilayer Automotive Paints	40
3.5 Characterization of Thin Trace Smear on Automotive Paints.....	40
CHAPTER IV RESULTS AND DISCUSSION.....	42
4.1 Characterization of Automotive Paints.....	42

4.1.1 Efficiency of Conventional ATR and Homemade μ ATR Accessories.....	42
4.1.1 Classification of Automotive Paints by FT-IR Spectra.....	46
4.2 Characterization of Multilayer Automotive Paints.....	58
4.2.1 Depth Profiling of Multilayer Automotive Paints	58
4.2.2 Characterization of Individual Layer on Cross-section of Multilayer Automotive Paints by the Homemade μ ATR Accessories.....	62
4.2.3 Characterization of Multilayer Automotive Paints by Cross-section Surface Line Mapping.....	70
4.2.4 Specular Reflection Measurement of Cross-section of Multilayer Automotive Paints.....	83
4.3 Characterization of Thin Trace Smears on Automotive Paint Support.....	88
CHAPTER V CONCLUSIONS.....	90
REFERENCES.....	92
APPENDICES.....	96
CURRICULUM VITAE.....	104

สถาบันวิทยบริการ
จุฬาลงกรณ์มหาวิทยาลัย

LIST OF FIGURES

x

Figure	Page
1.1 The cross-section of automotive paints: (A) sequence of layer over a metal (steel substrate) and (B) sequence of layer over a plastic substrate.....	1
2.1 Propagation of a linearly polarized electromagnetic wave in space. Electric (E) and magnetic (H) vectors are always perpendicular to each other and to the direction of propagation.....	9
2.2 Interactions of light with matter	10
2.3 Reflection and refraction of a plane wave at a dielectric interface based on Snell's Law.....	12
2.4 Light travels from an optically denser medium and impinges at the surface of the optically rarer medium ($n_1 > n_2$) with angle of incidence equals the critical angle	12
2.5 Various IREs configurations commonly used in ATR experimental setups: (a) Single reflection variable-angle hemispherical crystal and (b) Multiple reflection single-pass crystal	14
2.6 Relationship between the penetration depth and wavenumber for Ge crystal at different angle of incidence	15
2.7 Optical diagram for infrared microscope	17
2.8 The infrared radiation tracing with in the objective of infrared microscope..	17
2.9 The infrared radiation tracing within the diamond μ IRE	18
2.10 Transflectance spectrum of round brilliant cut natural diamond	20
2.11 The infrared radiation tracing within the Ge μ IRE.....	21
2.12 Schematic diagram show specular reflection measurement of sample.....	22
3.1 The homemade diamond μ ATR accessory: the diamond probing head, the adjustable reflection plane and the complete set of homemade accessory....	26
3.2 The homemade diamond μ ATR accessory: (A) Continuum infrared microscope attach to the Nicolet 6700 FT-IR spectrometer and (B) the complete set of the homemade diamond μ ATR accessory.....	27

Figure	Page
3.4 The homemade slide-on diamond μ ATR accessory: (A) Continuum infrared microscope attach to the Nicolet 6700 FT-IR spectrometer, (B) the slide-on diamond μ IRE was slide into the position of silde-on housing on the 15X Schwarzschild-Cassegrain infrared objective (C) the slide-on diamond μ IRE was fixed on the position of slide-on housing on the infrared objective, and (D) the complete set of the homemade slide-on diamond μ ATR accessory.....	29
3.5 (A) A schematic illustration of ray tracing within the infrared objective, (B) focused radiation traveling within the diamond μ IRE, and (C) image of the tip of diamond μ IRE under the visible light	30
3.6 The slide-on housing and composition of the homemade slide-on Ge μ IRE	32
3.7 The homemade slide-on Ge μ ATR accessory: (A) Continuum infrared microscope attach to the Nicolet 6700 FT-IR spectrometer, (B) the slide-on Ge μ IRE was slide into the position of silde-on housing on the 15X Schwarzschild-Cassegrain infrared objective (C) the slide-on Ge μ IRE was fixed on the position of slide-on housing on the infrared objective, and (D) the complete set of the homemade slide-on Ge μ ATR accessory	33
3.8 (A) A schematic illustration of ray tracing within the infrared objective, (B) focused radiation traveling within the Ge μ IRE, and (C) image of the tip of Ge μ IRE under the visible light	34
3.9 Schematic illustration of conventional ATR with hemispherical Ge IRE.....	35
3.10 Schematic illustration of the depth profiling measurement using a diamond μ IRE. The diamond was penetrated deeper by increasing applied pressure..	37
3.11 Schematic illustration of the multilayer automotive paint chip on acrylic plate at (A) the right angle of 90 degree and (B) the oblique angle 30 degree	38
4.1 ATR FT-IR spectra of a blue automotive paint acquired by three sampling techniques: (A) conventional ATR using hemispherical Ge IRE (30° angle of incidence), (B) the slide-on diamond μ IRE and (C) the slide-on Ge μ IRE.....	42

Figure	Page
4.2 ATR FT-IR spectra of the metal-contact surface of 17 different colors and shades of automotive paints acquired by conventional ATR using hemispherical Ge IRE	44
4.3 ATR FT-IR spectra of (A) the air-contact surface and (B) the metal-contact surface of 17 automotive paints acquired by the slide-on diamond μ IRE.....	45
4.4 ATR FT-IR spectra of (A) the air-contact surface and (B) the metal-contact surface of 17 automotive paints acquired by the slide-on Ge μ IR...	46
4.5 Comparison of both surfaces of (A) non-metallic paint and (B) metallic paint. The spectra were acquired by the Ge slide-on IRE.....	48
4.6 Reproducibility of the spectra acquired by the slide-on Ge μ IRE. All spectra were collected in triplicate: (A) black, (B) white, (C) yellow A, and (D) yellow B	51
4.7 Observed spectra of (A) green B, (B) red A, (C) blue B and (D) blue D acquired from the slide-on Ge μ IRE	52
4.8 ATR spectra of a multilayer silver gray paint from a car bumper. The spectra acquired as the diamond tip penetrate deep into the multilayer paint chip. F_1 indicated the shallowest diamond penetration which F_{14} indicated the deeper diamond penetration	59
4.9 ATR spectra of a multilayer gray paint from a car hood. The spectra acquired as the diamond tip penetrate deep into the multilayer paint chip. F_1 indicated the shallowest diamond penetration which F_6 indicated the deeper diamond penetration	60
4.10 ATR spectra of a multilayer blue paint from a car door. The spectra acquired as the diamond tip penetrate deep into the multilayer paint chip. F_1 indicated the shallowest diamond penetration which F_{12} indicated the deeper diamond penetration	61
4.11 ATR spectra of a multilayer white paint from a Mitsubishi fender. The spectra acquired as the diamond tip penetrate deep into the multilayer paint chip. F_1 indicated the shallowest diamond penetration which F_{10} indicated the deeper diamond penetration	62

Figure	Page
4.12 ATR spectra of a two-layered paint chip from a bumper of a silver gray car that was razorblade cut with a right angle (90 degree) acquired by (A) the slide-on diamond μ IRE and (B) the slide-on Ge μ IRE	63
4.13 ATR spectra of a two-layered paint chip from a bumper of a silver gray car that was razorblade cut with a oblique angle (30 degree) acquired by (A) the slide-on diamond μ IRE and (B) the slide-on Ge μ IRE	64
4.14 ATR spectra of a eight-layered paint chip from a hood of a gray car that was razorblade cut with a right angle (90 degree) acquired by (A) the slide-on diamond μ IRE and (B) the slide-on Ge μ IRE.....	65
4.15 ATR spectra of a eight-layered paint chip from a gray car hood that was razorblade cut with a oblique angle (30 degree) acquired by (A) the slide-on diamond μ IRE and (B) the slide-on Ge μ IRE	66
4.16 ATR spectra of a thirteen-layered paint chip from a blue car door that was razorblade cut with a oblique angle (30 degree) acquired by (A) the slide-on diamond μ IRE and (B) the slide-on Ge μ IRE	67
4.17 ATR spectra of a three-layered paint chip from a black Toyota Fortuner bumper that was razorblade cut with a oblique angle (30 degree) acquired by (A) the slide-on diamond μ IRE and (B) the slide-on Ge μ IRE	68
4.18 ATR spectra of a three-layered paint chip from a white Mitsubishi fender that was razorblade cut with a oblique angle (30 degree) acquired by (A) the slide-on diamond μ IRE and (B) the slide-on Ge μ IRE	69
4.19 ATR spectra of four layered paint chip from a blue BMW door that was razorblade cut with a oblique angle (30 degree) acquired by (A) the slide-on diamond μ IRE and (B) the slide-on Ge μ IRE	70
4.20 ATR spectra of a two-layered paint chip from a bumper of silver gray car acquired by (A) the slide-on diamond μ IRE and (B) the slide-on Ge μ IRE..	72
4.21 ATR spectra of an eight-layered paint chip from a hood of gray car acquired by (A) the slide-on diamond μ IRE and (B) the slide-on Ge μ IRE..	73
4.22 ATR spectra of a thirteen-layered paint chip from a door of blue car acquired by (A) the slide-on diamond μ IRE and (B) the slide-on Ge μ IRE..	75

Figure	Page
4.23 ATR spectra of a three-layered paint chip from a bumper of black Toyota Fortuner car acquired by (A) the slide-on diamond μ IRE and (B) the slide-on Ge μ IRE	80
4.24 ATR spectra of a three-layered paint chip from a fender of white Mitsubishi car acquired by (A) the slide-on diamond μ IRE and (B) the slide-on Ge μ IRE	82
4.25 Specular reflectance spectra of a two-layered paint chip from a silver gray car bumper: layer 1 and layer 2	84
4.26 The KK-transformed spectra of those Figure 4.25 of a two-layered paint chip from a silver gray car bumper; layer 1 and layer 2	84
4.27 Specular reflectance spectra of a three-layered paint from black Toyota Fortuner bumper; layer 1, layer 2 and layer 3	85
4.28 The KK-transformed spectra of those Figure 4.27 of a three-layered paint chip from a black Toyota Fortuner bumper; layer 1, layer 2 and layer 3.....	86
4.29 Specular reflectance spectra of a three-layered paint from white Mitsubishi fender; layer 1, layer 2 and layer 3	87
4.30 The KK-transformed spectra of those Figure 4.29 of a three-layered paint chip from a white Mitsubishi fender; layer 1, layer 2 and layer 3.....	87
4.31 The spectra were acquired by (A) a slide-on diamond μ IRE and (B) a slide-on Ge μ IRE. Comparison of the ATR spectra of (a) the blue paint support of damaged BMW car referred to known sample, (b) the black trace smear on the damaged car referred to unknown sample and (c) the bumper of Toyota Fortuner.....	89

LIST OF TABLES

Table	Page
1.1 Common extender pigments in automotive paint	2
1.2 Common coloring pigments in automotive paints	3
1.3 Typical Costing Binders.....	4
2.1 Information of materials used for internal reflection elements.....	13
3.1 Information of multilayer paint sample	24
4.1 Peak assignment of alkyd nitrocellulose.....	49
4.2 Peak assignment of acrylic nitrocellulose.	50
4.3 Major absorption bands of coloring pigments in automotive paints.....	53
4.4 Major absorption bands of common binders in automotive paints.....	55
4.5 Major absorption bands of common extender pigments in automotive paints.	57



 สถาบันวิทยบริการ
 จุฬาลงกรณ์มหาวิทยาลัย

LIST OF ABBREVIATIONS

ATR	: Attenuated total reflection
FT-IR	: Fourier transform infrared
Ge	: Germanium
ZnSe	: zinc selenide
IRE	: Internal reflection element
MSEF	: mean square electric field
IR	: infrared
KBr	: potassium bromide
KK	: Kramers-Kroing
K-M	: Kubelka-Munk
MCT	: mercury cadmium telluride
MIR	: mid infrared
m	: micron
S/N	: signal-to-noise
TIR	: total internal reflection

สถาบันวิทยบริการ
จุฬาลงกรณ์มหาวิทยาลัย

LIST OF SYMBOLS

A	: absorbance
I	: intensity
n	: refractive index
θ	: angle of incidence
θ_c	: critical angle
ν	: wavenumber
d_p	: penetration depth
μ	: micro



สถาบันวิทยบริการ
จุฬาลงกรณ์มหาวิทยาลัย

CHAPTER I

INTRODUCTION

1.1 Automotive Paints

Automotive paints are coating use to decorate a vehicle and give colored coating. Automotive paints help to cover and protect automobile from weather, UV radiation, acid rain, and rust corrosion. In industry, the automobile has multiple coating called multilayer coat or multilayer paint. Figure 1.1 showed the general coating consists of main four layers (for steel substrate). The bottom layer called the electrocoat that provided a good adhesion between subsequent layer and a car body and prevented rust of metal substrate. Plastic substrates, such as exterior trim and bumper, do not have this layer. Above this layer, the primer is prepared or retrieved surface to smooth and hides imperfection. This layer is mostly a white or gray which contains the basic pigment, extender and binder. Next layer, the basecoat provides the color to the paint through pigment. For metallic paint, alumina flakes are embedded in this layer. The top coat, a clear coat (or a binder layer) provides great appearance (glossiness) and helps to protect the basecoat. However, real coating process may have more or less than four layers.

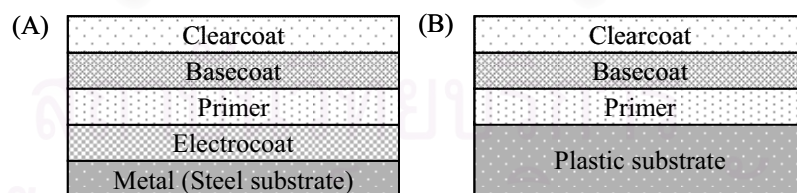


Figure 1.1 The cross-section of automotive paints: (A) sequence of layer over a metal (steel substrate) and (B) sequence of layer over a plastic substrate.

Different paints have different chemical compositions. The automotive paints are consisting of mainly two components. Firstly, the pigment component is contained with extender pigment and coloring pigment. The extender pigments were selected by the producers of automotive paints for adjusting physical properties, such as viscosity,

abrasion resistance, gloss, and matt including decreased production cost. Table 1.1 showed the common extender pigments in automotive paints [1]. The coloring pigments give paint color that consisted of inorganic pigment and organic pigment as shown in Table 1.2.

Table 1.1 Common extender pigments in automotive paint.

Group of extender pigment	Name of mineral
Silicates	Quartz Diatomaceous earth Synthetic silica Kaolin (Clay) Bentonite Talc Asbestine Mica (Muscovite) Mica (Phlogopite) Wallastonite Synthetic calcium silicate
Sulfates	Barytes Blanc fixe Gypsum Precipitated calcium sulfate Calcium sulfate anhydrite
Carbonate	Calcite Limestone Aragonite Dolomite

Table 1.2 Common coloring pigments in automotive paints.

Type of pigment	Pigments
Inorganic pigments	Chromates (yellows, oranges) Ferro cyanides (blues, maroons) Sulfides (yellows, oranges, reds) Iron oxides (variety of colors) Lead oxides (variety of colors) Copper oxides (variety of colors) Chromium oxides (variety of colors) Silcate/Phosphates (blues, Violets) Aluminum (metallic flake)
Organic pigments	Azos (yellows, oranges, reds) Phthalocyanines (blues, greens) Vats and anthraquinones (variety of colors) Quinacridones (reds, violets) Carbon and lampblack (blacks)

Secondly, the vehicle component is a combination of binder or resin, additive, filler, and solvent. The binder provides the support medium for the pigment and additive. Table 1.3 showed typical coating binder in automotive paints [1]. The additive added in a small quantity to improve properties and may or may not be remained in paint coated automotive such as driers, plasticizer, thickeners, and antifouling agents. The solvent used during the coating process were evaporated.

Table 1.3 Typical Costing Binders.

Binder	Information
Alkyd	Frequently cross-linked with an amine (melamine, urea) Frequently modified (styrene, vinyl toluene, acrylic, etc.)
Polyester	Similar to alkyds
Acrylic	Frequently modified (amines, alkyds, polyurethanes, styrene, epoxies, vinyl acetate, etc.)
Urethane	Tougher than acrylic Frequently modified (acrylics and alkyds)
Epoxy	Ether linkage, consequently strong bonding Frequently modified (amines, alkyds, polyurethanes, acrylics)
Vinyl	Substituted ethylene derivatives (chloride, dichloride, acetate, alcohol, benzene) Frequently used in latexes, especially copolymerized with acrylics Used as a modifier for other resins
Cellulose	Substituted ethylene derivatives (nitro, acetate, acetate butyrate, ethyl, methyl) Used as modifiers in other resins
Silicone	Polymer of silicone oil High heat stability Often used as modifier for other resins

1.2 Forensic Analysis of Automotive Paints

The examination and identification of automotive paints are important. In an accident, it is often found paint evidence on the road or on the victim car. The paint evidence was related with the events such as car accidents, robberies or burglaries. Forensic analysis of automotive paints often involves with two cases. First, the paint evidence from victim car was analyzed and compared with reference paint from a suspected car to determine whether two paint fragments could have the same origin or

not. Second, if no comparative material is available like hit-and-run case, the identification of paint evidence may provide the information of the type of paint, producer, year of production, and model by comparison with database spectra. Paint evidence maybe found in form of multilayer paint fragments or thin trace smears. Since the real paint evidence available for examination is very small, the suitable techniques can be applied.

Several techniques are used to characterize automotive paints. Getting started with optical microscopy that was characterized physical properties, they presented the differences in color, thickness, number of layers, and the morphology of paints. In many cases, paint cannot be differentiated from physical characterization thus the chemical analysis were requested such as X-ray fluorescence (XRF), scanning electron microscopy energy dispersive X-ray analysis (SEM-EDX), pyrolysis gas chromatography mass spectrometry (Py-GC-MS), Raman spectroscopy, and infrared spectroscopy (IR) [2].

XRF obtained the elemental composition [3-5]. SEM-EDX can be used to characterize the morphology and the elemental composition of paint [6]. The advantage of using SEM-EDX is determined the individual layer of multilayer paint without separated paint layer. However, both techniques cannot present chemical structure or chemical bonding of sample. Py-GC-MS is suitable to identify binder, additive and organic compound in the sample [7-10]. Disadvantages of Py-GC-MS are a destructive technique and not suitable to analyze multilayered-paint samples.

Raman spectroscopy can identify pigment and some extender in paint chip [11-14]. This technique is based on light scattering rather than adsorption. Raman scattering depends on the polar bond. Some paint components may give both infrared absorption bands and Raman bands but the intensity of absorption bands or scattering bands will be different. Some pigments may present Raman bands but they did not have infrared absorption bands. The advantage of Raman spectroscopy is no sample preparation and can provide information in low-frequency region where many inorganic pigments and extender have important vibration band. Disadvantage of Raman technique is the fluorescence effects, which sample heating lead to thermal

degradation or even pyrolysis or photochemical reactions. Strong fluorescence may overwhelm the weaker Raman scattering peaks. The fluorescence effect can be decreased by changing the laser wavelength, or reduced the recording time. However, fluorescence effects still occur for analyzing dark paints.

Infrared spectroscopy is one of the most popular techniques for characterization of automotive paint [1, 11, 12, 15-28]. It used for determination the general type of paint and identification the binder, main pigments and additives.

1.2.1 Fourier Transform Infrared (FT-IR) Spectroscopy of Automotive Paints

Fourier Transform Infrared (FT-IR) spectroscopy is widely used for forensic analysis of automotive paint. FT-IR spectra provide information directly relate to chemical structure of chemical composition in the analyzed material. As a result, this technique was employed for identifying binder, main pigment [23-28], and additive in paint. Several sampling techniques were analyzed paint evidence, such as reflection, transmission, and attenuated total reflection (ATR).

The reflectance mode is not frequently used to determine automotive paints for a reason of poor signal-to-noise ratio, spectral distortion (e.g. derivative-shaped peak due to anomalous distortion effect), and non-reproducibility techniques [1]. In general, the transmission mode was more favorable than reflectance mode.

For the multilayer paints, they need separation of each layer before analyzing or embedded and microtomed method. From the development of infrared microscopy, the aperture size can be adjusted to decrease the sampling area to limit in each layer of multilayer paint chip without separation layer. But the disadvantage of decreasing the aperture is reduces signal-to-noise ratio.

The embedding and microtoming methods are required for a small and fragile paint fragment [21]. The problems from embedding media (e.g. wax, polyester, and epoxy resin) are interfering with the sample, curing temperature, shrinking after

curing, reaction with sample, and do not easily microtomed that cause difficulty in sample preparation.

Transmission mode is required the very thin sample that the infrared light can transmit. The paint chip was embedded in a suitable resin and then using a microtome to cut (5-15 μm in thickness). However, the transmission analysis cannot analyze trace smear on paint support that may be difficult to isolate. Additionally, the opaque pigment maybe obstructed transmission of light.

The ATR FT-IR can be used to analyze single layer paint and trace smear, but the analysis of multilayer paint chip is still difficult as it requires the separation for the individual paint layer [15, 18, 19].

1.2.2 ATR FT-IR Microspectroscopy of Automotive Paints

Attenuated total reflection Fourier Transform Infrared (ATR FT-IR) spectroscopy is one of the many FT-IR sampling techniques that provide molecular information of sample surface. In the ATR technique, the sample is placed against an internal reflection element (IRE). The IRE is made of material with high refractive index such as germanium (Ge), silicon (Si) or zinc selenide (ZnSe). The total internal reflection occurs at the interface as the angle of incidence greater than the critical angle is utilized. The conventional ATR with hemispherical Ge IRE (25 mm in diameter) has large sampling area ($\sim 5 \times 5 \text{ mm}^2$). It cannot analyze small paint evidence or multilayer paint without a separation of paint layer.

From the limitation of the commercial ATR accessory, a homemade diamond μATR accessory and a homemade Ge μATR accessory were developed by Sensor Research Unit, Department of Chemistry, Faculty of Science, Chulalongkorn University. The novel diamond μIRE with a gem quality round brilliant cut natural diamond and the Ge μIRE with a dome-shaped Ge was employed for spectral acquisition using an infrared microscope. Due to the small sampling area of the culet of diamond μIRE and the tip of Ge μIRE , a small sample can be analyzed. In this work, diamond μIRE and Ge μIRE were employed for forensic analysis of

automotive paints such as paint coated on metal, multilayer paint chip, and paint trace smear.

1.3 Objectives of the Research

The objective of this work is to develop techniques for characterization of automotive paint by ATR FT-IR microspectroscopy and employed for forensic analysis.

1.4 Scope of the Research

1. To characterize automotive paints with different colors and shades by conventional ATR with hemispherical Ge IRE, the slide-on diamond μ IRE and the slide-on Ge μ IRE and compare efficiency.
2. To characterize multilayered automotive paint chip without separating individual paint layer.
3. To characterize thin trace smear on automotive paint by the slide-on diamond μ IRE and the slide-on Ge μ IRE.

สถาบันวิทยบริการ
จุฬาลงกรณ์มหาวิทยาลัย

CHAPTER II

THEORETICAL BACKGROUND

2.1 Fundamentals of Infrared Spectroscopy

Infrared spectroscopy is one of the most often used spectroscopic techniques to the study of matter. It is the study of the interaction of infrared radiation with the sample. Light is an electromagnetic wave because it is composed of electric wave (electric vector (E)) and magnetic wave (magnetic vector (H)) [29]. These two waves are in planes perpendicular to each other as shown in Figure 2.1. The amplitude of the electric vector changes over time and has the form of the sine wave.

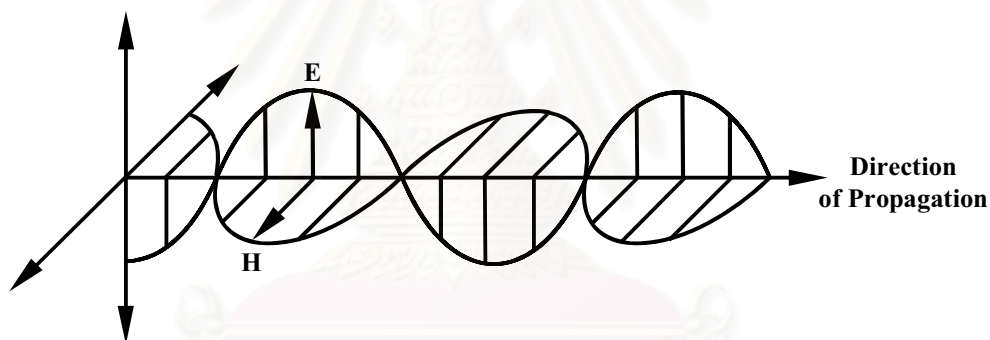


Figure 2.1 Propagation of a linearly polarized electromagnetic wave in space. Electric (E) and magnetic (H) vectors are always perpendicular to each other and to the direction of propagation.

The distance of a wave is the wavelength. The wavenumber of a light is inversely varied as the wavelength. If wavelength is measured in cm, then wavenumber is reported in cm^{-1} . Wavenumber is the units that used to denote different type of light. Higher wavenumber light has more energy than lower wavenumber light. Mid-infrared radiation will be defined between 4000 and 400 cm^{-1} .

When infrared radiation interacts with matter, it can be absorbed and causing the chemical bonds in the molecule to vibrate. The vibration of chemical bonds in a material was presented by infrared absorbance. Functional groups within molecules

absorb infrared radiation in different wavenumber. A plot of infrared intensity versus wavenumber is called infrared spectrum that related to the chemical functional group of a sample.

When the electromagnetic radiation impinges on the matter, interactions between the incident radiation and the molecules will alter the incident beam. The incident radiation can be reflected, scattered, transmitted, or absorbed by the sample depending on the experiment. A schematic illustration for an interaction between light and matter is illustrated in Figure 2.2 [29].

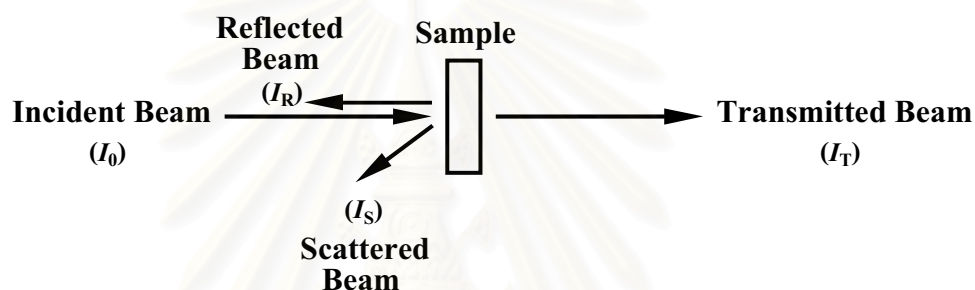


Figure 2.2 Interactions of light with matter.

The total amount of incident energy is the sum of reflected, scattered, transmitted, and absorbed light. This process can be expressed by the following relationship [29]:

$$I_0 = I_R + I_S + I_T + I_A \quad (2.1)$$

where I_0 is the intensity of the incident radiation, I_R , I_S , and I_T are the reflected, scattered, and transmitted radiations, respectively. I_A is the radiation absorbed by matter. The intensity of each radiation depends on the intensity and wavelength of the incident radiation, the optical properties of the specimen, the concentrations of species, and the geometry of the experimental setup.

The sample absorbed a fraction of the incident radiation. In order to measure the region and amount of light being absorbed by the sample, we need to measure the ratio of the sample attenuated (I) and nonattenuated (I_0) intensities of the radiation. In

transmission measurement the ratio is proportional to the transmittance of the sample. This relationship can be quantitatively related to the chemical composition of the sample by the Beer-Lambert law as [29]:

$$I / I_0 = e^{-A(\bar{\nu})} = e^{-c_2 \varepsilon(\bar{\nu}) l} \quad (2.2)$$

where $A(\bar{\nu})$ is the sample absorbance at a given wavenumber $\bar{\nu}$, c_2 is the concentration of the absorbing functional group, $\varepsilon(\bar{\nu})$ is the wavenumber-dependent absorption coefficient, and l is the film thickness for the IR beam at a normal incidence to the sample surface.

2.2 Attenuated Total Reflection Fourier Transform Infrared (ATR FT-IR) Spectroscopy

Attenuated total reflection Fourier transform infrared (ATR FT-IR) spectroscopy is one of the many FT-IR sampling techniques where the infrared radiation is employed for accessing molecular information of surfaces and interfaces under total internal reflection (TIR) phenomenon. In experimental, a sample need only be placed in optical contact with the surface of the IRE to record its ATR spectra.

2.2.1 A Principle of Light Reflection and Refraction

Refraction and reflection occur, when an electromagnetic radiation passes from one medium to another that has a different refractive index. A change of beam direction takes place because of the differences in propagation velocity through two media. If light propagates through an incident medium with refractive index n_1 and enters a medium with refractive index n_2 (Figure 2.3), the light path will be changed and the extent of refraction is given by the following relationship, known as Snell's law [29]:

$$n_1 \sin \alpha_1 = n_2 \sin \alpha_2 \quad (2.3)$$

where α_1 and α_2 are the angles of incidence and refraction, respectively.

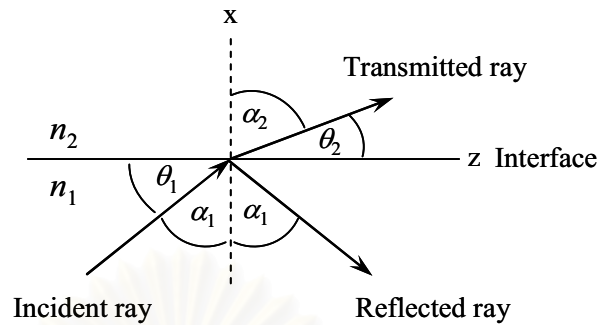


Figure 2.3 Reflection and refraction of a plane wave at a dielectric interface based on Snell's law.

Total internal reflection occurs when radiation traveling in a higher refractive index material impinges on the interface with a lower refractive material at an incident angle larger than the critical angle. The critical angle, θ_c , can be derived from Snell's law and given by Equation 2.4 [29].

$$\theta_c = \sin^{-1}(n_2 / n_1). \quad (2.4)$$

where n_2 is the lower refractive index and n_1 is the higher index. The critical angle is the incident angle that the corresponding refracted angle equal 90° as shown in Figure 2.4. For any angle of incidence that larger than the critical angle, all the light is totally reflected off the interface.

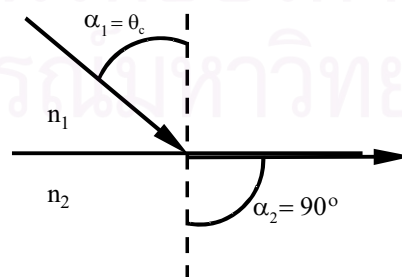


Figure 2.4 Light travels from an optically denser medium and impinges at the surface of the optically rarer medium ($n_1 > n_2$) with angle of incidence equal the critical angle.

In ATR technique, the reflectivity is a measure of the interaction of the electric field with the material and the resulting spectrum is also a characteristic of the material.

2.2.2 Internal Reflection Element (IRE)

ATR spectroscopy has long been used for various samples from aqueous solutions to bulk materials. A variety of the internal reflection element (IRE) or ATR prism that must have a high refractive index and be transparent throughout the mid-infrared spectral region and accessories have been developed. Table 2.1 showed optical properties of some infrared transmitting materials [30].

In practice, internal reflection crystals can have many shapes. They can divide into two main types, single reflection type with a hemispherical IRE and multiple reflection type with a trapezoidal IRE, as shown in Figure 2.5. Hemispherical IREs are used in variable-angle or fixed-angle, single-reflection ATR attachments. The hemisphere allows the angle of incidence to be changed over a wide range without changing the divergence of the incident radiation. A choice must be made in the working angle or range of angles of incidence, number of reflections, aperture, number of passes, surface preparation, and material from which it is made [31].

Table 2.1 Information of materials used for internal reflection elements.

Material	Usable wavenumber range (cm ⁻¹)	Reflective index at 1000 cm ⁻¹	Hardness (kg mm ⁻²)
Germanium	5,500-600	4.02	780
Silicon	8,300-1500, 360-120	3.42	1150
Zinc selenide	20,000-460	2.43	120
Diamond	45,000--~2,500, ~1,650-200	2.417	8820

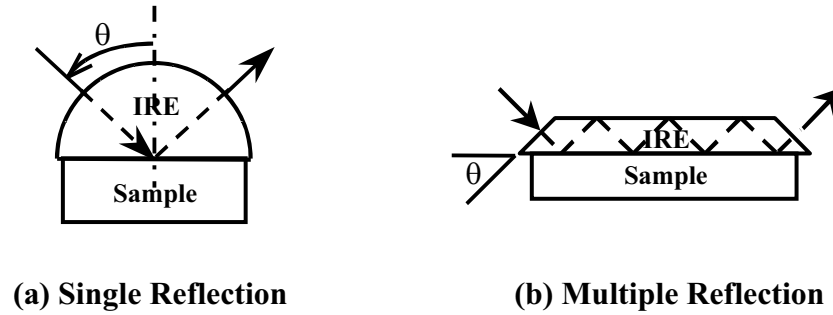


Figure 2.5 IRE configurations commonly used in ATR experimental setups: (a) Single reflection variable-angle hemispherical crystal and (b) Multiple reflection single-pass crystal.

2.2.3 ATR Spectral Intensity

The magnitudes of the interaction between light and the sample can be expressed in terms of absorbance. The absorbance depends on both the material properties (e.g., refractive index of the IRE and refractive index of the sample) and the experimental parameters (e.g., angle of incidence, frequency, and polarization of the incident beam). Under the ATR condition, the absorption in absorbance unit can be expressed in terms of experimental parameters and material characteristic by [32]:

$$A(\theta, \nu) = \frac{2\pi\nu}{\ln(10)n_{IRE} \cos\theta} n_{Sample}(\nu) k_{Sample}(\nu) d_p(\theta, \nu) \langle E_0^2(\theta, \nu) \rangle \quad (2.5)$$

where $A(\theta, \nu)$ is absorbance, θ is the angle of incidence, ν is the frequency of the incident radiation (i.e., in wavenumber unit), n_{Sample} and k_{Sample} , respectively, are the refractive index and the absorption index of the sample, $d_p(\theta, \nu)$ is the penetration depth, and $\langle E_0^2(\theta, \nu) \rangle$ is the *mean square evanescent electric field (MSEvF)*

2.2.4 Penetration Depth

ATR FT-IR spectroscopy is a surface sensitive technique. The electromagnetic field penetrating into the sample is commonly referred to an evanescent wave. The depth of penetration of the evanescent wave is defined as the distance from the

surface interface of the IRE/sample that the intensity of the evanescent wave has been reduced to $1/e$ ($\sim 37\%$) of its value at the surface and can be calculated as [31]:

$$d_p = \frac{1}{2\pi\nu n_0 (\sin^2 \theta - (n_1/n_0)^2)^{1/2}} \quad (2.7)$$

where $d_p(\theta, \nu)$ is the penetration depth. The penetration depth also depends on experimental conditions and material characteristics.

The penetration depth can be controlled either by varying the angle of incidence or by selection of IRE. Different IREs have different refractive index. For example, the penetration depth with ZnSe ($n_I = 2.4$) as the IRE is greater than that of Ge ($n_I = 4.0$). The penetration depths of Ge IRE at different angle of incidence are shown in Figure 2.6.

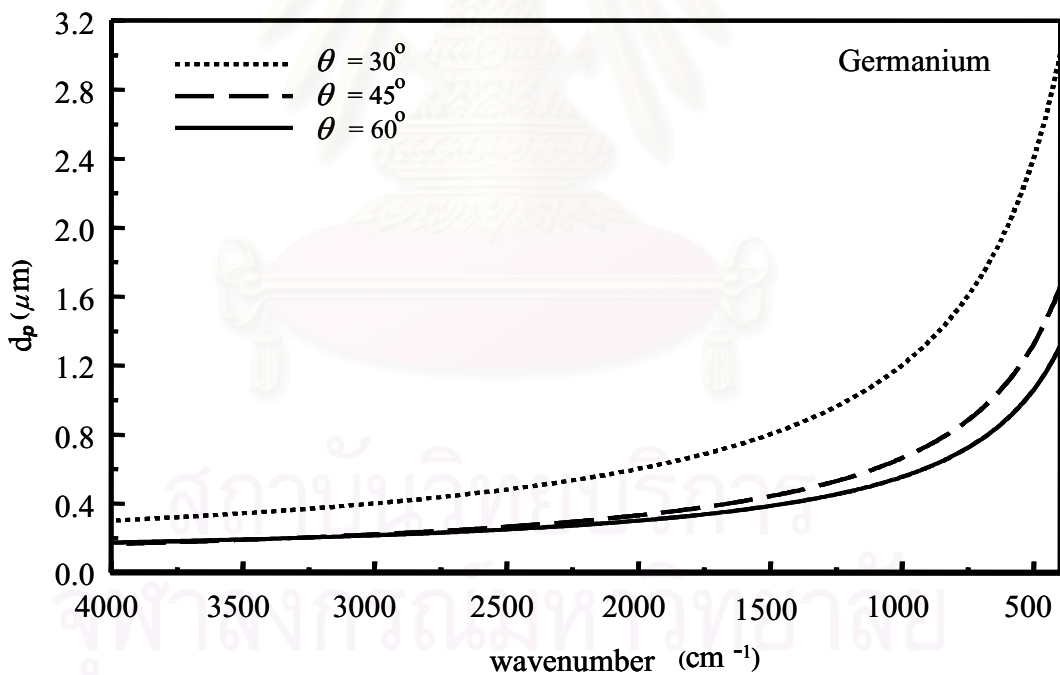


Figure 2.6 Relationship between the penetration depth and wavenumber for Ge crystal at different angle of incidence.

It also indicates that the penetration depth depending largely on the frequency of the incident beam. As the frequency of the infrared light increases, the penetration depth decreases. However in FT-IR practice, it is often convenient to express

frequency in terms of wavenumber, the penetration depth decreases when wavenumber increases. This also leads to a decrease of relative band intensities in the ATR spectrum with increasing wavenumber. In addition, the penetration depth is also depending on the angles of incident. If the angle of incident is increased, the penetration depth will be decreased and the spectral intensity will be decreased.

2.2.5 Limitation of ATR FT-IR Spectroscopy

ATR FT-IR spectroscopy is a surface sensitive technique. However, it has several limited applications [32]. One of them is a contact between the sample and IRE. In order to obtain good ATR spectra, a very good contact between the sample and IRE is required. If there is an air gap between the sample and the IRE, the smaller is the observed spectral intensity. For a solid material with a rough surface, its ATR spectrum may not be observed. To solve this problem, the high pressure is applied at the sample against the IRE. However, the brittle IRE may be damaged by an excessive pressure. Another limitation for conventional ATR technique is that have large sampling area, the spectral information of a small sample cannot be obtained.

2.3 ATR FT-IR Microscopy

Combining infrared spectroscopy with microscopy has extended the application of vibrational spectroscopy to the analysis of small samples. Microscopes became common attachments to industrial and forensic laboratory FT-IR spectrometers in the mid-1980s [30, 33]. The optical diagram of an infrared microscope is shown in Figure 2.7.

A ray tracing within the 15X Schwarzschild Cassegrain infrared objective are shown in Figure 2.8. The concave primary mirror and the convex secondary mirror of the objective focus radiation onto the reflecting plane with angles of incidence ranging from 15.6° to 35.5° . ATR spectra are always collected by using the reflection mode based on the phenomenon known as total internal reflection, by coupling the focused radiation into specially designed μ IREs made of high refractive index materials and by making the angle of incidence at the sampling surface greater than the critical angle.

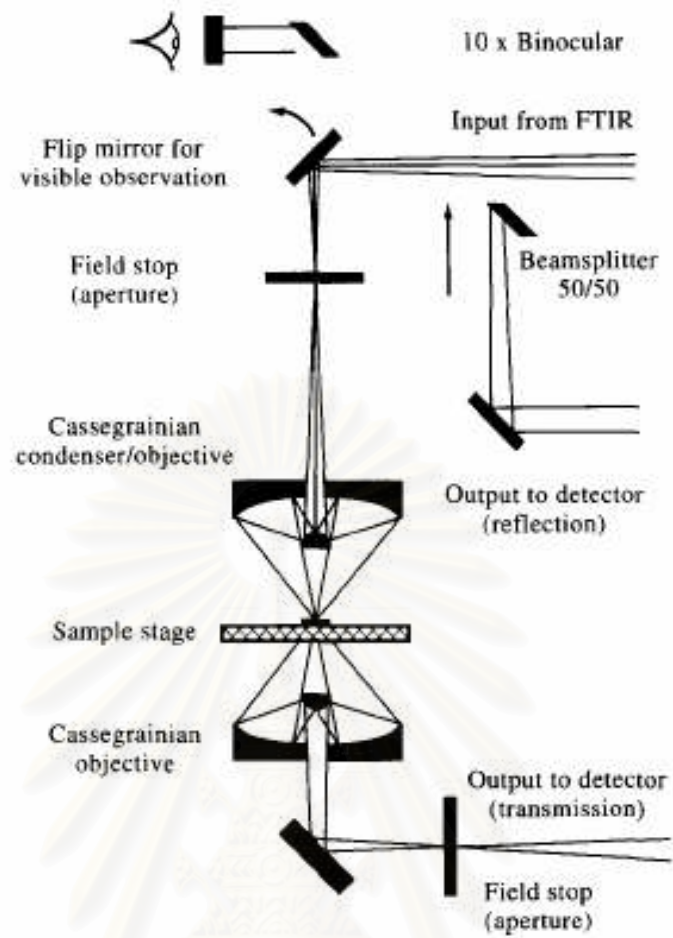


Figure 2.7 Optical diagram for infrared microscope.

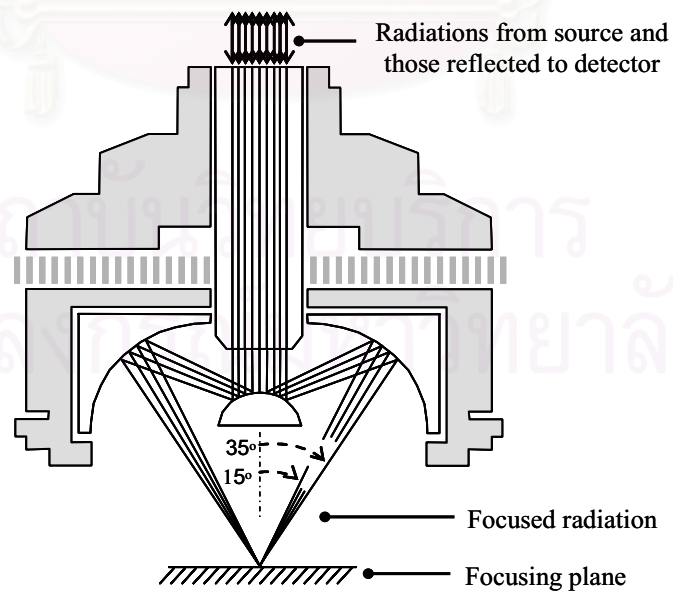


Figure 2.8 The infrared radiation tracing within the objective of infrared microscope.

2.3.1 The Homemade Slide-on Diamond μ IRE

Diamond can be employed as an IRE because its high refractive index ($n_{diamond} = 2.417$) is greater than that of sample ($n_{organic} = 1.5$). An internal reflection elements (IRE) made of a ~ 0.1 ct gem quality round brilliant cut natural diamond type IaB with low nitrogen impurity was employed for ATR FT-IR spectral acquisition using an infrared microscope. In principle, a gem quality brilliant cut diamond was cut in such a proportion that the number of total internal reflection (TIR) within the diamond is enhanced. To increase the number of total internal reflection, the cutting proportion of the diamond is carefully designed with respect to its refractive index, size, shape, and carat weight. The number of total internal reflection (TIR) depends on the angle and positions that light enter the diamond. The greater the number of total internal reflection reflections, the better the fire and brilliance of the diamond. This phenomenon is due to the dispersion of light associated with its traveling distance and the total internal reflection inside diamond.

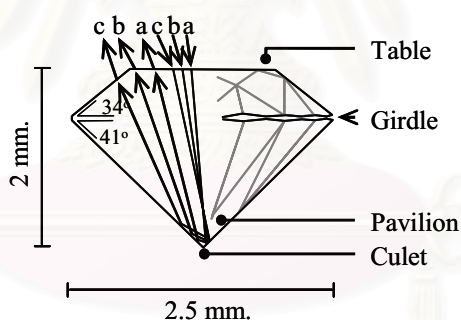


Figure 2.9 The infrared radiation tracing within the diamond μ IRE.

To collect ATR spectra using a faceted diamond as an IRE, the infrared radiation is coupled into and is collected from the table facet with a normal incidence. The radiation totally reflects at the pavilion facet. Examples of ray tracings within the sharp-tip diamond IRE with a Tolkowsky's recommended cut proportion are shown in Figure 2.9. According to the traveling path of the coupled radiation, the re-emerging radiation from the table facet is defined as the *transflected radiation* [34]. Due to the complex cut the surfaces of the facet diamond, the coupled radiations that impinge the table facet with different angles and/or positions undergo different reflections inside the faceted diamond before emerging into air at any facets. The TIR phenomenon in

the diamond IRE occurs at the pavilion facet instead of the culet (i.e., the sharp tip of the faceted diamond). For a diamond with a near ideal cut proportion, the angle of incidence at the pavilion facet of diamond/air or diamond/organic medium is greater than the critical angle. The critical angle (θ_c) is equal to 38.36° for the diamond/organic material interface and 24.44° for the diamond/air interface [34]. As a result, ATR FT-IR absorption of a material having an optical contact with the pavilion facet can be realized. A good contact between the diamond IRE and a solid sample, especially a hard and rigid solid, can always be achieved simply by pressing the specimen against the culet of the diamond.

Let us consider the energy of the transflected radiation, there are three sources for the energy losses: the reflection loss as the beam impinges the faceted surfaces due to the radiation is specularly reflected at the air/diamond interface and is internally reflected at the diamond/air interface with an angle smaller than the critical angle (i.e., the critical angle at the diamond/air interface equals 24.44°), the absorption by the diamond IRE that associated with defects and impurities in the diamond crystal structure, and the ATR absorption by the material undergo total internal reflection at the pavilion facet. When a faceted diamond is employed as an IRE, the transflected absorption of the diamond IRE and the ATR-absorption of the material are additively present in the observed spectrum.

Diamond is absorbing in the mid-infrared region as shown in Figure 2.10. Transflectance spectrum has three major absorption bands: *one-phonon* at 1400-900 cm^{-1} , *two-phonon* at 2650-1500 cm^{-1} , and *three-phonon* at 3900-2650 cm^{-1} [34, 35]. The one-phonon absorption is due to nitrogen impurity. The absorption magnitude in this region depends on the concentration of nitrogen impurities. Diamond with high nitrogen content always shows over absorption in this region. The employed IRE is a natural diamond type IaB with relatively low nitrogen content, the observed spectral did not interfere with the absorption bands of the diamond. The two-phonon region is indicated the specifically absorption of the diamond crystal structure that always over absorbing in this region. The three-phonon region is associated with hydrogen impurity in the diamond structure.

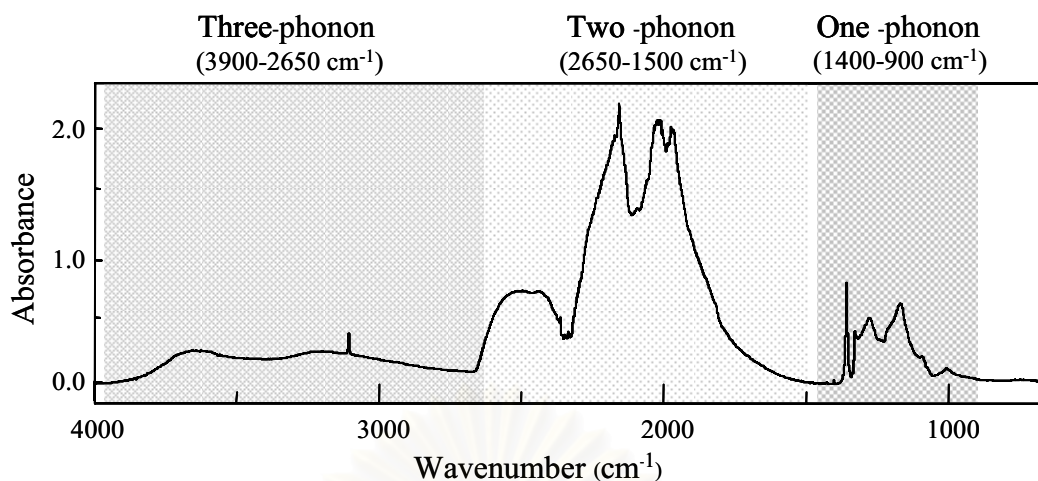


Figure 2.10 Transflectance spectrum of round brilliant cut natural diamond.

2.3.2 The Homemade Slide-on Ge μ IRE

The cone-shaped Ge μ IRE was employed an IRE due to the small tip configuration and small sampling area. Unlike the diamond μ IRE, the TIR phenomenon in the Ge μ IRE occurs at the tip of the cone-shaped Ge as shown in Figure 2.11. To ensure a good contact between the Ge tip and a solid sample, the circular tip of the IRE was made a small hemispherical surface. Since the contact area is small, a good contact was achieved with a minimal force exerting on the tip. The hemispherical dome of the cone-shaped Ge μ IRE facilitates the coupling of the focused radiation traveling into the IRE by minimizing the reflection loss at the air/Ge interface. If a nearly perfect coupling was assumed, the radiation transmitted through the air/Ge interface of the dome and impinged the Ge/air interface of the tip without a significantly change in the angle of incidence (i.e., the refraction at the air/Ge interface was minimized). For the total internal reflection (TIR), the incident angle must greater than the critical angle. The critical angle between the Ge μ IRE ($n_{\text{Ge}} = 4.0$) with air ($n_{\text{air}} = 1.0$) and an organic sample ($n_{\text{organic}} = 1.5$) are 14.48° and 22.02° , respectively. While the angle of incidence from the objective microscope was covered range from 15.6° to 35.5° . To eliminate interference from the internal reflection associated with the radiation having an angle of incidence smaller than the critical angle, an opaque circular adhesive tape was placed on the center of the hemispherical dome. The observed spectrum is free of refractive-index type peak shape originated

by internal reflection at the tip due to the un-wanted radiation was blocked. ATR FT-IR spectra of a small sample or a small area can be acquired.

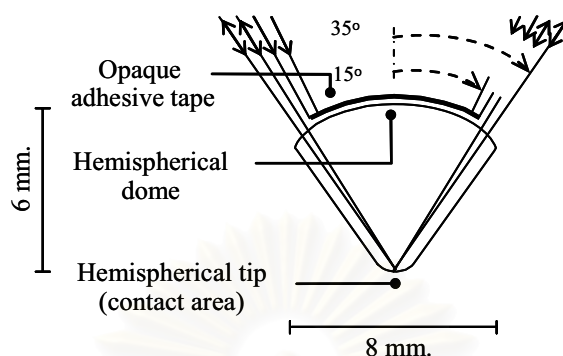


Figure 2.11 The infrared radiation tracing within the Ge μ IRE.

2.4 Specular Reflection

Reflection technique involves the reflection of the infrared light off the sample (particularly for solids). It is considered to be a simpler technique than the transmission technique. When an infrared radiation is directed onto the surface of solid sample two types of reflected radiations are obtained: specular and diffuse reflection.

Specular reflectance is defined as reflection in which the angle of incidence on the sample is exactly equal to the angle of reflection as shown in Figure 2.12. In order to produce a good spectrum, the surface of the sample must be smooth and flat. The reflected intensity also depends upon the index of refraction. Since the refractive index of material goes through an anomalous dispersion in the region of absorption band, the true specular reflectance spectrum qualitatively resembles the dispersion in refractive index. The result is a spectrum that shows strong dispersion features at the absorption frequencies, which is not easily interpreted. A mathematical process known as the *Kramers-Kronig (KK) transformation* can convert the specular reflectance spectrum into transmission-like spectrum. This transform can be readily carried out by the computer associated with the FT-IR spectrometer and the suitable software furnished by all FT-IR manufacturers. The transform works well only if the spectrum is purely specular (no diffuse reflection) and the dispersion is low at both the beginning and the end of the range being transformed [36, 37].

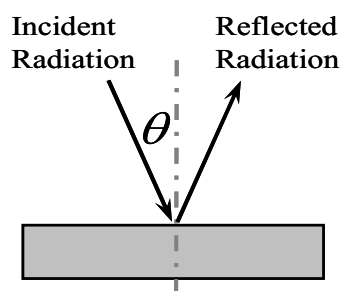


Figure 2.12 Schematic diagram of specular reflection measurement of sample.



สถาบันวิทยบริการ
จุฬาลงกรณ์มหาวิทยาลัย

CHAPTER III

EXPERIMENTAL SECTION

ATR FT-IR spectroscopy was applied for surface characterization of automotive paints with forensic analysis purpose. Three types of automotive paints were investigated: different colors and shades of automotive paint; multilayer automotive paint from different cars; and smear trace on automotive paint. The different colors and shades of automotive paint were identified by conventional ATR with hemispherical Ge IRE comparison with two homemade μ ATR accessories; a slide-on diamond μ IRE and the slide-on Ge μ IRE. The identification of each paint layer of multilayer automotive paints can be providing the information for forensic purpose. The multilayer automotive paint from different cars were analyzed depth profiling by a diamond μ IRE and each layer on cross-section of paint fragment by the slide-on diamond μ IRE, the slide-on Ge μ IRE and specular reflection without separation of paint layers. In addition, multilayer automotive paint were identified by cross-section surface line mapping with the slide-on diamond μ IRE and the slide-on Ge μ IRE. In car accident, the evidence almost is in trace smear form. It is necessary to examine the paint trace smear that found on the vehicle. The thin and smear trace on automotive paint were determined by the slide-on diamond μ IRE and the slide-on Ge μ IRE.

3.1 Materials and Equipments

3.1.1. Automotive Paint Samples

1. Different colors and shades of automotive paint (from Nippon paint, Thailand) coated on metal plate (paint thickness \sim 23-27 μ m).
 - 1.1 Non-metallic paint
(i.e, gray D, white, yellow A, yellow B, red A, red B, orange, green A, green B, blue A, blue B, blue D, and black)
 - 1.2 Metallic paint
(i.e, gray A, gray B, gray C, and blue C)

- Multilayer automotive paint (from different cars).

Table 3.1 Information of multilayer paint sample.

Source	Top coat color	Number of layer via optical images
Bumper (body kit)	Silver gray	Two
Hood	Gray	Eight
Door	Blue	Thirteen
Bumper of Toyota Fortuner	Black	Three
Fender of Mitsubishi car	White	Three
Door of BMW car	Blue	Four

- Thin trace smear on automotive paint (from the BMW paint fragment).

3.1.2 Instruments

- Nicolet 6700 FT-IR spectrometer equipped with a mercury-cadmium-telluride (MCT) detector.
- ContinuumTM infrared microscope with 15X Cassegrain infrared objective and 10X glass objective.
- Variable-angle single-reflection attenuated total reflection accessory (The SeagullTM, Harrick Scientific, USA) with a hemispherical germanium (Ge) IRE (25 mm diameter).
- Homemade diamond μ ATR accessory with a gem-quality round brilliant cut diamond as IRE.
- Homemade slide-on diamond μ ATR accessory with a gem-quality round brilliant cut diamond as IRE.
- Homemade slide-on germanium (Ge) μ ATR accessory with a cone-shaped Ge as IRE.

3.1.3 Default Spectral Acquisition Parameter

Nicolet 6700 FT-IR Spectrometer

Instrumental Setup

Source	Standard Globar TM Infrared Light Source
Detector	MCT
Beam splitter	Ge-coated KBr

Acquisition Parameters

Spectral resolution	4 cm ⁻¹
Number of scans	256 scans
Spectral format	Absorbance
Mid-infrared range	4000-650 cm ⁻¹

Advanced Parameters

Zero filing	none
Apodization	Happ-Genzel
Phase correction	Mertz

ContinuumTM Infrared Microscope

Instrumental Setup

Detector	MCT
Objective	15X Schwarzschild-Cassegrain
Aperture size	150 μm x 150 μm

3.2 Homemade μATR Accessories

3.2.1 Homemade Diamond μATR Accessory

The homemade diamond μATR accessory consists of two parts as shown in Figure 3.1. The first part is the probing head which designed for mounting the diamond. A gem quality round brilliant cut natural diamond type IaB (0.1 ct) with extremely low nitrogen content was employed as the IRE. The probe head accessory has a sample holder for a solid sample can be brought into contact with the culet of the diamond. The second part is the adjustable reflection plane. The three knobs

setting on the corner of this plate were designed for adjusting the table facet of the diamond perpendicular to the incident radiation in order to obtain a high energy throughput. The homemade diamond μ ATR accessory was placed onto the stage of ContinuumTM infrared microscope that connected to the Nicolet 6700 FT-IR spectrometer, as shown in Figure 3.2. The spectral acquisitions of infrared microscope were performed in reflectance mode. The incident infrared radiation from the infrared microscope was coupled onto the table facet of the diamond. The amount of light is controlled by the aperture of the microscope. The infrared radiation was focused at the culet of the diamond. The sample focus can be adjusted by the knobs of the homemade accessory and the stage of the microscope in order to obtain high energy throughput. Due to the diamond is the hardest known material, it can penetrate into the hard and rigid sample by pressing the sample against the diamond. Thus, the depth profile of sample was studied by homemade diamond μ ATR accessory.

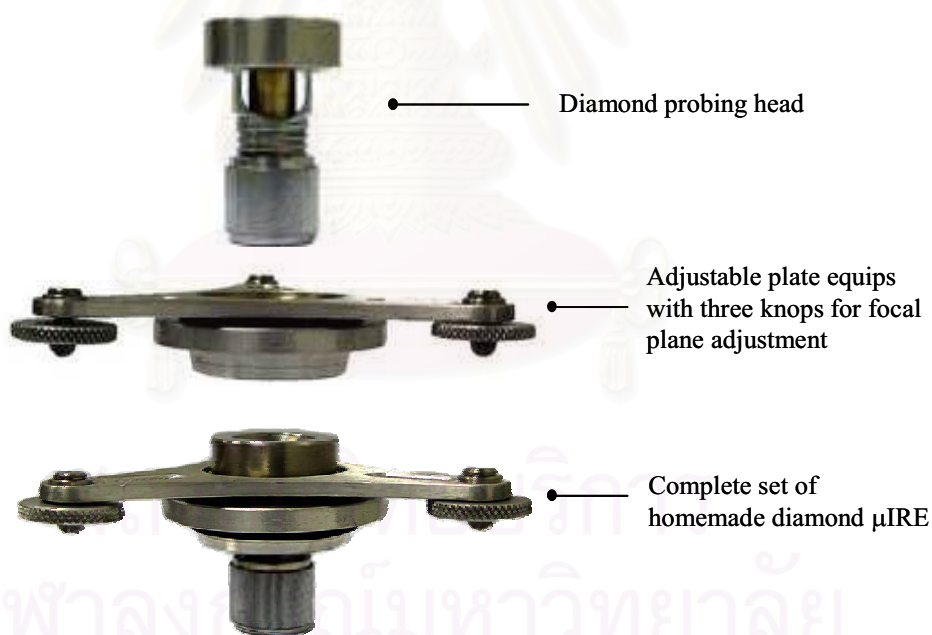


Figure 3.1 The homemade diamond μ ATR accessory: the diamond probing head, the adjustable reflection plane and the complete set of homemade accessory.

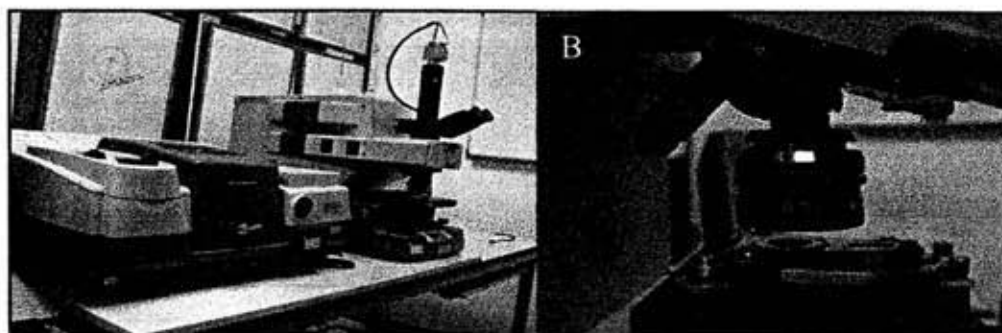


Figure 3.2 The homemade diamond μ ATR accessory: (A) Continuum infrared microscope attach to the Nicolet 6700 FT-IR spectrometer and (B) the complete set of the homemade diamond μ ATR accessory.

3.2.2 Homemade Slide-on Diamond μ ATR Accessory

The homemade slide-on diamond μ ATR accessory was developed from the homemade diamond μ ATR accessory which was limited from size of sample holder and cannot select sampling spot on the surface sample. The homemade slide-on diamond μ ATR accessory consists of two components as shown in Figure 3.3. First, the slide-on housing was designed for placing the slide-on diamond μ IRE on the objective infrared microscope. Second, the slide-on diamond μ IRE was designed for mounting the sharp-tip diamond IRE and slid into the slide-on housing. A gem quality round brilliant cut natural diamond type IaB (0.1 ct) with an extremely low nitrogen content was employed as an IRE. The alignment can be adjusted the diamond slide-on IRE in order to obtain high energy throughput. The slide-on diamond μ IRE was slid into the slide-on housing that had been fixed on the built-in 15x Schwarzschild-Cassegrain infrared objective that connected to the Nicolet 6700 FT-IR spectrometer. Then the slide-on diamond μ IRE was locked by the knob with the slide-on housing. The complete set of the homemade slide-on diamond μ ATR accessory are shown in Figure 3.4. The spectral acquisitions of microscope were performed in reflectance mode. The amount of light is controlled by the aperture of the microscope. The incident radiation from the infrared microscope was coupled into the table facet of diamond and was undergoing total internal reflection at the pavilion facet of diamond as shown in Figure 3.5. The slide-on diamond μ IRE has a small tip that contact with a sample and small sampling area ($\sim 30 \mu\text{m}$ in diameter).

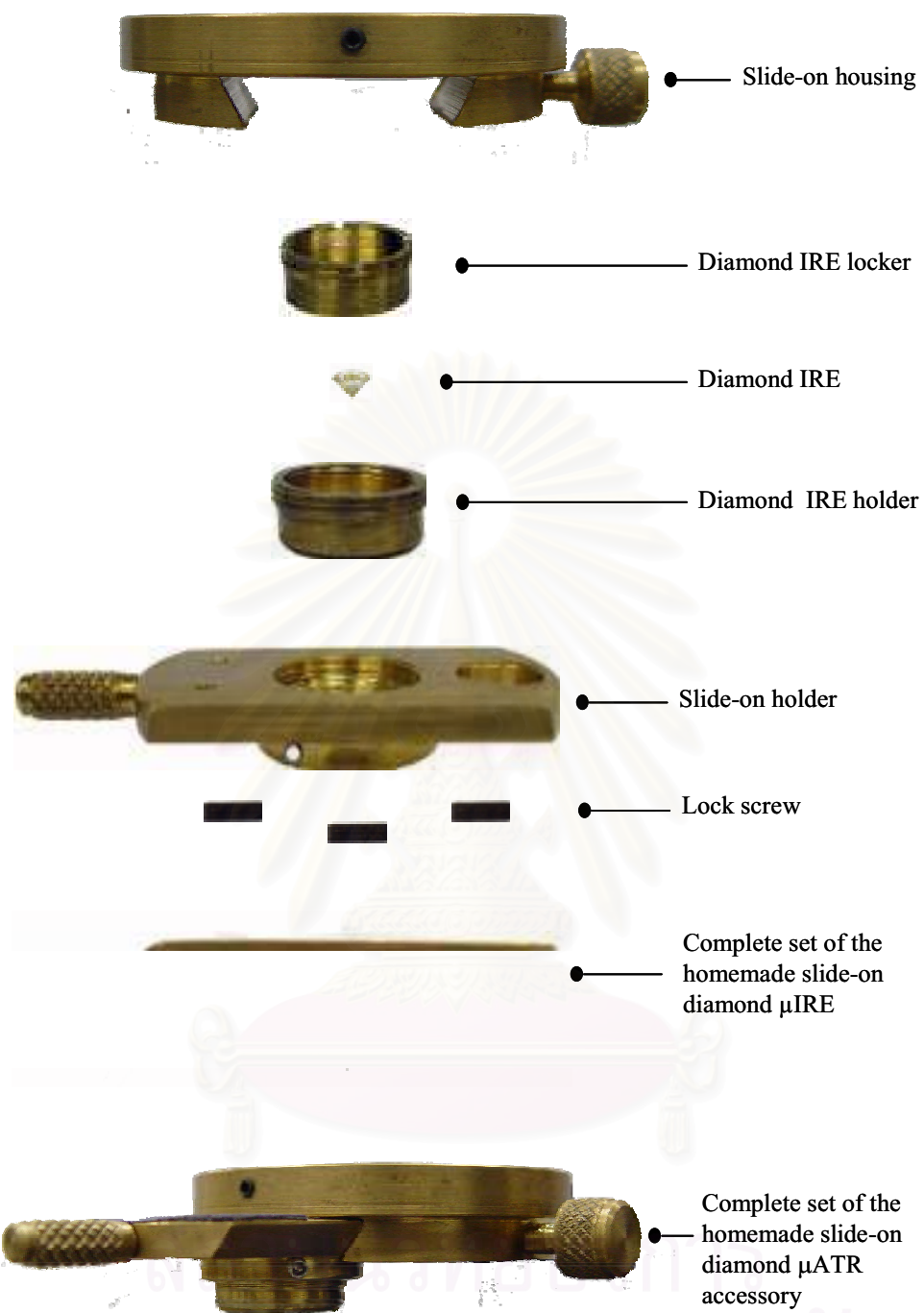


Figure 3.3 The slide-on housing and composition of the homemade slide-on diamond μ IRE.

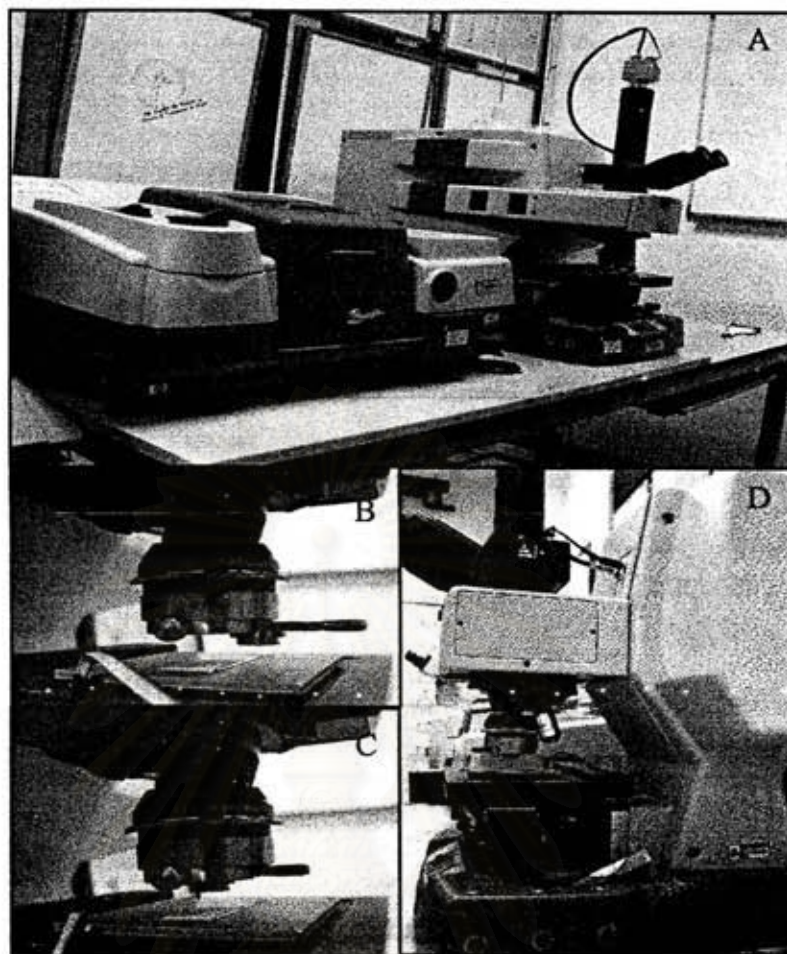


Figure 3.4 The homemade slide-on diamond μ ATR accessory: (A) Continuum infrared microscope attach to the Nicolet 6700 FT-IR spectrometer, (B) the slide-on diamond μ IRE was slid into the position of slide-on housing on the 15X Schwarzschild-Cassegrain infrared objective (C) the slide-on diamond μ IRE was fixed on the position of slide-on housing on the infrared objective, and (D) the complete set of the homemade slide-on diamond μ ATR accessory.

จุฬาลงกรณ์มหาวิทยาลัย

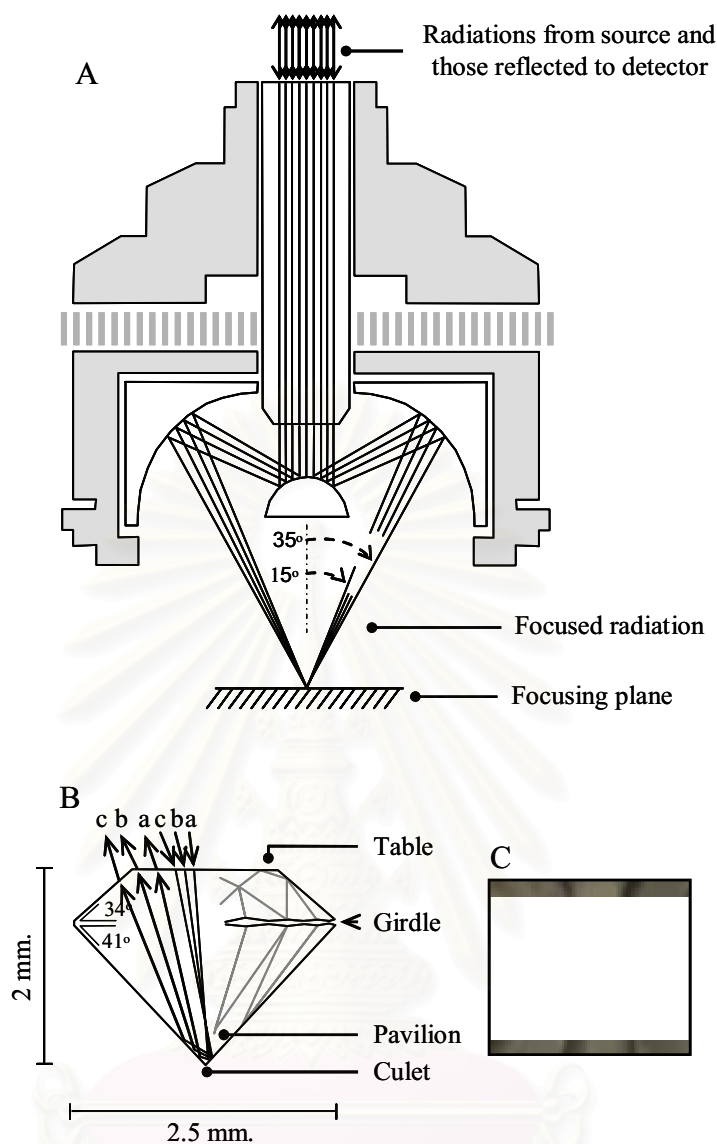


Figure 3.5 (A) A schematic illustration of ray tracing within the infrared objective, (B) focused radiation traveling within the diamond μ IRE, and (C) image of the tip of diamond μ IRE under the visible light.

3.2.3 Homemade Slide-on Ge μ ATR Accessory

The homemade slide-on germanium (Ge) μ ATR accessory was developed from a commercial ATR accessory with hemispherical Ge IRE which was limited from a large sampling area ($5 \times 5 \text{ mm}^2$), limited from size of sample holder, and result in a poor contact between sample and IRE. The homemade slide-on Ge μ ATR accessory consists of two components as shown in Figure 3.6. First, the slide-on housing was

designed for placing the slide-on Ge μ IRE on the objective infrared microscope. Second, the slide-on Ge μ IRE was designed for mounting the cone-shaped Ge IRE and slid into the slide-on housing. The alignment can be adjusted the Ge slide-on IRE in order to obtain high energy throughput. The slide-on Ge μ IRE was slid into the slide-on housing that had been fixed on the built in 15x Schwarzschild-Cassegrain infrared objective that connected to the Nicolet 6700 FT-IR spectrometer, as shown in Figure 3.7. Then the slide-on Ge μ IRE was locked by the knob with the slide-on housing. Then the slide-on Ge μ IRE was locked by the knob. The incident radiation from the infrared microscope was coupled into the dome-shaped Ge IRE and was undergoing total internal reflection at the tip of Ge, as shown in Figure 3.8. The amount of light is controlled by the aperture of the microscope. The slide-on Ge μ IRE has a small tip that contact with a sample and small sampling area (less than $\sim 100 \mu\text{m}$ in diameter).

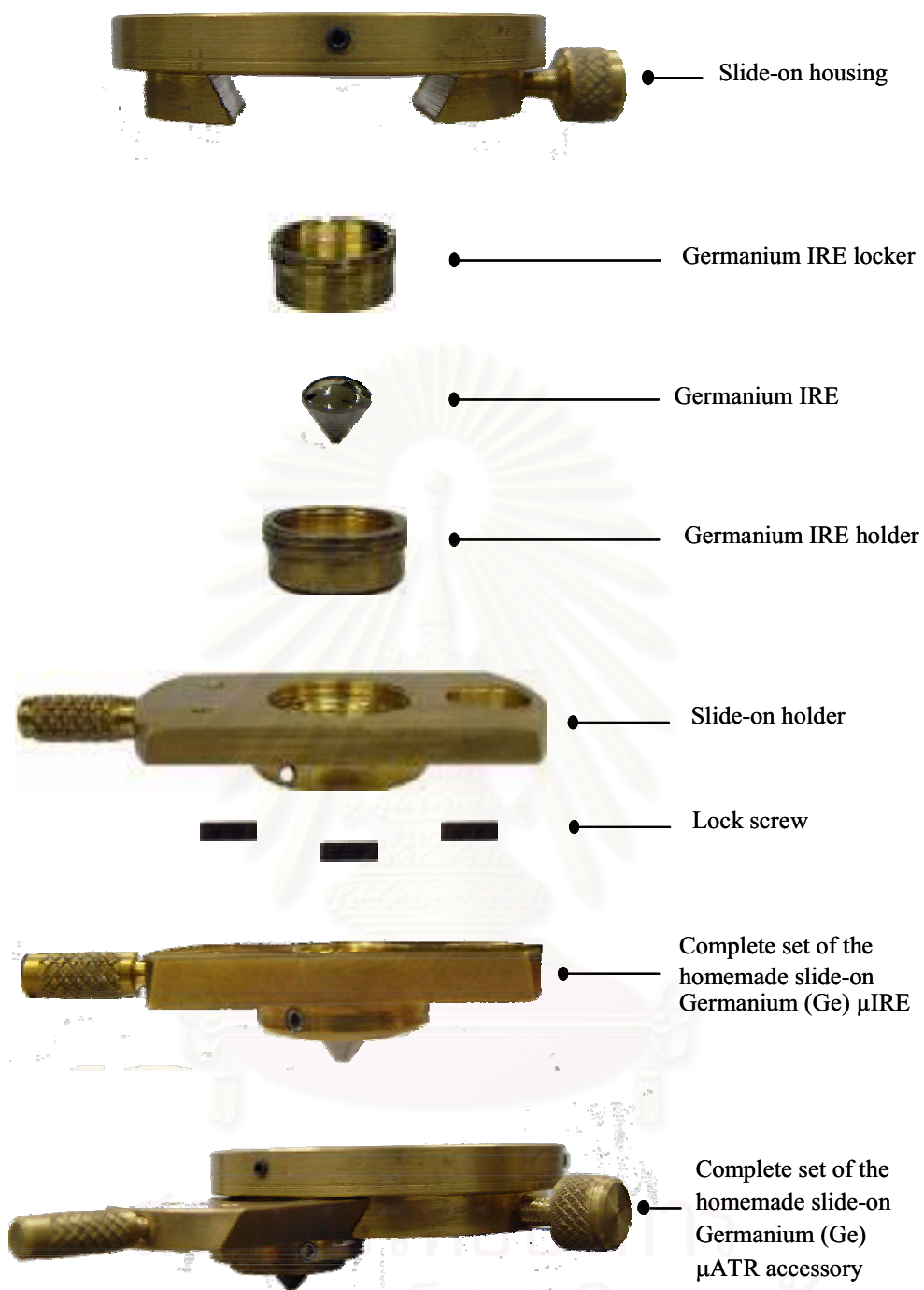


Figure 3.6 The slide-on housing and composition of the homemade slide-on Ge μ IRE.

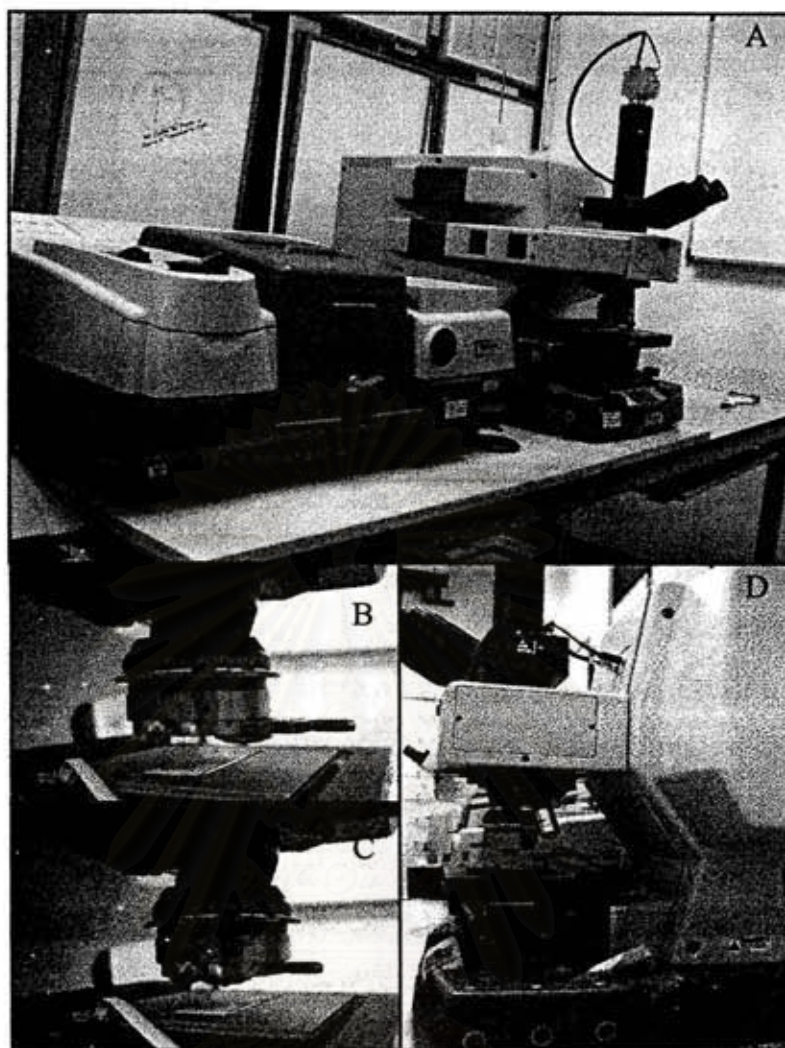


Figure 3.7 The homemade slide-on Ge μ ATR accessory: (A) Continuum infrared microscope attach to the Nicolet 6700 FT-IR spectrometer, (B) the slide-on Ge μ IRE was slid into the position of slide-on housing on the 15X Schwarzschild-Cassegrain infrared objective (C) the slide-on Ge μ IRE was fixed on the position of slide-on housing on the infrared objective, and (D) the complete set of the homemade slide-on Ge μ ATR accessory.

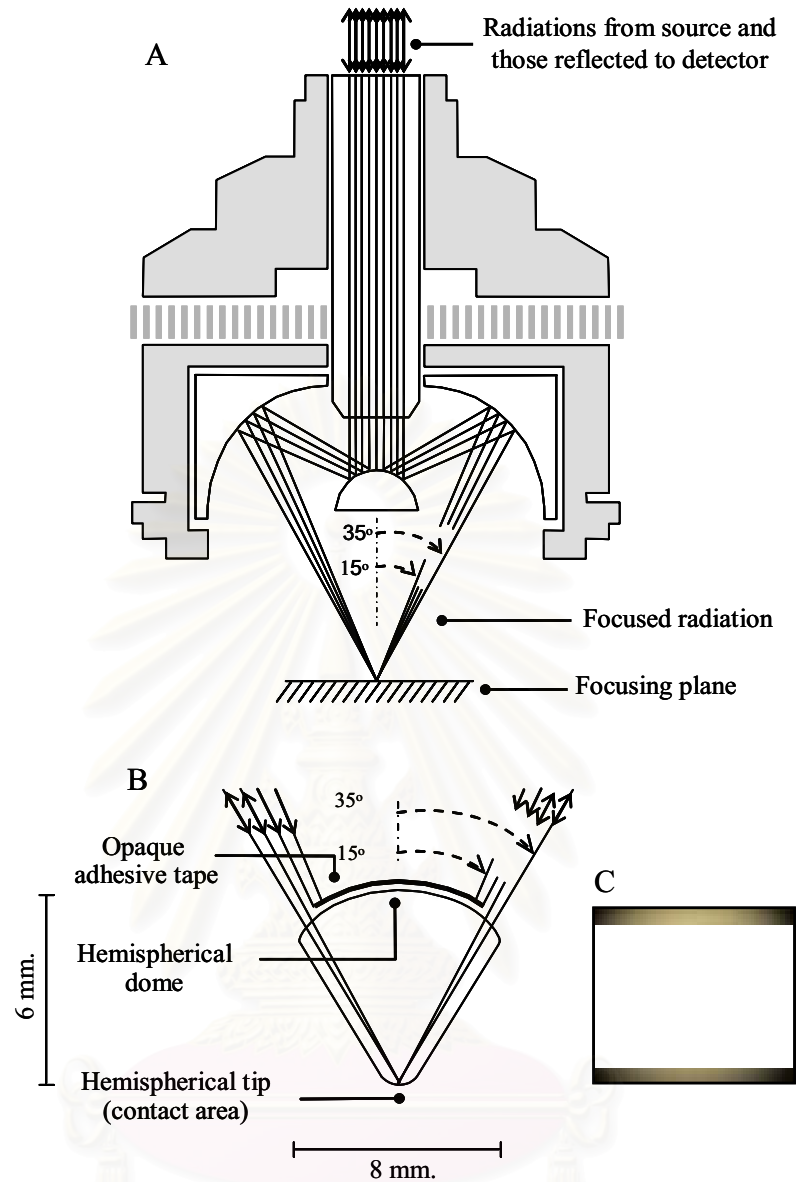


Figure 3.8 (A) A schematic illustration of ray tracing within the infrared objective, (B) focused radiation traveling within the Ge μ IRE, and (C) image of the tip of Ge μ IRE under the visible light.

3.3 Characterization of Different Colors and Shades of Automotive Paints

3.3.1 Experimental Procedure using the Commercial ATR Accessory

The automotive paints with different colors and shades coated on metal substrate were obtained from general coating binder supplied by Nippon paint (Thailand). The automotive paint was separated from the metal substrate by a *thermal shock technique*. A metal substrate will be destroyed surface of the hemispherical Ge IRE. The paint coated metal $5 \times 5 \text{ mm}^2$ was immersed in liquid nitrogen reservoir for few seconds. After that paint chip was peeled off from metal substrate by adhesive tape. The metal-contact surface of paint chip was analyzed.

All ATR spectra were collected by Nicolet 6700 FT-IR spectrometer with a commercial ATR accessory (the Seagull™, Harrick Scientific, USA). A hemispherical Ge IRE (25 mm in diameter) was employed as IRE, as shown in Figure 3.9. The angle of incidence was 30° . The background spectrum was collected through IRE without sample contact. For spectral acquisition of samples, the paint chip was brought into contact with the bottom surface of the IRE under an applied pressure. The ATR spectra of samples were then acquired.

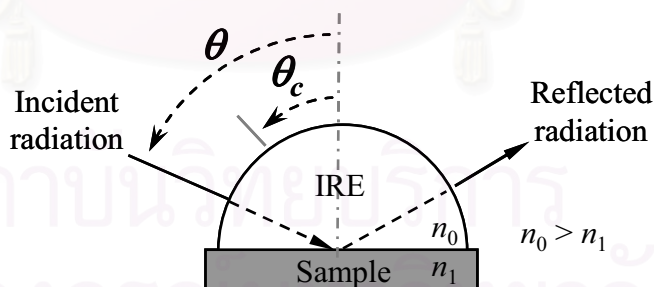


Figure 3.9 Schematic illustration of conventional ATR with a hemispherical Ge IRE.

3.3.2 Experimental Procedure using the Homemade μ ATR Accessories

The automotive paints with different colors of coated on metal substrate were obtained from general coating binder supplied by Nippon paint (Thailand). Both of the metal-contact surface and the air-contact surface of paint chip were analyzed. For the metal-contact surface of paint chip, the automotive paint was separated from the metal substrate by a *thermal shock technique*. The paint coated metal was immersed in liquid nitrogen reservoir for few seconds. Paint chip was peeled off from metal substrate by adhesive tape and then was analyzed. The air-contact surface of paint chip was directly analyzed from paint coated on metal substrate.

All ATR spectra were collected by a ContinuumTM infrared microscope attached to the Nicolet 6700 FT-IR spectrometer. For both homemade μ ATR accessories, the automotive paint chip was placed on the microscope stage. An analyzed sampling position on the surface was selected through a built-in objective. The slide-on μ IRE was slid into the position of the slide-on housing and locked by the knob at the same position where sampling surface coincides with the focal point. The aperture size of the infrared radiation was set at $150 \times 150 \mu\text{m}^2$. The background spectrum was collected through μ IRE without sample contact. For spectral acquisition of samples, the microscope stage was elevated until the sample contact the tip of the IRE at sampling position.

3.4 Characterization of Multilayer Automotive Paints

3.4.1 Depth Profiling of Multilayer Automotive Paints

Experimental Procedure for the Homemade Diamond μ ATR Accessory

Depth profiling of multilayer automotive paint from different cars were studied by varying diamond penetration under a constant aperture as shown in Figure 3.10. The $5 \times 5 \text{ mm}^2$ multilayer paint fragment was placed horizontally into a sample holder without separation of paint layer.

All ATR spectra were collected by a ContinuumTM infrared microscope that attached to the Nicolet 6700 FT-IR spectrometer. The diamond μ IRE was mounted into the homemade accessory. A multilayer automotive paint was placed against the culet of diamond and then the pressure was applied. Diamond μ IRE was placed on the stage of the infrared microscope. The aperture size of the infrared radiation was set at $150 \times 150 \mu\text{m}^2$. Reflection of the incidence radiation from the table facet of diamond IRE was employed as a background spectrum. For spectral acquisition of samples, the stage of microscope was raised in order to bring sample contact to the diamond IRE. The selected sampling area must focus at the culet of diamond IRE. The obtained spectrum was subtracted by spectrum of diamond in order to obtain the characteristic absorption bands of the sample. The ATR spectra of samples were acquired. The same procedure was repeated by increasing applied pressure. The diamond penetration was controlled by revolving pressure applicator. With the increased pressure, the diamond tip penetrated deeper into the multilayer automotive paint.

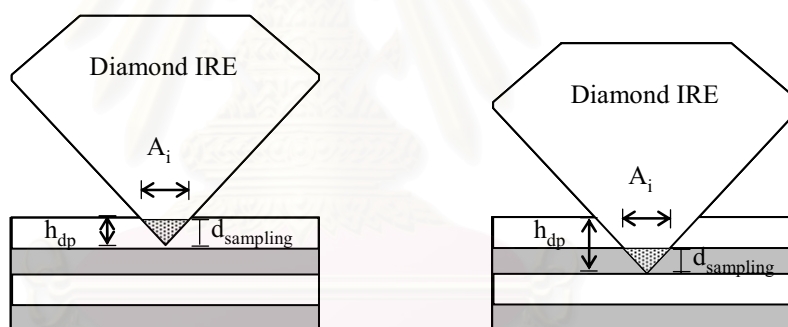


Figure 3.10 Schematic illustration of the depth profiling measurement using a diamond μ IRE. The diamond was penetrated deeper by increasing applied pressure.

3.4.2 Characterization of Individual Layer on Cross-section Surface of Multilayer Automotive Paints by the Homemade μ ATR Accessories

The multilayer automotive paint fragments from different cars were examined. Individual layer on cross-section surface of the multilayer paint fragment was measured by the slide-on diamond μ IRE and the slide-on Ge μ IRE. The paint fragment was glued on acrylic plate at a right angle and an oblique angle 30 degree.

After that the paint fragment was perpendicular cut by a razor blade, as shown in Figure 3.11.

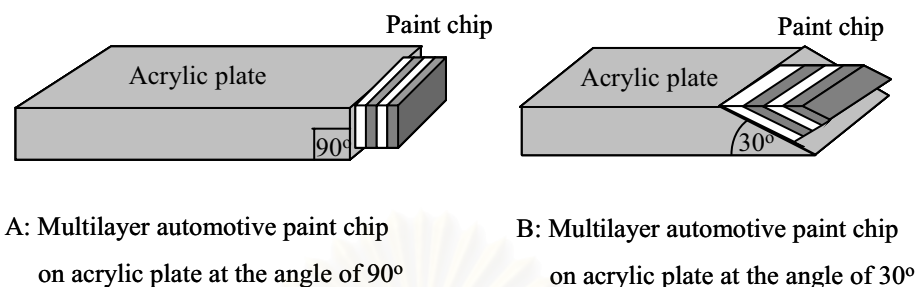


Figure 3.11 Schematic illustration of the multilayer automotive paint chip on acrylic plate at (A) the right angle of 90 degree and (B) the oblique angle 30 degree.

To collect an ATR FT-IR spectrum with the Continuum™ infrared microscope that attached to the Nicolet 6700 FT-IR spectrometer. The multilayer paint fragment stuck on an acrylic plate was placed on the microscope stage. An analyzed sampling position on the center of cross-section surface of each layer was selected through a built-in objective of infrared microscope. A slide-on IRE was slid into the position of slide-on housing and locked by the knob at the same position where sampling surface coincide with the focal point. The aperture size of the infrared radiation was set at $150 \times 150 \mu\text{m}^2$. The background spectrum was collected through IRE without sample contact. For spectral acquisition of samples, the microscope stage was elevated until the sample contacted the tip of the IRE at the selected sampling position. The sample was collected at the same degree of contact for all measurement by using a contact alert sensor plate. The microscope stage was stopped when the contract alert sensor indicated at a critical force exerted on the sensor plate. ATR FT-IR spectrum of the sample at the position of contact was collected. After the spectral acquisition was measured, the stage of microscope was lowered. The IRE was cleaned and was prepared for the next experiment.

3.4.3 Characterization of Multilayer Automotive Paints by Cross-section Surface Line Mapping

A line mapping of multilayer automotive paints can be performed due to the small contact area of the μ IRE, the non-destructive technique, and the microscope can be easily operated by automatically moving stage up and down. Fragments of multilayer automotive paint from different cars were examined without a separation layer of paint. The paint fragment was glued on an acrylic plate with an oblique angle of 30 degree and perpendicular cut to the layers by using a razor blade in order to increase the distance along the cross-section surface. Surface line mapping was measured on cross-section surface of the multilayer paint fragment.

All ATR spectra were collected by a ContinuumTM infrared microscope that attached to the Nicolet 6700 FT-IR spectrometer. The spectra were collected in mid-infrared range of 4000-650 cm^{-1} with 64 co-addition scans. The multilayer paint fragment glued on an acrylic plate was placed on the microscope stage. To create a line mapping, a line grid pattern along the thickness direction of the cross-section paint chip was pre-defined through a built-in objective. Distance of sampling positions on the surface of the cross-section paint chip can also be created from step-size. The step-size was set at 25 μm . A slide-on IRE was slid into the position of slide-on housing and locked by the knob. The aperture size of the infrared radiation was set at $150 \times 150 \mu\text{m}^2$. The background spectrum was collected through IRE without a sample. The spectral acquisitions at the defined positions were automatically controlled by the OMNICTM and AltusTM software package (Thermo Electron Corporation, Madison, WI, USA). The microscope stage was automatically raised until the paint fragment contacted the tip of the IRE. The sample was collected at the same degree of contact for all measurement by using a contact alert sensor plate. The elevation of microscope stage was stopped when the force exerted on the sensor plate and the spectra acquisition was started. After finishing acquisition, the stage of microscope was lowered and was driven to the next position by the automatic XY stage controller. The stage was automatically raised and a new spectral acquisition starting. A process was repeating until all positions of line mapping were analyzed.

3.4.4 Specular Reflection of Individual Layer on Cross-section Surface of Multilayer Automotive Paints

The multilayer automotive paint fragments were examined by specular reflection. The paint fragment was glued on an acrylic plate with an oblique angle of 30 degree and perpendicular cut to the layers by using a razor blade in order to increase the sampling area of cross-section surface. The individual paint layer on cross-section surface of the multilayer paint fragment was measured.

The specular spectra of individual layer of multilayer automotive paint were collected by the ContinuumTM infrared microscope that attached to the Nicolet 6700 FT-IR spectrometer. The microscope was operated in the reflectance mode. Reflection with normal incidence from a gold mirror was employed as a background spectrum. For spectral acquisition of samples, the multilayer paint fragment stuck on acrylic plate was placed on the microscope stage. A sampling spot on the cross section surface was selected through a built-in objective of microscope. The aperture size of the infrared radiation was set depending on the thickness of the layer of paint fragment. The incident infrared radiation was focused at a sample surface by adjusting the stage of the microscope. The infrared radiation was coupled to the surface of sample by a built-in 15X Cassegrainian objective. The specularly reflected radiation was collected by the same objective while the observed spectrum was expressed in reflectance unit. Since the observed specular reflection spectrum exhibits the reflective index type feature, the result spectrum was transformed into an absorption-type spectrum by Kramers-Kronig (KK) transformation. The transformation process was easily performed by a built-in subroutine in the OMNICTM software.

3.5 Characterization of Thin Trace Smear on Automotive Paints by the Homemade μ ATR Accessories

In a car accident case, two cars were damaged. Most paint fragments were in form of the abrasive smear that cannot separate them. Thin trace smear on automotive paint was analyzed by the slide-on diamond μ IRE and slide-on Ge μ IRE. From the real accident case, the blue BMW car was hit by another unknown car. The thin black trace was smeared on a damaged blue car. Both of the blue BMW paint chip (blue

paint support) referred to known sample and the black trace smear referred to unknown sample were determined.

All ATR spectra were collected by a Continuum™ infrared microscope that attached to the Nicolet 6700 FT-IR spectrometer. The automotive paint chip was placed on the microscope stage. A sampling position on the surface was selected through a built-in objective and then the paint support and the thin trace smear sample were analyzed. A slide-on μ IRE was slid into the position of the slide-on housing and locked by the knob. The aperture size of the infrared radiation was set at $150 \times 150 \mu\text{m}^2$. The background spectrum was collected through IRE without sample contact. For spectral acquisition of samples, the microscope stage was raised until the sample contacted the tip of the IRE at sampling position. The ATR spectral were acquired at the same position where sampling surface coincided with the focal point.



สถาบันวิทยบริการ
จุฬาลงกรณ์มหาวิทยาลัย

CHAPTER IV

RESULTS AND DISCUSSION

4.1 Characterization of Automotive Paints

4.1.1 Efficiency of Conventional ATR and Homemade μ ATR Accessories

Automotive paints of different colors and shades coated on metal substrate were analyzed by three techniques: conventional ATR with hemispherical Ge IRE, slide-on diamond μ IRE, and slide-on Ge μ IRE. The ATR FT-IR spectra of a blue paint acquired by those three techniques were shown in Figure 4.1.

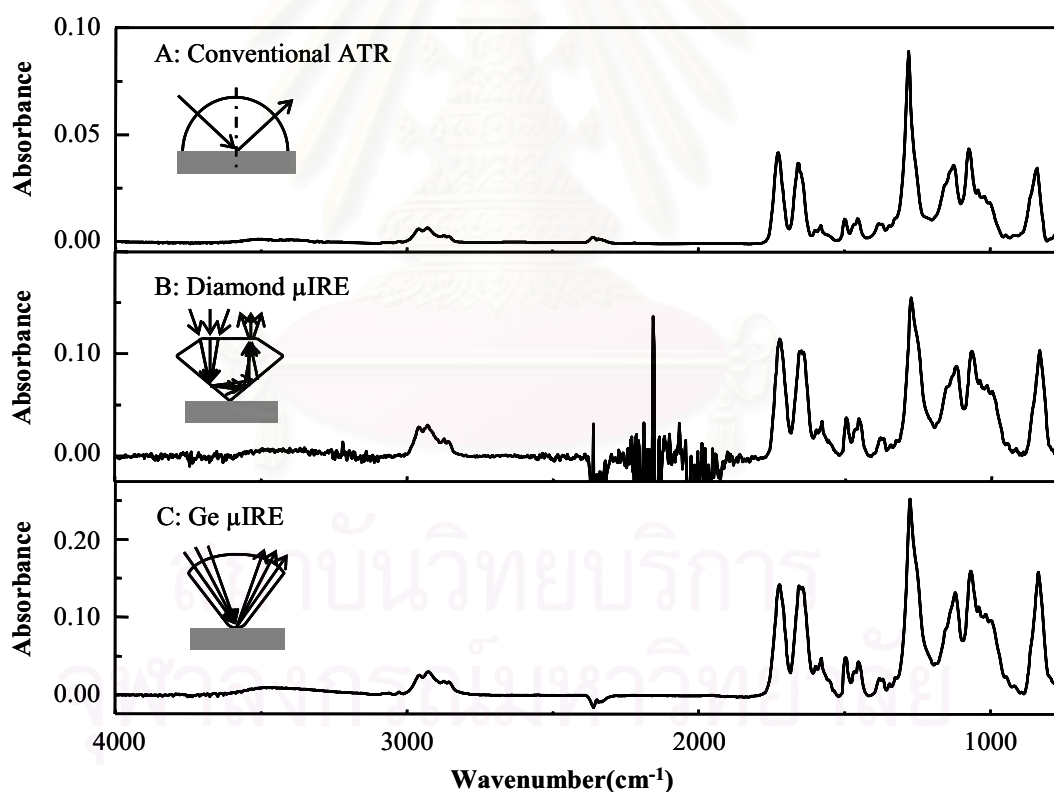


Figure 4.1 ATR FT-IR spectra of a blue automotive paint acquired by three sampling techniques: (A) conventional ATR using hemispherical Ge IRE (30° angle of incidence), (B) the slide-on diamond μ IRE, and (C) the slide-on Ge μ IRE.

The spectra of all techniques were identical. However, the relative absorbance of slide-on diamond μ IRE, and slide-on Ge μ IRE were higher than that of the conventional ATR. This is due to a better contact between the μ IRE and the sample. The ATR FT-IR spectrum acquired by the slide-on diamond μ IRE showed high noise level at 2400-1900 cm^{-1} due to the over absorption in the two-phonon region of the diamond. However, it did not affect the analysis of automotive paint since most of the organic material and polymer do not have an absorption band in this region.

Figure 4.2, 4.3, and 4.4, respectively, showed ATR FT-IR spectra of 17 different colors and shades of automotive paints acquired by the conventional ATR with hemispherical Ge IRE, the slide-on diamond μ IRE, and the slide-on Ge μ IRE. The paints were non-metallic paints (gray D, white, yellow A, yellow B, red A, red B, orange, green A, green B, blue A, blue B, blue D and black) and metallic paints (gray A, gray B, gray C and blue C). The outside surface (air-contact surface) of the paints was directly analyzed as the paints coated on metal plate. Since the metal substrate may destroy the surface of hemispherical Ge IRE, the conventional ATR cannot be employed for the spectral acquisition of the air-contact surface. Thus the paint was separated from the metal substrate by adhesive tape in order to analyze the paint surface attached to the metal. The slide-on diamond μ IRE and the slide-on Ge μ IRE were employed for direct analysis of the paint coated on metal plate without an additional sample preparation. The gray D paint was not analyzed by conventional ATR because it could not be separated from the metal substrate by adhesive tape. The obtained spectra from the slide-on diamond μ IRE lost chemical information in the region 2400-1900 cm^{-1} due to the saturated absorption of diamond in that region. The homemade slide-on diamond μ IRE and slide-on Ge μ IRE were employed for the analyses of the paint chip without interference of substrate. The major advantage of the homemade slide-on diamond μ IRE and slide-on Ge μ IRE was the small tip that can create a good contact with the sample. The conventional ATR with hemispherical Ge IRE has 5 x 5 mm^2 sampling area while the homemade slide-on IREs have sampling area of 30 μm diameter for the slide-on diamond μ IRE and less than 100 μm diameter for the slide-on Ge μ IRE. In addition, sample for the analysis with the conventional ATR was constrained by the sample holder. The sample must have a width less than 2 cm. in order to be able to fit into the sample holder. The analysis by

both μ IREs did not have a constraint on the sample size, a large sample can be placed on the stage of microscope.

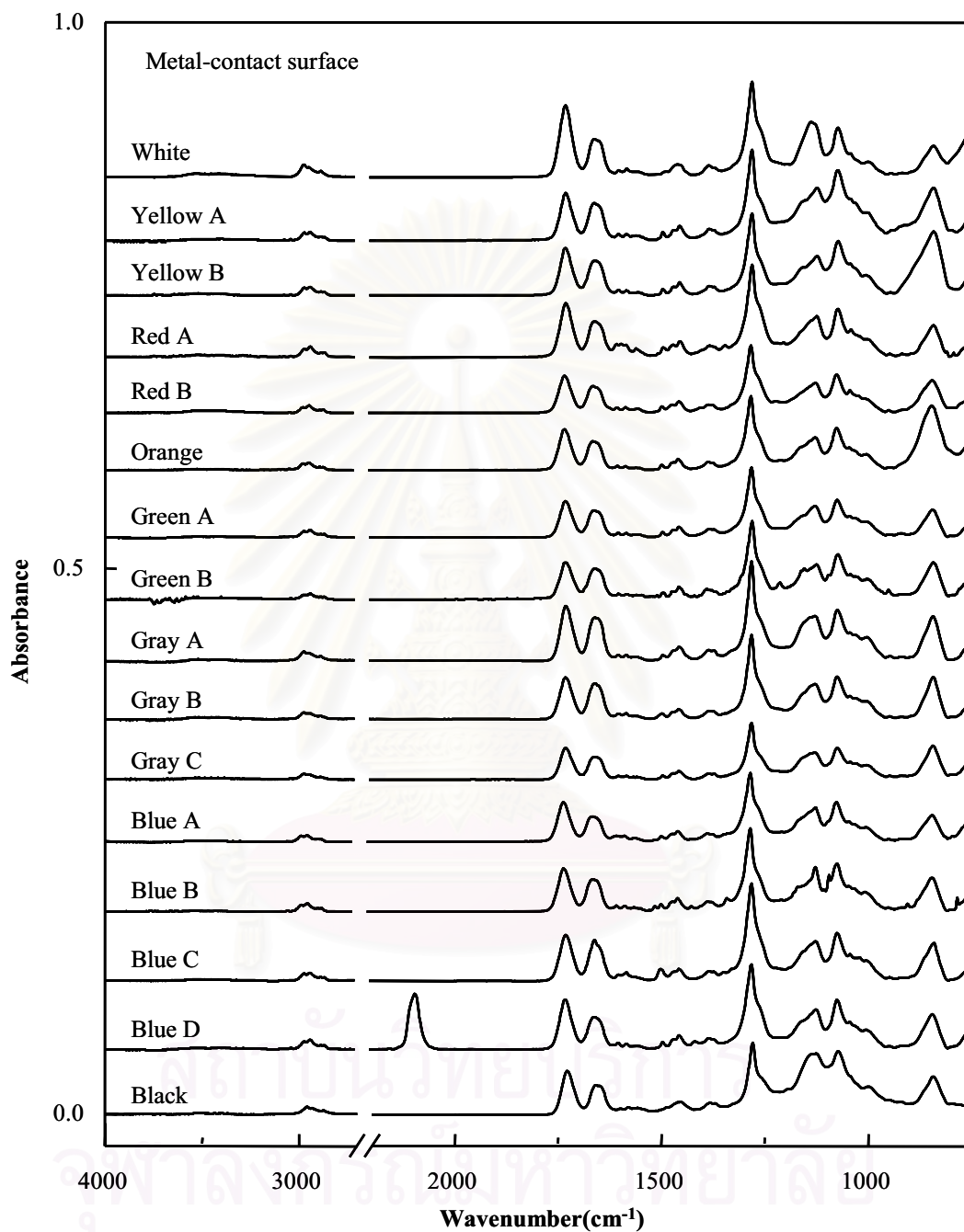


Figure 4.2 ATR FT-IR spectra of the metal-contact surface of 17 different colors and shades of automotive paints acquired by conventional ATR using hemispherical Ge IRE.

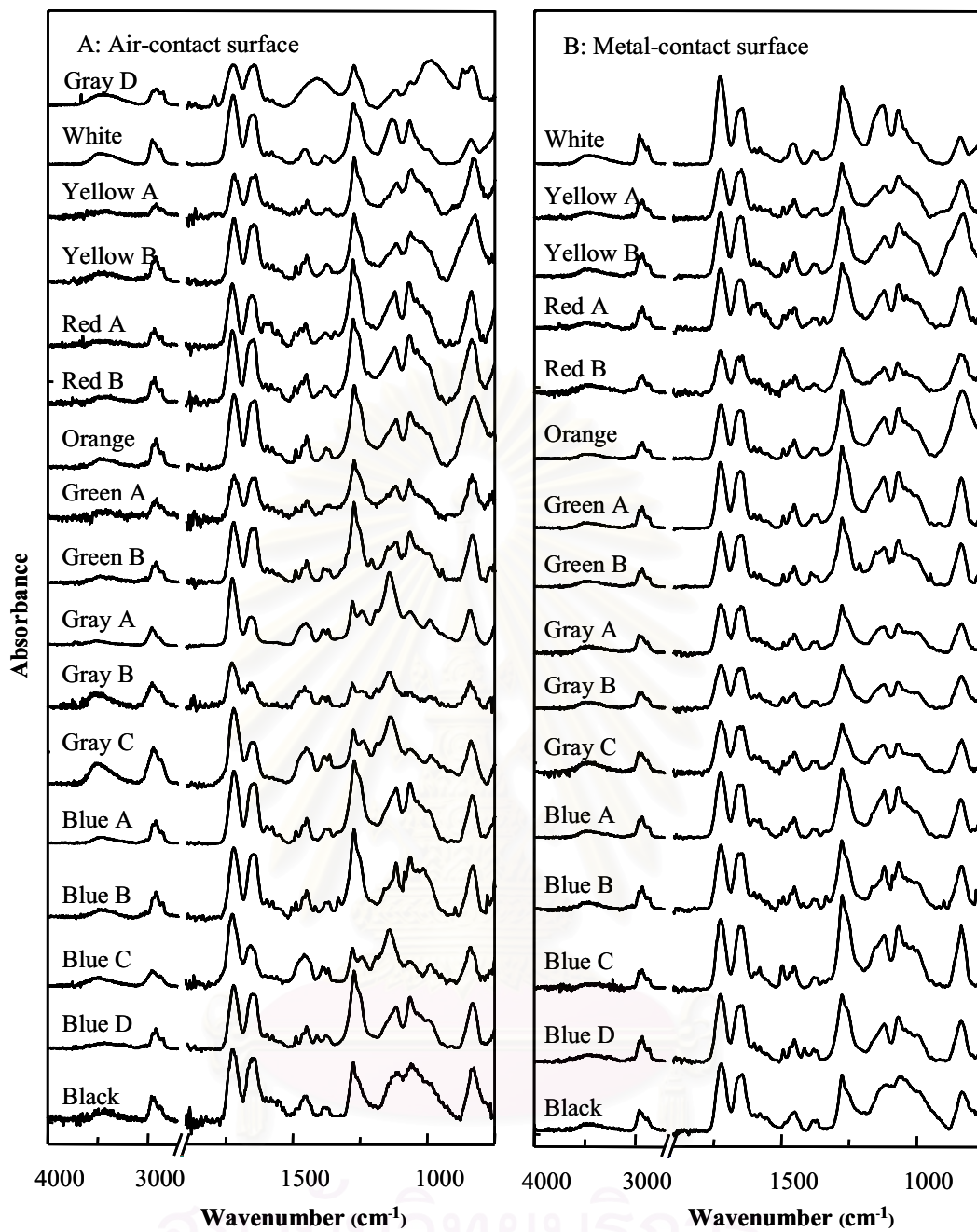


Figure 4.3 ATR FT-IR spectra of (A) the air-contact surface and (B) the metal-contact surface of 17 automotive paints acquired by the slide-on diamond μ IRE.

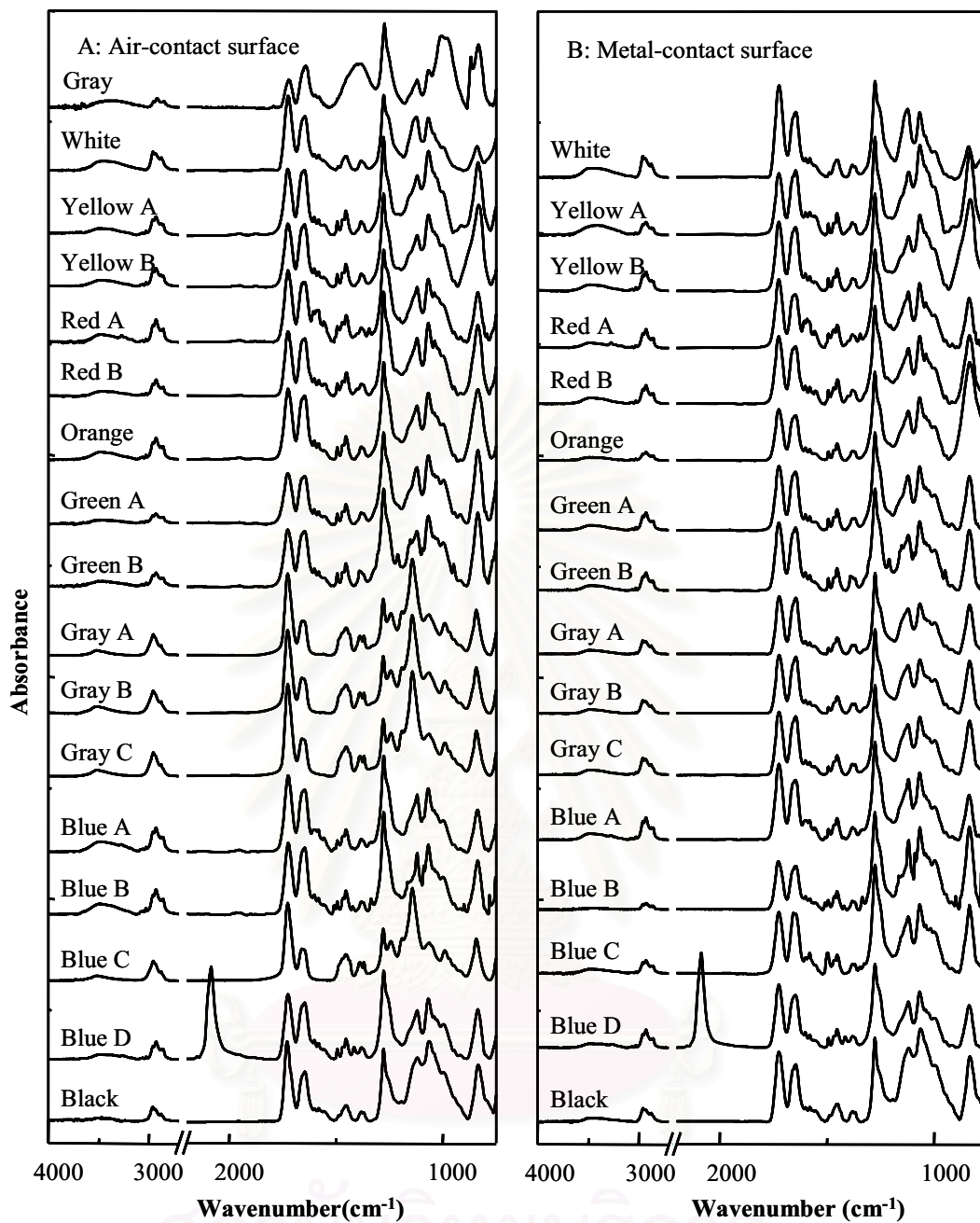


Figure 4.4 ATR FT-IR spectra of (A) the air-contact surface and (B) the metal-contact surface of 17 automotive paints acquired by the slide-on Ge μ IRE.

4.1.2 Classification of Automotive Paints by FT-IR Spectra

From the spectra acquired by the slide-on Ge μ IRE shown in Figure 4.4, the spectrum of blue D showed a unique absorption feature of cyano $C\equiv N$ stretching band at 2086 cm^{-1} of the Prussian blue pigment. This easily indicated that the blue D

containing the Prussian blue pigment as a dark blue color pigment. From the observed spectrum, most of the paints can be distinguished by their chemical information derived from the observed ATR FT-IR spectra.

Figure 4.5 showed the ATR FT-IR spectra of the outside surface (air-contact surface) and the inside surface (metal-contact surface) of a non-metallic paint (blue B) and metallic paint (gray B). The ATR FT-IR spectra of the air-contact surface and metal-contact surface of all non-metallic paints indicated that they were alkyd nitrocellulose. Nitrocellulose is characterized by strong bands at 1658 cm^{-1} (asymmetric $-\text{NO}_2$ stretching), 1278 cm^{-1} (symmetric $-\text{NO}_2$ stretching), and 842 cm^{-1} (N-O stretching). The absorption band at 3080 , 3060 , and 3028 cm^{-1} are the characteristic of C-H stretching vibration of aromatic in alkyd resin. The absorption bands of C=C stretching vibration occurred at 1601 and 1580 cm^{-1} . The bands at 1730 , 1119 , and 1070 cm^{-1} are the absorptions of C=O, C-O-C, and C-O, stretching vibration, respectively. A summary of the ATR spectral assignments of alkyd nitrocellulose is presented in Table 4.1. The ATR FT-IR spectra of the metal-contact surface of the metallic paint indicated that it was alkyd nitrocellulose. However, the observed spectrum indicated that the air-contact surface of the metallic paints was acrylic nitrocellulose. The observed spectrum of acrylic nitrocellulose shows typical absorption bands of nitrocellulose at 1658 , 1278 , and 842 cm^{-1} . The absorption band at 1450 cm^{-1} is due to the CH deformations. The absorption band at 1242 cm^{-1} is attributed to C-O-C stretching. The band at 1061 cm^{-1} is ascribed to O-CH₂ stretching. A summary of the ATR spectral assignments of acrylic nitrocellulose is presented in Table 4.2. Identification of acrylic nitrocellulose and alkyd nitrocellulose can be easily noticed the absorption bands of aromatic in alkyd nitrocellulose structure at $3000\text{-}3100\text{ cm}^{-1}$ and $1600\text{-}1580\text{ cm}^{-1}$. The metallic paints have a shiny metal flakes imbedded in the clear acrylic nitrocellulose top coat.

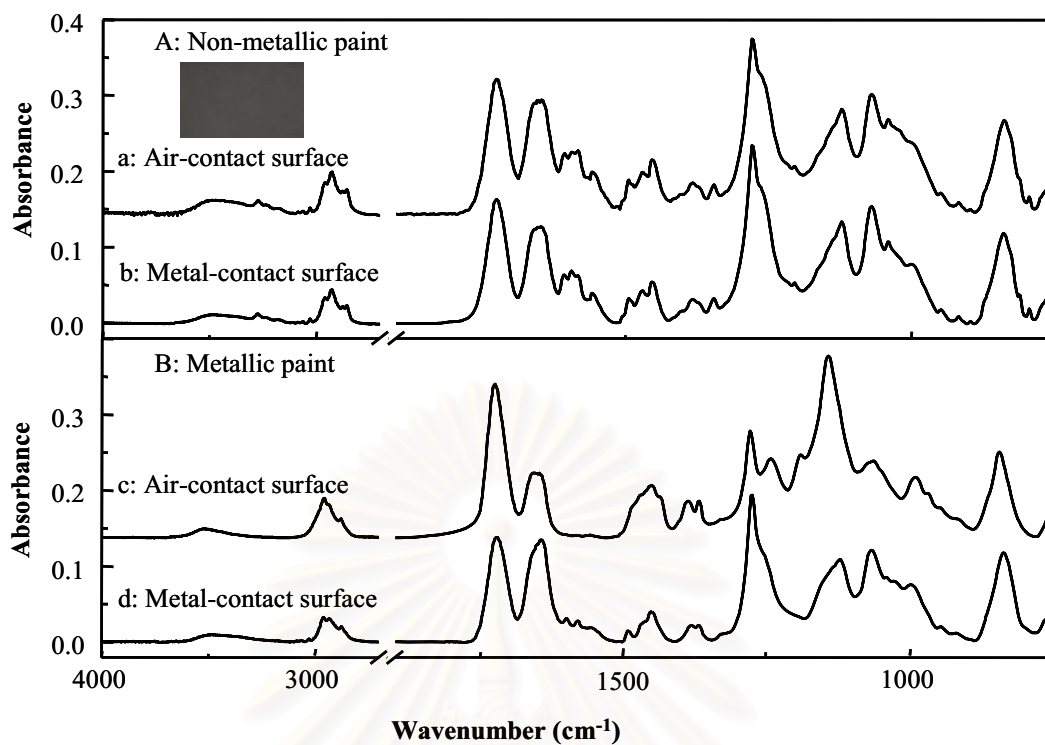


Figure 4.5 Comparison of both surfaces of (A) non-metallic paint and (B) metallic paint. The spectra were acquired by the Ge slide-on IRE.

Table 4.1 Peak assignments of alkyd nitrocellulose.

Wavenumber (cm ⁻¹)	Functional group
3500-3300	O-H stretching
3080,3060,3028	C-H stretching of aromatic
2957	asymmetric C-H stretching of -CH ₃
2926	asymmetric C-H stretching of -CH ₂
2873	symmetric C-H stretching of -CH ₃
2855	symmetric C-H stretching of -CH ₂
1730	C=O stretching
1659	asymmetric -NO ₂ stretching
1601	C=C stretching
1580	C=C stretching
1495	out of plane CH ₂ deformation
1452	out of plane CH ₃ deformation
1400	O-CH ₂ wagging
1385	in of plane CH ₃ deformation
1367	CH ₃ deformation
1275	symmetric -NO ₂ stretching
1250	C-C-O stretching
1119	C-O-C stretching
1070	C-O stretching
1038	O-CH ₂ stretching
839	N-O stretching

Table 4.2 Peak assignments of acrylic nitrocellulose.

Wavenumber (cm ⁻¹)	Functional group
3500-3300	O-H stretching
2954	asymmetric C-H stretching of -CH ₃
2928	asymmetric C-H stretching of -CH ₂
2875	symmetric C-H stretching of -CH ₃
2857	symmetric C-H stretching of -CH ₂
1730	C=O stretching
1658	asymmetric -NO ₂ stretching
1480	out of plane CH ₂ deformation
1450	out of plane CH ₃ deformation
1392	O-CH ₂ wagging
1368	CH ₃ deformation
1278	symmetric -NO ₂ stretching
1242	C-C-O stretching
1190	(O=)C-O stretching
1145	C-O-C stretching
1061	O-CH ₂ stretching
842	N-O stretching

สถาบันวิทยบริการ
จุฬาลงกรณ์มหาวิทยาลัย

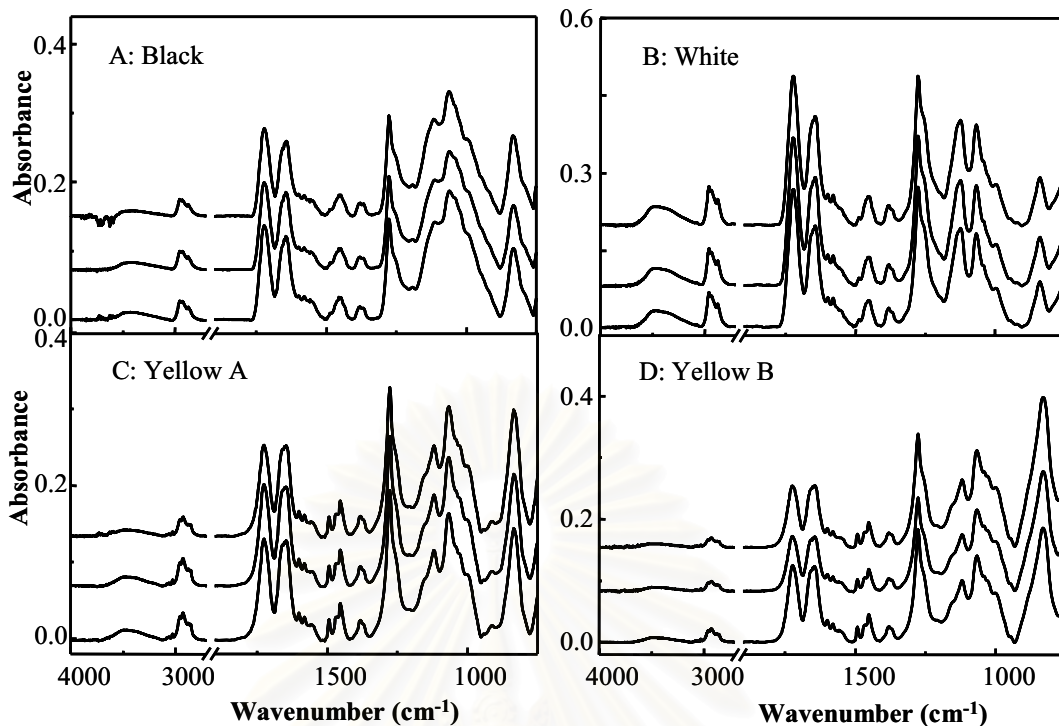


Figure 4.6 Reproducibility of the spectra acquired by the slide-on Ge μ IRE. All spectra were collected in triplicate: (A) black, (B) white, (C) yellow A, and (D) yellow B.

The reproducibility and repeatability of ATR FT-IR spectra acquired by the slide-on Ge μ IRE were shown in Figure 4.6. All spectra were collected at different positions on the surface of the coated metal substrates. The observed spectra indicated that the re-collected spectra were identical in the first spectrum taken. Each paints showed unique spectral features. As a result, paint chips with similar or the same color can be differentiated based on the observed ATR FT-IR spectra.

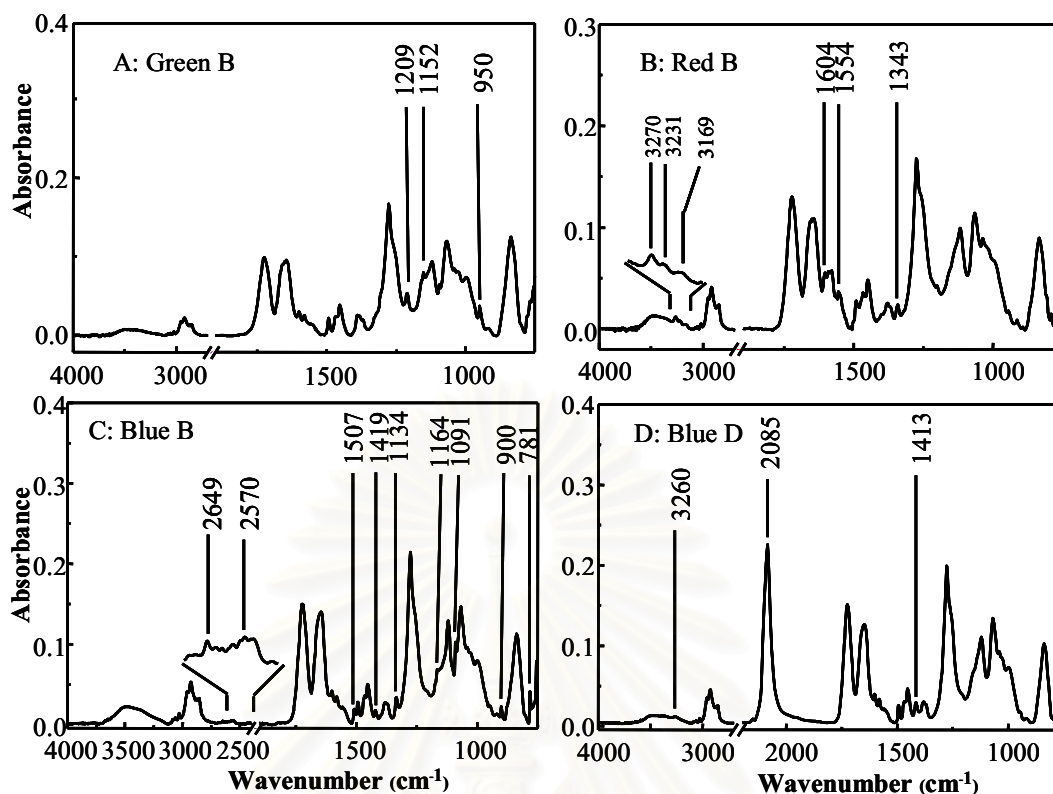


Figure 4.7 Observed spectra of (A) green B, (B) red A, (C) blue B and (D) blue D acquired from the slide-on Ge μ IRE.

The spectra in Figure 4.7 show the characteristic absorption bands of paint. The observed spectra show weak band that maybe contribute to the pigment in the paint. The weak bands of the observed spectra were compared with the infrared database of pigment to identify which the pigment was used in paint. Table 4.3 showed major absorption bands of coloring pigments for automotive paints from infrared reference spectra. The identification of coloring pigment maybe interfered by the binder and extender pigment having higher concentration compared with the coloring pigment. The observed spectrum of green B non-metallic alkyd nitrocellulose enamel (A) show peak at 1209, 1152 and 920 cm^{-1} that contributed to absorption bands of phthalocyanine green pigment as shown in Table 4.3. Phthalocyanine green contains cyanine functional group. The spectrum of red B non-metallic alkyd nitrocellulose enamel (B) shows weak band at 3270, 3231, 3169, 1604, 1554 and 1343 cm^{-1} appearing to be contributed by quinacridone red pigment. Quinacridone red composes of C=O and N-H functional group. The ATR spectrum of blue B non-metallic alkyd nitrocellulose enamel (C) which contains a phthalocyanine blue pigment that indicated the weak band at 2649, 2570, 1507, 1419, 1134, 1164, 1191, 900 and 781

cm^{-1} . Phthalocyanine blue contains cyanine functional group. The ATR spectrum of blue B non-metallic alkyd nitrocellulose enamel (D) showed peak at 3260, 2085 and 1413 cm^{-1} indicating that the same as major absorption bands of the Prussian blue pigment. Prussian blue has $\text{C}\equiv\text{N}$ stretching band at 2086 cm^{-1} of cyano functional group.

Table 4.3 Major absorption bands of coloring pigments in automotive paints.

Chemical name	Pigment	Wavenumber (cm^{-1})
Copper (II) chlorophthalocyanine ($\text{Cu}(\text{C}_{32}\text{H}_{16}\text{ClN}_8)$)	Phthalocyanine green	1615
		1497
		1391
		1308
		1211
		1152
		949
5,12-Dihydro-quinol[2,3-b] acridine-7,14-dione ($\text{C}_{20}\text{H}_{12}\text{N}_2\text{O}_2$)	Quinacridone red	3270
		3228
		3168
		1604
		1583
		1551
		1479
1342		
Iron (III) hexacyanoferrate (II) ($\text{Fe}_4[\text{Fe}(\text{CN})_6]_3$)	Prussian blue	3250
		2089
		1412

Table 4.3 (continued) Major absorption bands of coloring pigments for automotive paints.

Chemical name	Pigment	Wavenumber (cm ⁻¹)
Copper (II) phthalocyanine (Cu(C ₃₂ H ₁₆ N ₈))	Phthalocyanine blue	3450
		2645
		2572
		1611
		1506
		1419
		1333
		1165
		1120
		1093
		900
870		
Titanium (IV) dioxide (TiO ₂)	Rutile	750
	Anatase	610 (rutile)
		450 (rutile)
		640 (anatase)
		515 (anatase)
		395 (anatase)
Calcium phosphate (Ca ₃ (PO ₄) ₂)	Bone black or	1087
	Ivory black	1035

Two paint chips with the same binder can be distinguished based on pigments and additives. Nitrocellulose with acrylic or alkyd modified was favored in repainted finish coating. Besides the nitrocellulose binder, the automotive paints have several binder types (such as acrylic enamel, alkyd enamel, acrylic melamine enamel, alkyd melamine enamel, polyester melamine enamel, alkyd urea enamel, acrylic urethane enamel, epoxy resin). The major absorption bands of common binders for automotive paints were shown in Table 4.3. The information in this Table was supported from

prior research that analyzing about automotive paint. In next part, we use the major absorption bands in this Table to identify types of binder.

Table 4.4 Major absorption bands of common binders in automotive paints.

Binder type	Wavenumber (cm ⁻¹)	Functional group
Acrylic enamel	1730	C=O stretching
	1270	C-O stretching
	1240	C-C-O stretching
	1150	C-O-C stretching
	1070	O-CH ₂ stretching
	840	CH ₂ twisting
Alkyd enamel	1730	C=O stretching
	1450	CH ₂ deformation
	1270	C-O stretching
	1120	O-CH ₂ stretching
	1070	C-O stretching (phthalate)
	740	CH ₂ rocking
Nitrocellulose lacquer	1650	asymmetric -NO ₂ stretching
	1280	symmetric -NO ₂ stretching
	840	N-O stretching
Acrylic melamine enamel	1730	C=O stretching
	1550	C-N stretching
	1480	CH ₂ deformation
	1370	in plane CH ₃ deformation
	1270	C-O stretching
	1240	C-C-O stretching
	1170	C-O-C stretching
	1090	O-CH ₂ stretching
	815	Out of plane C-H bending

Table 4.4 (continued) Major absorption bands of common binders in automotive paints.

Binder type	Wavenumber (cm ⁻¹)	Functional group
Alkyd melamine enamel	1730	C=O stretching
	1550	C-N stretching
	1270	C-O stretching
	1120	O-CH ₂ stretching
	1070	C-O stretching (phthalate)
	815	Out of plane C-H bending
	740	CH ₂ rocking
Polyester melamine enamel	1730	C=O stretching
	1550	C-N stretching
	1300	CH ₂ wagging
	1240	C-O stretching
	815	Out of plane C-H bending
	750	CH ₂ rocking
Alkyd urea enamel	1730	C=O stretching
	1650	C=O stretching (urea)
	1540	C-N stretching
	1270	C-O stretching
	1120	O-CH ₂ stretching
	1070	C-O stretching (phthalate)
	740	CH ₂ rocking
Acrylic urethane enamel	1730	C=O stretching
	1530-1520	C-N stretching
	1240	C-O stretching
	1180-1150	C-N stretching
	1070	O-CH ₂ stretching
Epoxy resin	1510	Out of plane C-H bending in p-substituted aromatic ring
	830	In plane C-H wagging

Some paints had the same binder but different pigments (both extender pigment and coloring pigment). Table 4.5 showed major absorption bands of common extender pigments for automotive paints. The information in this Table was supported from previously research and can be employing for examining the kind of extender pigments in automotive paints. The extender pigments may have the same chemical formula but different crystalline forms. Usually, the extender pigment used to modify gloss, texture, and opacity of the paint.

Table 4.5 Major absorption bands of common extender pigments in automotive paints.

Chemical name	Extender	Wavenumber (cm ⁻¹)
Calcium carbonate (CaCO ₃)	Calcite	1440 (broad)
	Limestone	875
	Aragonite	715
Calcium sulfate (CaSO ₄)	Gypsum or	1120 (broad)
	Calcium sulfate	1160
	anhydrite	675 and 600
Barium sulfate (BaSO ₄)	Barytes	1120 (broad)
		1180
		980
Aluminum silicate (Al ₂ SiO ₅)	Kaolin (clay) Bentonite	1040 and 1010 (broad)
		1105
		910
Magnesium silicate (3MgO.4SiO ₂ .H ₂ O)	Talc	1019 (broad)
		670
Potassium aluminum silicate (KAl ₃ Si O ₄) ₃	Mica	1030 (broad)
Calcium silicate (Ca ₂ SiO ₄)	Wollastonite Synthetic calcium silicate	1020 and 1090 (broad)
		920 (multiple band)
Silicon dioxide (SiO ₂)	Quartz	1100 (broad)
	Diatomaceous earth	
	Synthetic silica	

The ATR FT-IR spectra can be employed for the identification and distinguishing between the different colors and shades of automotive paints. This is due to the fact that the observed infrared spectra are directly associated chemical structure and composition of the paint. Each paint has its own unique infrared absorption pattern. The two homemade μ ATR accessories, the slide-on diamond μ IRE and the slide-on Ge μ IRE can be employed for the paint chip characterization. This technique does not require an additional sample preparation.

4.2 Characterization of Multilayer Automotive Paints

4.2.1 Depth Profiling of Multilayer Automotive Paints

Depth profiling of multilayer automotive paints were determined by the homemade diamond μ ATR accessory. The diamond was able to penetrate into the multilayer paint fragment by pressing the sample against the diamond. By performing controlled penetration of the culet of diamond through the sample and/or illuminating the pavilion facet near the culet with constant aperture sizes, spectral information of a specific layer at a certain distance from the surface can be selectively collected. The illuminated portion of the diamond tip near the culet can be adjusted via the opening aperture of the focusing optics. Thus, only parts of the material attached to the diamond IRE at the illuminated pavilion facet interact with the coupled radiation and have contribution in the observed spectrum.

Figure 4.8 showed the depth profiling ATR FT-IR spectra of two-layered paint from silver gray car bumper. To classify type of binder in each single layer, major absorption bands of common binders (Table 4.4) and flowchart of infrared classification for automotive paint (Figure 11. in Appendices) were used. At the smallest applied pressure the spectra indicated acrylic urethane clear coat. Acrylic urethane is characterized by absorption bands at 1723 cm^{-1} (C=O stretching), 1522 cm^{-1} (C-N stretching), 1240 cm^{-1} (C-O stretching), and 1070 cm^{-1} (O-CH₂ stretching). At the greater applied pressure and deep penetration, the absorption band magnitudes of acrylic urethane are decreased while the new bands appeared. The appearances of the new bands revealed the spectral feature of alkyd urea enamel and talc. The observed spectra show typical absorption bands of alkyd urea at 1724 cm^{-1} (C=O

stretching of acrylic), 1650 cm^{-1} (C=O stretching of urea), 1540 cm^{-1} (C-N stretching), 1276 cm^{-1} (C-O stretching), 1120 cm^{-1} (O-CH₂ stretching), and 1070 cm^{-1} (C-O stretching). The strong absorption band at 1019 cm^{-1} is the characteristic of Si-O-Si stretching vibration of talc that is the extender pigment. The observed spectra indicated that the diamond μ IRE can detect the change of spectral feature from acrylic urethane to the alkyd urea enamel as the diamond tip penetrated deeper into the silver gray bumper fragment.

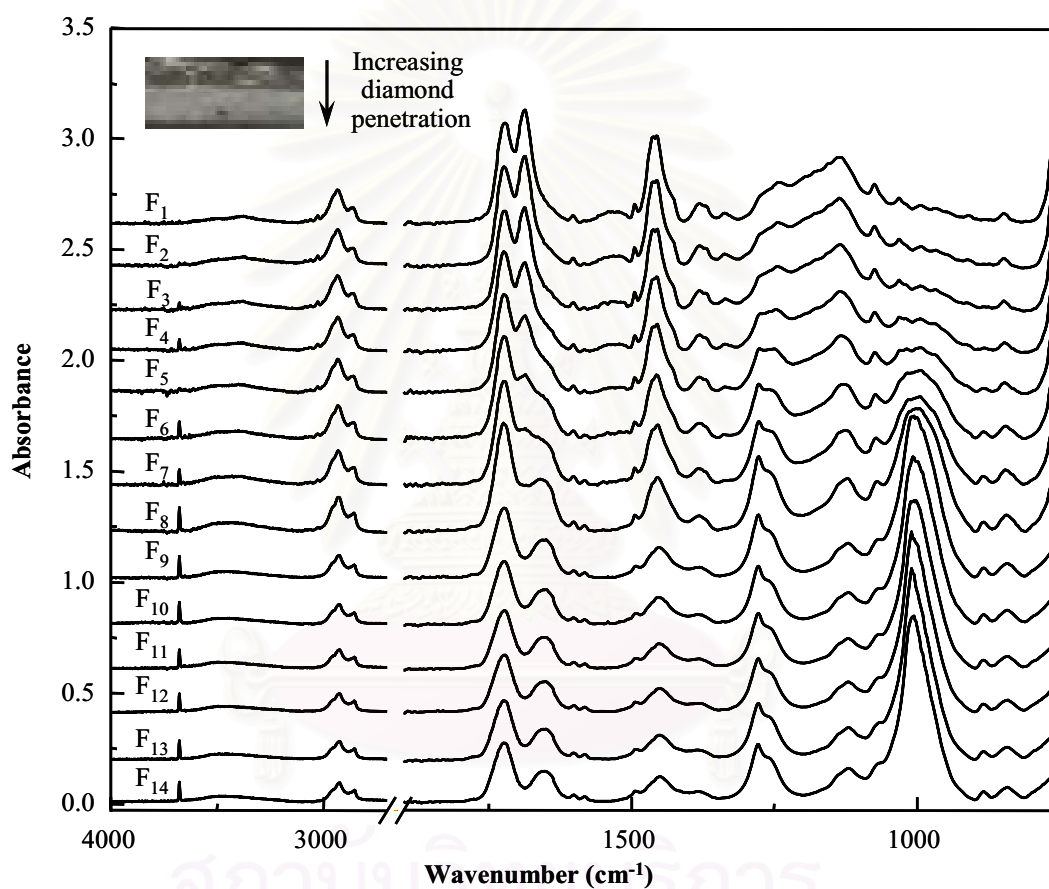


Figure 4.8 ATR spectra of a multilayer silver gray paint from a car bumper. The spectra acquired as the diamond tip penetrate deep into the multilayer paint chip. F₁ indicated the shallowest diamond penetration which F₁₄ indicated the deeper diamond penetration.

Figure 4.9 showed the ATR spectra of an eight-layered paint chip from a gray car hood. The chemical information of the multilayer paint was observed as the diamond penetrated deeper into multilayer paint chip. The observed spectra indicated that the top coat was acrylic urethane clear coat. When diamond penetration deeper,

the spectra were not changed. All observed spectra showed the same spectral feature. As the diamond tip penetrated deeper, the brittle paint fragment was broken. As a result, the diamond tip did not have any contact with other layers.

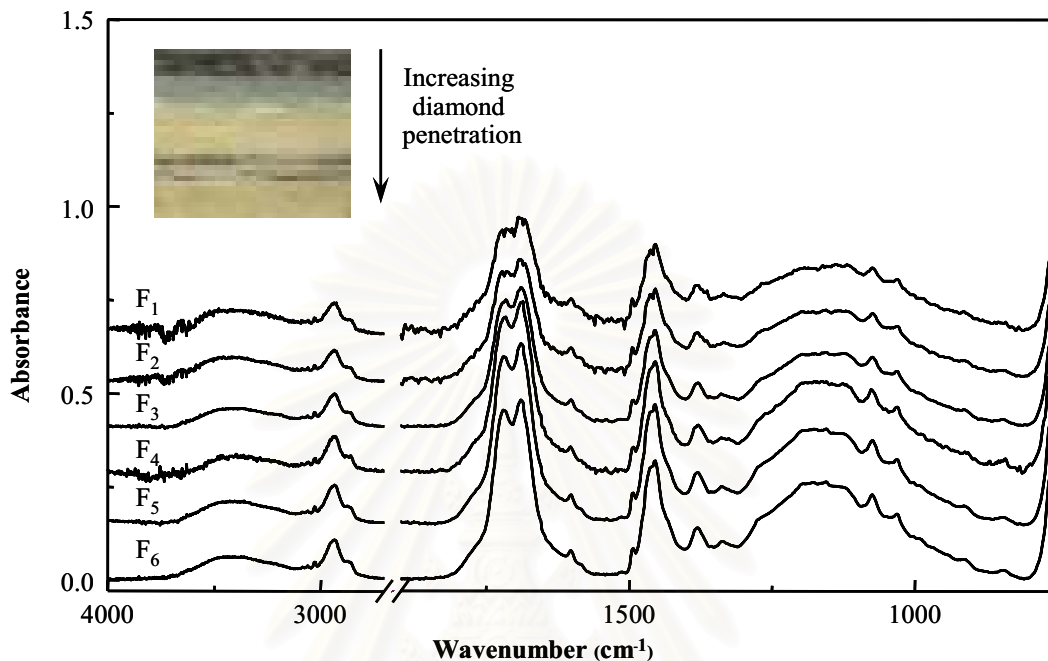


Figure 4.9 ATR spectra of a multilayer gray paint from a car hood. The spectra acquired as the diamond tip penetrate deep into the multilayer paint chip. F₁ indicated the shallowest diamond penetration which F₆ indicated the deeper diamond penetration.

Figure 4.10 showed ATR spectra of a thirteen-layered paint chip from a blue car door. The chemical information of the multilayer paint was observed as the diamond penetrated deeper into multilayer paint chip. The observed spectra indicated that the top layer was acrylic urethane clear coat. At deeper diamond penetration depth, the spectra did not change. All observed spectra showed the same spectral feature. Due to the diamond tip did not penetrate into another layer. Because the tough polymer top coat flowed with the diamond tip so the top coat is obstructed the lower layer from making a contact with the diamond tip.

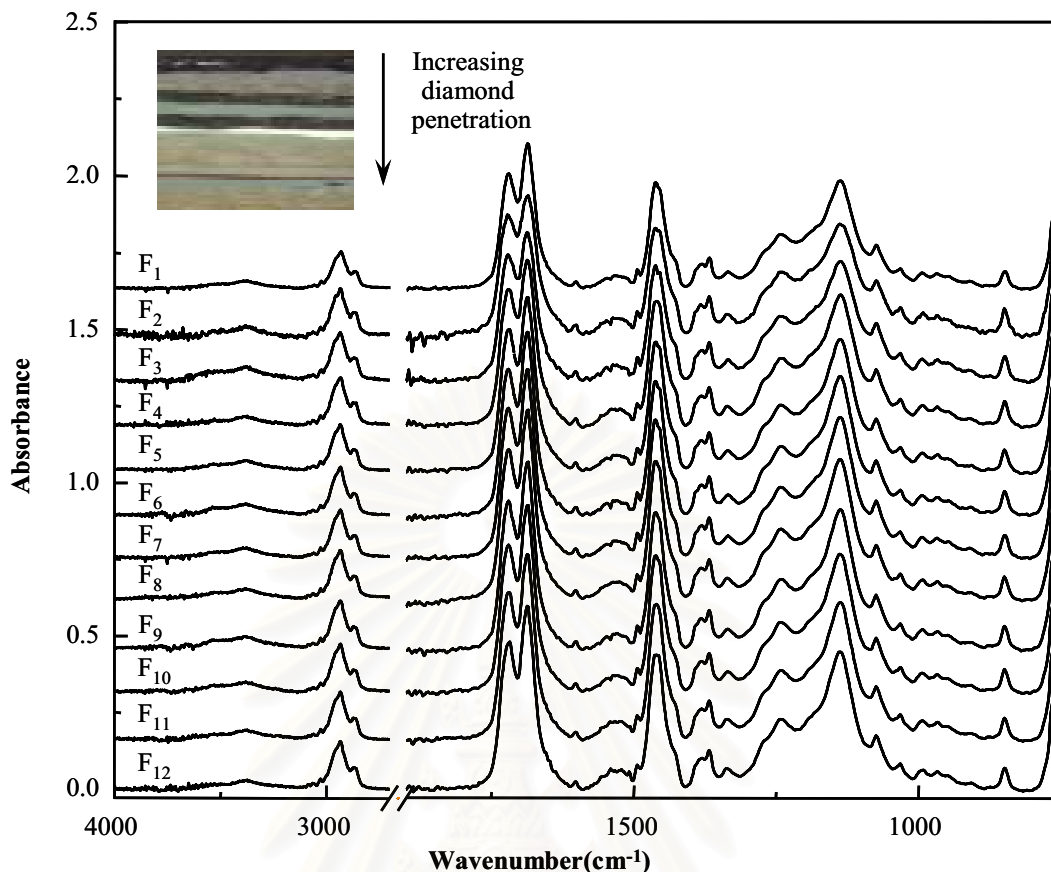


Figure 4.10 ATR spectra of a multilayer blue paint from a car door. The spectra acquired as the diamond tip penetrate deep into the multilayer paint chip. F_1 indicated the shallowest diamond penetration which F_{12} indicated the deeper diamond penetration.

Figure 4.11 showed ATR spectra of a three-layered paint from a white Mitsubishi fender. The chemical information of the multilayer paint was observed as the diamond penetrated deeper into multilayer paint chip. The observed spectra indicated that the top layer was acrylic urethane clear coat. When diamond penetration deeper, the spectra were not changed. All observed spectra showed the same spectral feature. Due to the diamond tip did not penetrate into another layer, the tough top coat deformed and flowed with the pavilion of diamond. As a result, the diamond tip did not have any contact with other layers.

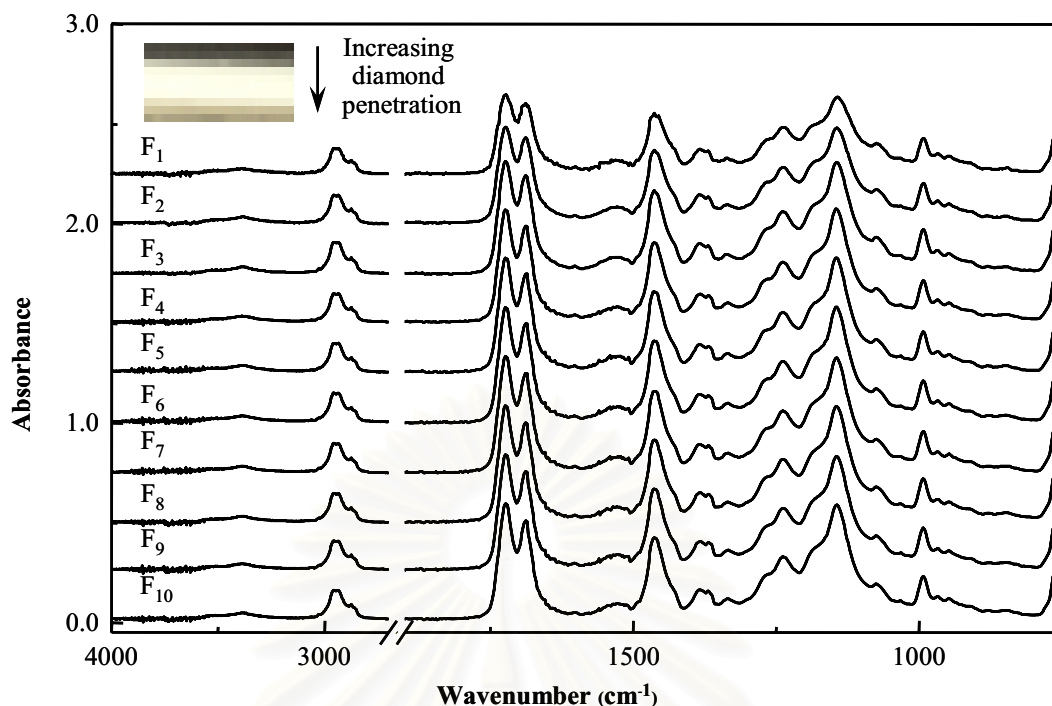


Figure 4.11 ATR spectra of a multilayer white paint from a Mitsubishi fender. The spectra acquired as the diamond tip penetrate deep into the multilayer paint chip. F_1 indicated the shallowest diamond penetration which F_{10} indicated the deeper diamond penetration.

This result suggested that the diamond μ IRE is not suitable to apply for depth profiling analysis of brittle sample or tough top coat. However, the spectra acquired from the top coat of different cars indicated that difference.

4.2.2 Characterization of Individual Layer on Cross-section of Multilayer Automotive Paints by the Homemade μ ATR Accessories

ATR FT-IR spectra of a multilayer paint were acquired at the center of an individual layers. The paint chips were razorblade cut with a right angle (90 degree) and an oblique angle (30 degree) in order to increase the distance along the cross-section surface. By simply placing the culet of the diamond μ IRE or the tip of the Ge μ IRE on the analyzed surface, ATR FT-IR spectra of the contact surface were acquired.

The two-layered paint chip was obtained from silver gray car bumper. ATR spectra of a multilayer automotive paint were acquired by an individual layer

measurement. The typical result in Figure 4.12 shows that the paint chip is razor blade cut with a right angle (90 degree) and Figure 4.13 that the paint chip is razor blade cut with an oblique angle (30 degree) in order to increase the area along the cross-section surface from $\sim 80 \mu\text{m}$ to $\sim 170 \mu\text{m}$ (as shown in insert of Figure 4.12 and Figure 4.13, respectively). The spectra of both original sampling area and increased sampling area were the same due to sampling area of the slide-on diamond μIRE and the slide-on Ge μIRE are smaller than area of each layer on cross-section surface. The analysis started with the first layer from air-contact surface. From the acquired spectra, the first layer of paint chip was acrylic urethane enamel and the second layer was alkyd urea enamel with high concentration of talc. The observation of the acquired spectra in Figure 4.12 and 4.13 was in agreement with the spectra acquired by depth profiling measurement (Figure 4.8). The spectra acquired by the slide-on diamond μIRE and the slide-on Ge μIRE were slightly different due to the inherent differences of both IREs. The peak shape and relative peak intensity were slightly different since both IREs difference in the optical constant and the angle of incidence at the contact surface. However, all the peak positions were the same.

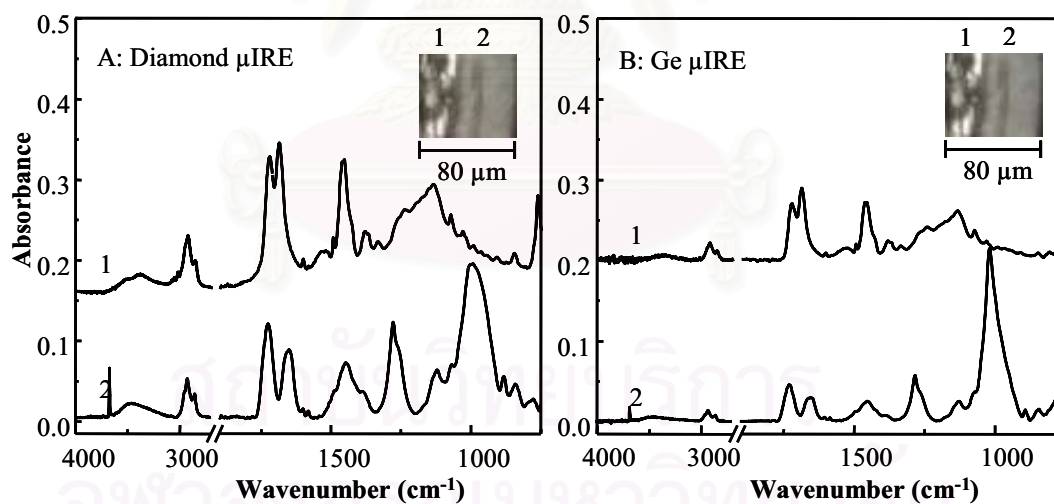


Figure 4.12 ATR spectra of a two-layered paint chip from a bumper of a silver gray car that was razor blade cut with a right angle (90 degree) acquired by (A) the slide-on diamond μIRE and (B) the slide-on Ge μIRE .

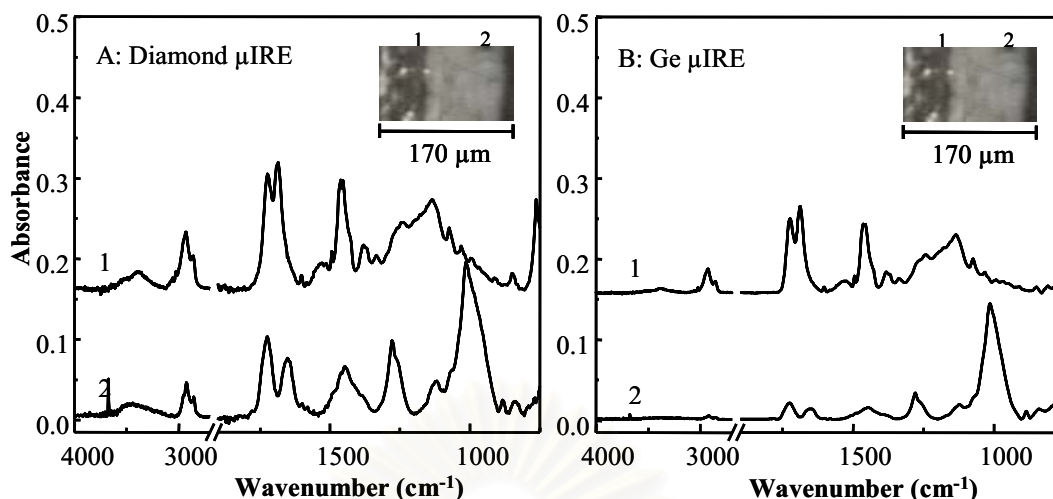


Figure 4.13 ATR spectra of a two-layered paint chip from a bumper of a silver gray car that was razor blade cut with an oblique angle (30 degree) acquired by (A) the slide-on diamond μ IRE and (B) the slide-on Ge μ IRE.

Figure 4.14 and Figure 4.15, respectively showed ATR FT-IR spectra of each layer on cross-section surface of an eight-layered paint chip that obtained from gray car hood. The distance along cross-section surface increased from $\sim 500 \mu\text{m}$ (by razorblade cut with an angle 90 degree) to $\sim 1050 \mu\text{m}$ (by inclining cut at 30 degree). The spectra No. 1, 2, 3, and 8 of both original sampling area and increased sampling area were the same due to sampling area of the slide-on diamond μ IRE and the slide-on Ge μ IRE are smaller than area of each layer on cross-section surface of paint chip. But the spectra No. 4, 5, 6, and 7 of both original sampling area and increased sampling area were slightly different due to area of each layer on cross-section surface of paint chip are smaller than sampling area of the slide-on diamond μ IRE and the slide-on Ge μ IRE. Those spectra were interfered from near layer. From the first layer, the paint chip consisted of acrylic urethane enamel (layer 1), alkyd urea enamel (layer 2), alkyd primer (layer 3), acrylic enamel (layer 4), alkyd urea enamel (layer 5-7) and alkyd primer (layer 8), respectively. Although the optical images of the layer 5, 6 and 7 showed different colors, the observed spectra showed that they were made of the same matrix. But sixth layer may have a red pigment that cannot present in infrared absorbance. The acquired spectra from the first layer in Figure 4.14 and 4.15 were in agreement with the top coat spectrum acquired by depth profiling measurement (Figure 4.9). The spectra acquired by the slide-on diamond μ IRE and

the slide-on Ge μ IRE were slightly different due to the inherent differences of both IREs.

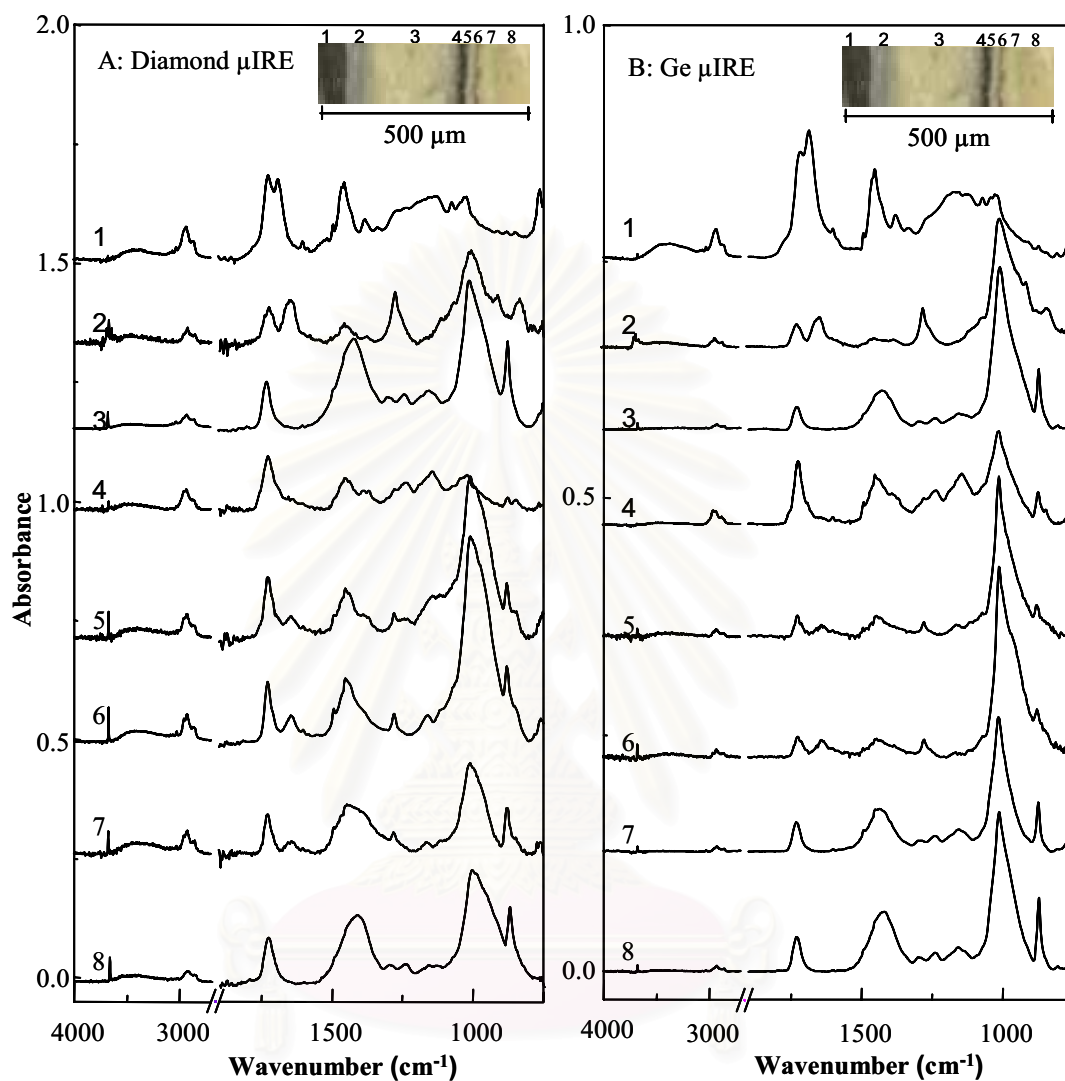


Figure 4.14 ATR spectra of an eight-layered paint chip from a hood of a gray car that was razor blade cut with a right angle (90 degree) acquired by (A) the slide-on diamond μ IRE and (B) the slide-on Ge μ IRE.

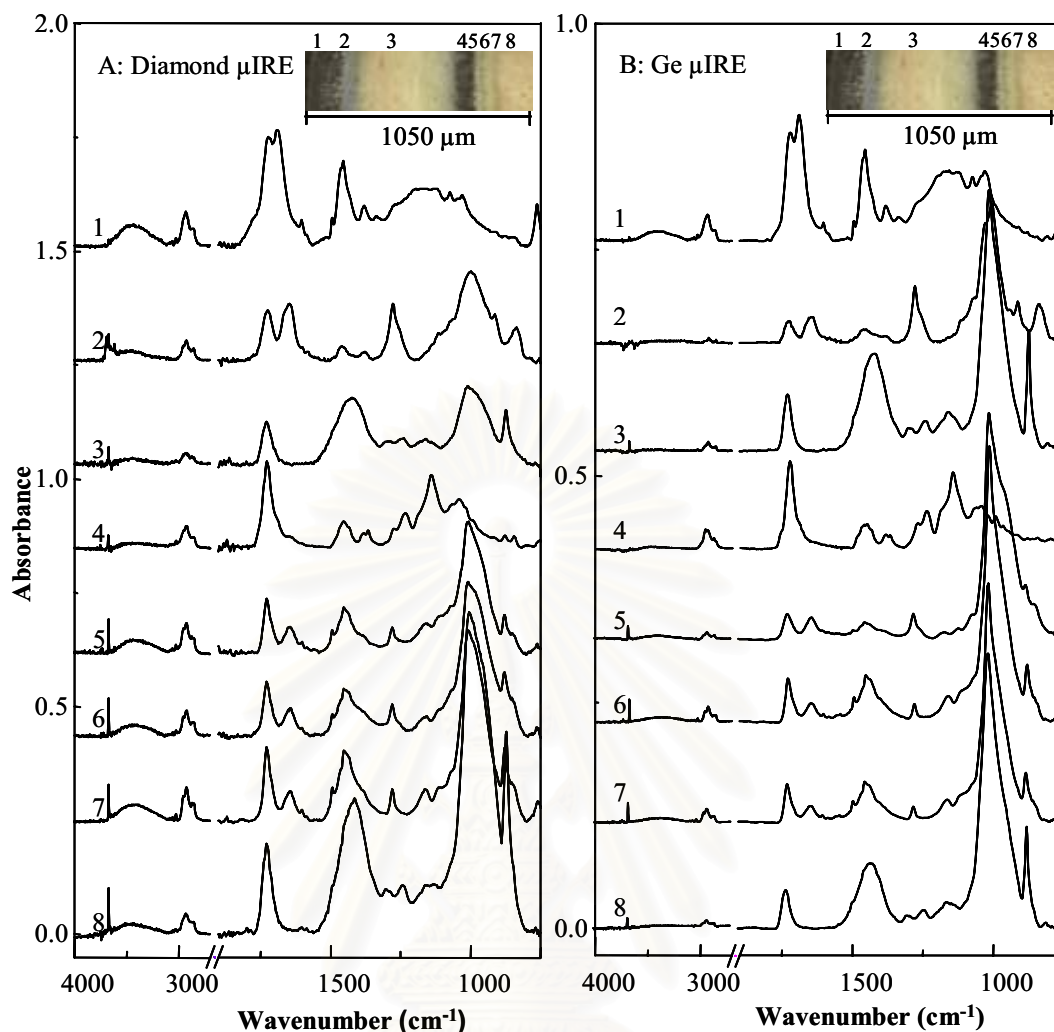


Figure 4.15 ATR spectra of an eight-layered paint chip from a gray car hood that was razor blade cut with an oblique angle (30 degree) acquired by (A) the slide-on diamond μ IRE and (B) the slide-on Ge μ IRE.

Figure 4.16 showed the ATR FT-IR spectra of each layer on cross-section surface of a thirteen-layered paint chip that obtained from a blue car door. The distance along cross-section surface that increased from $\sim 1071 \mu\text{m}$ to $\sim 2468 \mu\text{m}$ by razorblade cut with an oblique angle at 30 degree. The thickness of each layer was not equal. For thin layer, the analyzed position could be selected since the homemade μ IREs had small sampling area. From the first layer, the paint chip consisted of acrylic urethane enamel (layer 1), alkyd urea enamel (layer 2), alkyd primer (layer 3), acrylic enamel (layer 4), alkyd urea enamel (layer 5), acrylic enamel (layer 6), alkyd nitrocellulose (layer 7), alkyd urea enamel (layer 8), alkyd primer (layer 9), alkyd urea enamel (layer 10-12), and alkyd primer (layer 13), respectively. Although some layers were difficult to be differentiated, the optical images shown that the first layer were

chemically different from the forth layer and the sixth layer. The layers 10, 11 and 12 were the different colors via optical images, the observed spectra clearly shown that they had the same composition. Layer 10 was difference in intensity at 1647 cm^{-1} , 880 cm^{-1} , and 838 cm^{-1} , this was due to the absorption was interfered by the layer 9.

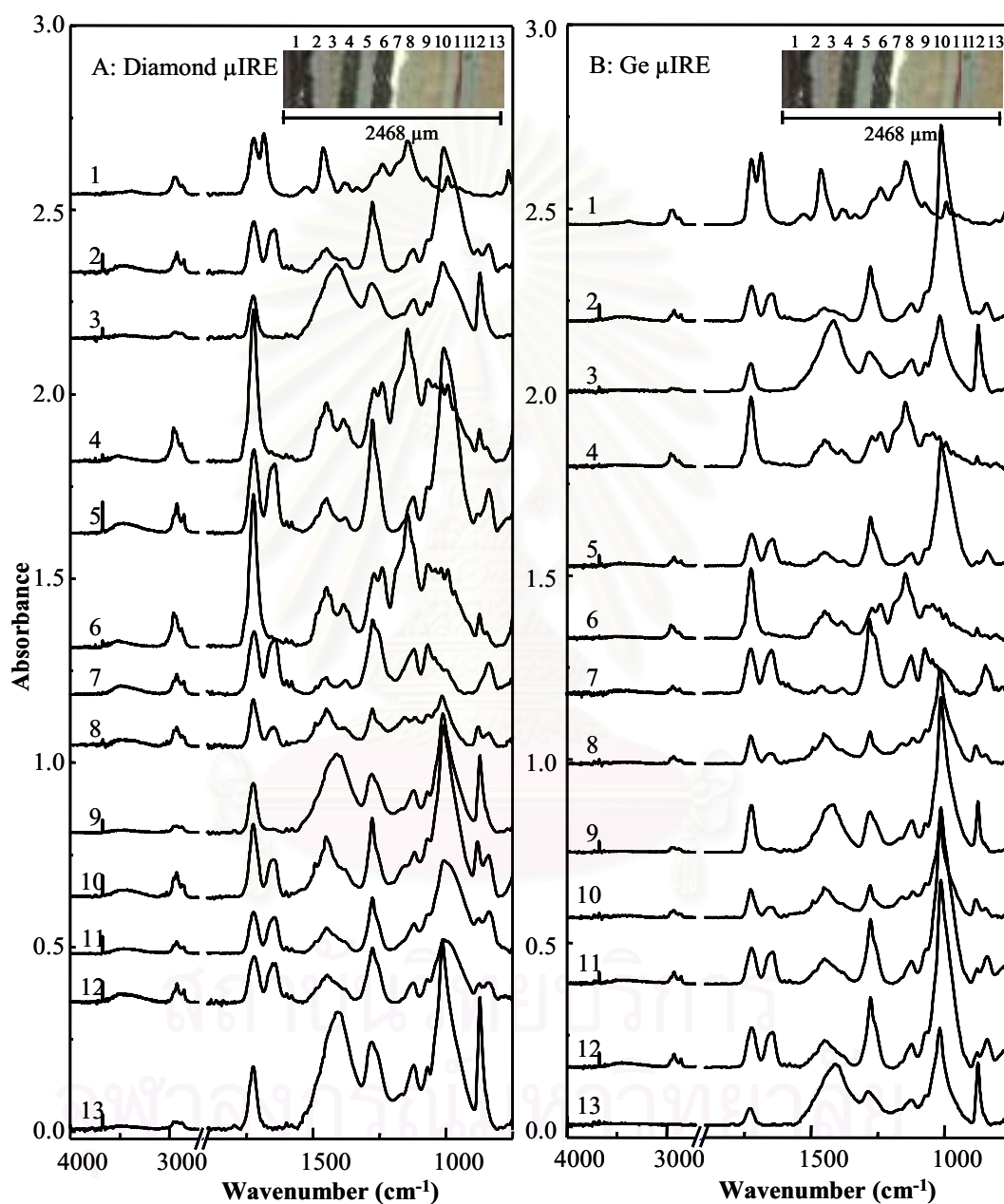


Figure 4.16 ATR spectra of a thirteen-layered paint chip from a blue car door that was razorblade cut with an oblique angle (30 degree) acquired by (A) the slide-on diamond μ IRE and (B) the slide-on Ge μ IRE.

Figure 4.17 showed ATR FT-IR spectra of a three-layered paint chip by analyzing an individual layer on cross-section surface. The paint fragment obtained from a black Toyota Fortuner bumper that was inclined cut at 30 degree in order to increase the distance along cross-section surface from $\sim 140 \mu\text{m}$ (original thickness) to $\sim 270 \mu\text{m}$. ATR FT-IR spectra of surface that the culet of the diamond μIRE or the tip of the Ge μIRE contact on the center of individual on cross-section surface were acquired. Starting the first layer from the air-contact surface to the end layer showed in spectrum No.1 to spectrum No.3, respectively. The chemical information from spectrum No.1 indicated that the first layer is acrylic urethane enamel. The chemical information in spectrum No.2 indicated that the material was acrylic urethane too. The chemical information of both layers were different due to spectra feature of the first layer and the second layer were different. The spectrum No.3 showed chemical information indicated that it was polypropylene and talc that favor using in a pickup truck bumper. The characteristic absorption bands of C-H stretching in polypropylene appeared at 2949, 2918, 2867 and 2838 cm^{-1} . The absorption band at 1459 and 1376 cm^{-1} are associated to the CH_3 bending. The absorption band at 1166 cm^{-1} is related to the C-C stretching vibration.

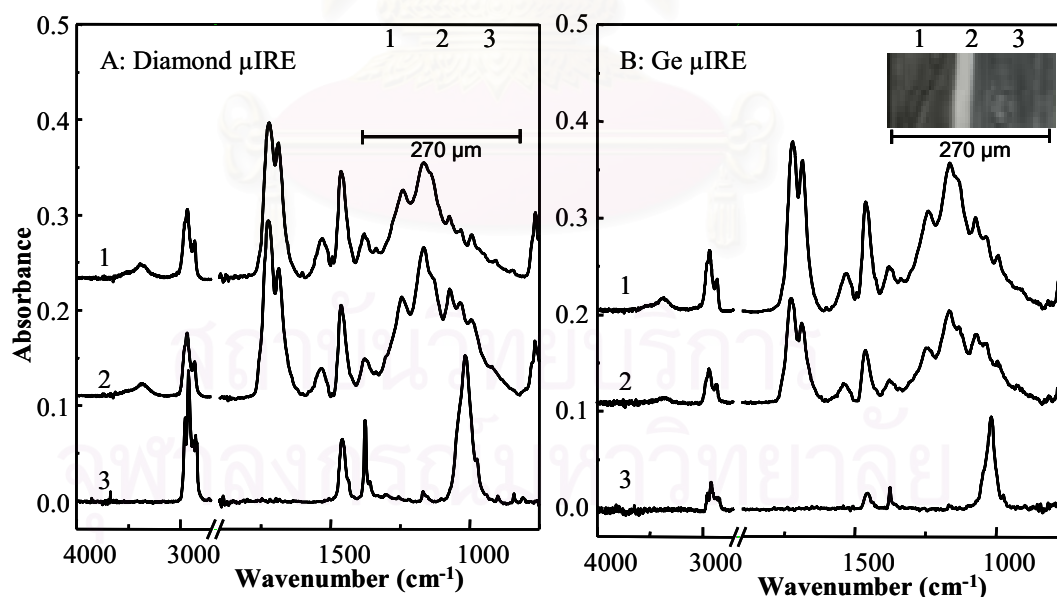


Figure 4.17 ATR spectra of a three-layered paint chip from a black Toyota Fortuner bumper that was razorblade cut with an oblique angle (30 degree) acquired by (A) the slide-on diamond μIRE and (B) the slide-on Ge μIRE .

ATR FT-IR spectra of a white three-layered paint chip from a fender of Misubitshi car by analyzing at the center of an individual layer on cross-section surface are shown in Figure 4.18. The paint fragment was inclined cut at 30 degree in order to increase the distance along cross-section surface from $\sim 300 \mu\text{m}$ (original thickness) to $\sim 500 \mu\text{m}$. ATR FT-IR spectra of surface that the culet of the diamond μIRE or the tip of the Ge μIRE contacts on the center of individual on cross-section surface were acquired. The analysis was started at the first layer from the air-contact surface. The chemical information from the first layer (spectrum No.1) indicated that the analyzed sample is acrylic urethane enamel. The second layer (spectrum No.2) showed chemical information indicated that it was acrylic urethane. Since spectra feature of the first layer and the second layer were different, the chemical information of both layer were different. The chemical information in third layer (spectrum No.3) indicated that the material was alkyd primer with high concentration of talc and calcium carbonate. The top coat spectra acquired by depth profiling (Figure 4.11) were the same in agreement from the spectra of the first layers.

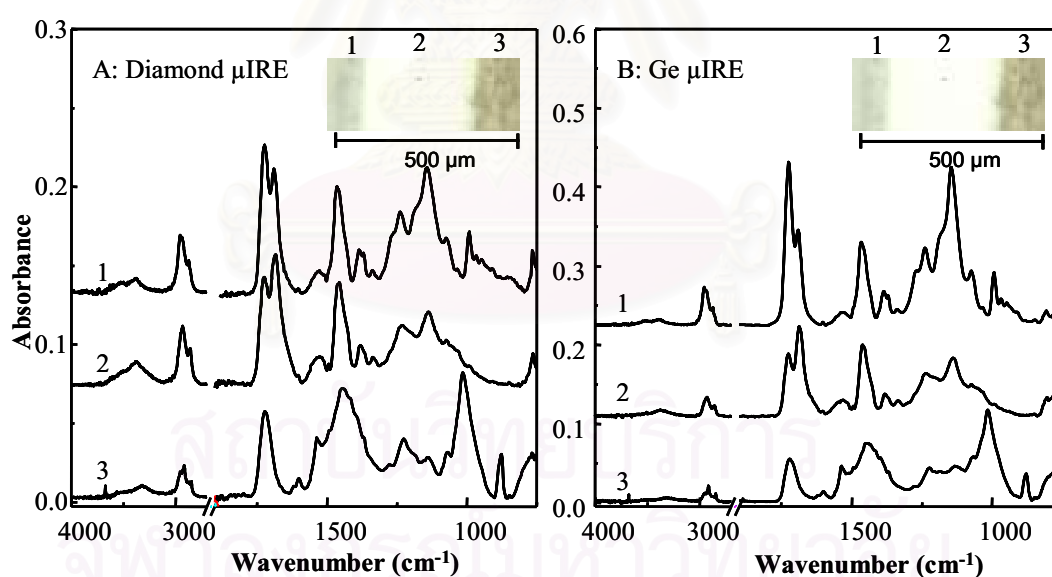


Figure 4.18 ATR spectra of a three-layered paint chip from a white Mitsubishi fender that was razorblade cut with an oblique angle (30 degree) acquired by (A) the slide-on diamond μIRE and (B) the slide-on Ge μIRE .

ATR FT-IR spectra of a blue four-layered paint chip from a door of BMW car by analyzing at the center of an individual layer on cross-section surface are shown in Figure 4.19. The paint fragment was inclined cut at 30 degree in order to increase the

distance along cross-section surface from $\sim 380 \mu\text{m}$ (original thickness) to $\sim 720 \mu\text{m}$. ATR spectra of surface that the culet of the diamond μIRE or the tip of the Ge μIRE contact on the center of individual on cross-section surface were acquired. The analysis was started at the first layer from the air-contact surface. From the first layer, the paint chip consisted of acrylic urethane enamel (layer 1), acrylic urethane with kaolin (layer 2), alkyd with kaolin extender pigment (layer 3), and alkyd primer with high concentration of talc (layer 4), respectively.

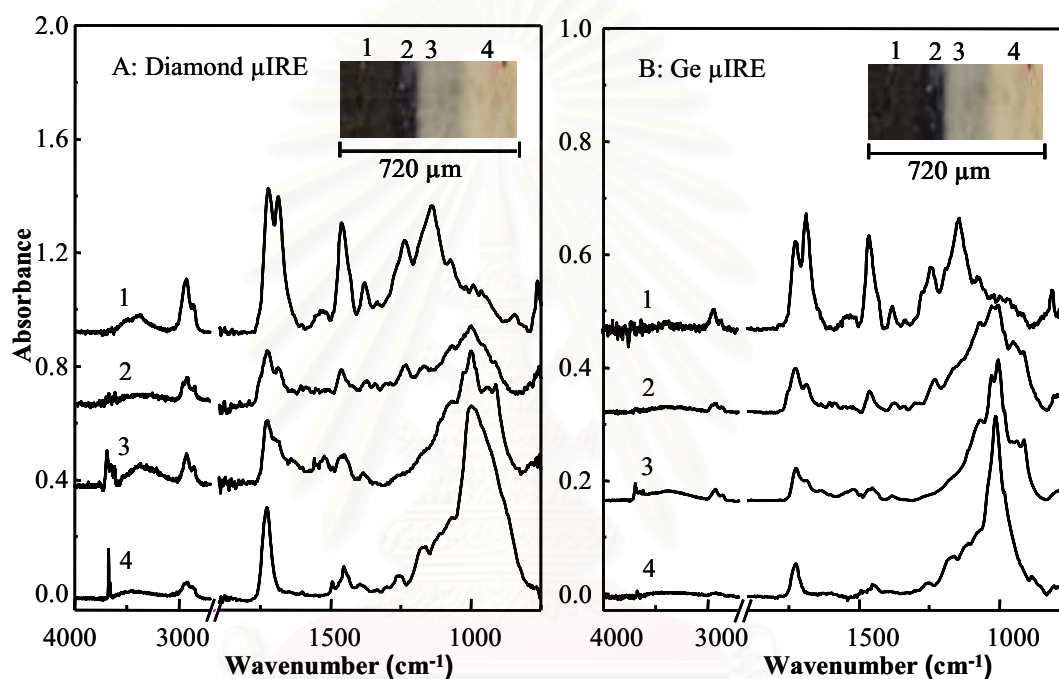


Figure 4.19 ATR spectra of a four-layered paint chip from a blue BMW door that was razorblade cut with an oblique angle (30 degree) acquired by (A) the slide-on diamond μIRE and (B) the slide-on Ge μIRE .

The slide-on diamond μIRE and the slide-on Ge μIRE can identify individual on cross-section surface of multilayer paint chips without separation layer.

4.2.3 Characterization of Multilayer Automotive Paints by Cross-section Surface Line Mapping

Since the slide-on diamond μIRE and the slide-on Ge μIRE have a small sampling area, non-destructive analysis, and the microscope stage can be easily operated by automatically moving, line mapping technique can be used to characterize

at each small point on cross-section surface of multilayer automotive paint chip. The paint chips were cut with an oblique angle at 30 degree in order to increase the distance along the cross-section surface without additional sample preparation. The line map was drawn via the built-in objective. By simply placing the culet of diamond μ IRE and the tip of the Ge μ IRE the analyzing surface, ATR FT-IR spectra of the contact surface can be easily acquired because of a relatively small step size of the line-map. The sample was collected at the same degree of contact for all measurement by using a contact alert sensor plate on the microscope stage. For all characterization of multilayer paint by surface line mapping, the slide-on diamond μ IRE and the slide-on Ge μ IRE were investigated at the same sampling area.

ATR FT-IR spectra of multilayer automotive paint acquired by slide-on diamond μ IRE and slide-on Ge μ IRE were shown in Figure 4.20 (A) and Figure 4.20 (B), respectively. The two-layered paint fragment was obtained from body kit bumper of a silver gray car. Starting from the first layer at the air-contact surface, the line map was drawn along the thickness direction of the paint chip as shown in the insert of Figure 4.20. The obtained spectra clearly revealed the spectra change from acrylic urethane layer (spectra No. 1-2) to alkyd urea and talc layer (spectra No. 4-5). The observed spectra show the thin layer of alkyd with talc and calcium carbonate (spectra No. 3) between acrylic urethane layer and alkyd urea layer. In an accident case, the real evident sample available may have interfered from near layer. Surface line mapping can clearly present the changing between two adjacent layers. The observation in Figure 4.20 showing the agreements with the spectra of an individual layer were selectively acquired at the center of the layer shown in Figure 4.13. The spectra acquired by the slide-on diamond μ IRE were slightly different from those acquired by the slide-on Ge μ IRE, especially of those of high absorption band. This is related to the inherently differences between both IREs. The differences in the optical constant and the angle of incidence at the contact surface making the peak shape and relative peak intensity are slightly different. However, the corresponding spectra show the same spectral features (i.e., peak positions and number of peaks).

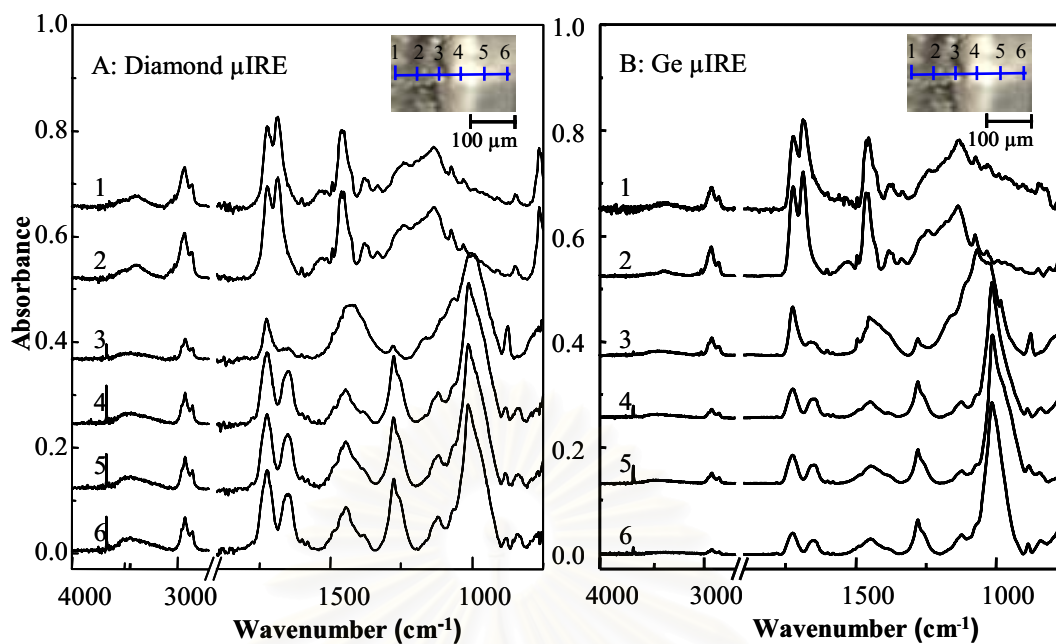


Figure 4.20 ATR spectra of a two-layered paint chip from a bumper of silver gray car acquired by (A) the slide-on diamond μ IRE and (B) the slide-on Ge μ IRE.

Figure 4.21 (A) and (B) showed the spectra acquired by the slide-on diamond μ IRE and the slide-on Ge μ IRE, respectively. The eight-layered paint chip was obtained from a hood of a gray car. Insert of Figure 21 showed line map along the thickness of the paint chip. The analysis was started from the bottom layer. The paint chip consists of acrylic urethane enamel (spectra No. 1-5), acrylic enamel (spectra No. 6-7), alkyd urea enamel (spectra No. 8-11), alkyd primer (spectra No. 12-20), acrylic enamel (spectra No. 21-22), alkyd urea enamel (spectra No. 23-26) and alkyd primer (spectra No. 27-30). The spectral feature was showing the agreement with the spectra analyzed from each layer as shown in Figure 4.15. The obtained spectra and the optical image showed the first layer of acrylic urethane was consisted of a thin layer of acrylic enamel (spectra No. 6-7). The spectra acquired by the slide-on diamond μ IRE and slide-on Ge μ IRE were slightly different due to the inherently differences between both IREs and the slide-on Ge μ IRE was required smooth surface. A rough surface did not allow a good contact between the Ge IRE and the solid surface.

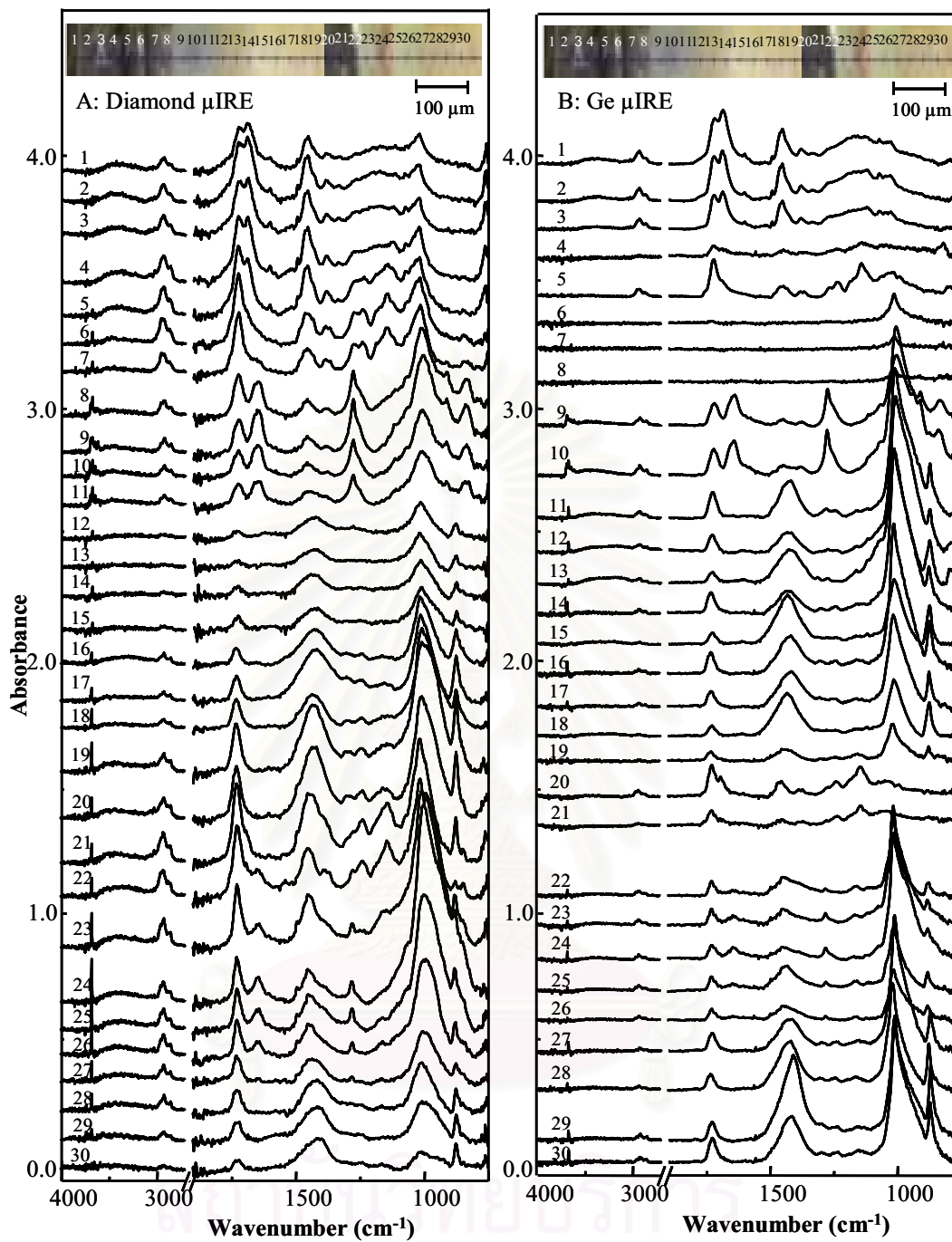


Figure 4.21 ATR spectra of an eight-layered paint chip from a hood of gray car acquired by (A) the slide-on diamond μ IRE and (B) the slide-on Ge μ IRE.

Figure 4.22 showed spectra of a thirteen-layered paint chip from blue car door acquired by (A) the slide-on diamond μ IRE and (B) the slide-on Ge μ IRE. The line map was started at the first layer (air-contact surface) along the thickness of paint chip as shown in insert. The paint chip consists of acrylic urethane enamel (spectra No. 1-6), acrylic enamel (spectra No. 7-12), alkyd urea enamel (spectra No. 13-19), alkyd primer (spectra No. 20-29), acrylic enamel (spectra No. 30-35), alkyd urea enamel (spectra No. 36-46), acrylic enamel (spectra No. 47-50), alkyd nitrocellulose (spectra No. 51-52), alkyd urea enamel (spectra No. 53-58), alkyd primer (spectra No. 59-73), alkyd urea enamel (spectra No. 74-83), and alkyd primer (spectra No. 84-97). The spectral feature was showing the agreement with the spectra analyzed from each layer as shown in Figure 4.16. The spectra acquired by the slide-on Ge μ IRE had lower intensity than the spectra acquired by the slide-on diamond μ IRE. Due to the sharp tip of diamond can penetrate down into the sample thus that has a good contact between diamond and rough surface while the tip of Ge just touch on the sample. Another reason, refractive index of diamond ($n_{Diamond} = 2.417$) is lower than that of Ge ($n_{Ge} = 4$). The refractive index inversely varied as penetration depth (d_p) thus the penetration depth of radiation of diamond are greater than that of Ge.

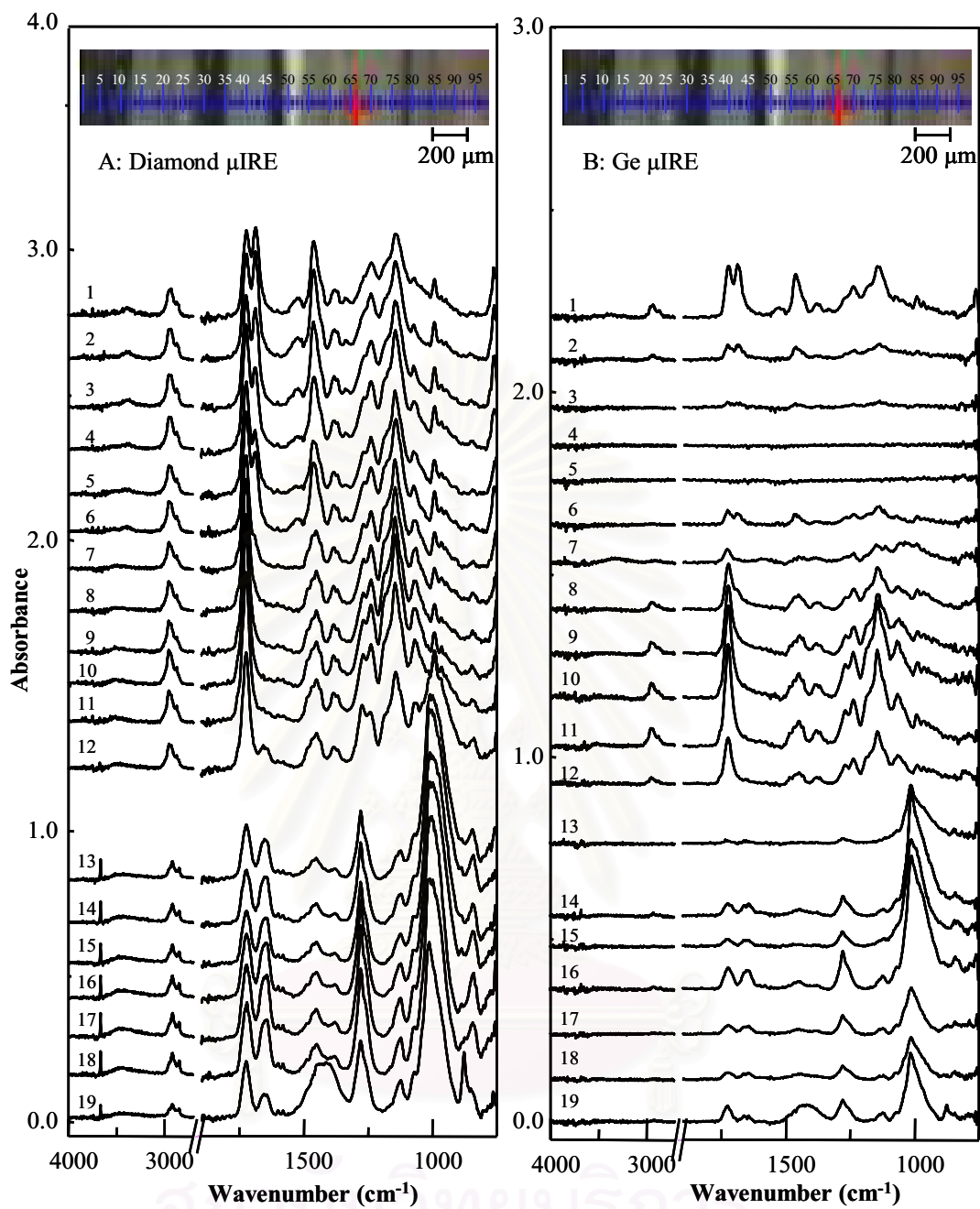


Figure 4.22 ATR spectra of a thirteen-layered paint chip from a door of blue car acquired by (A) the slide-on diamond μ IRE and (B) the slide-on Ge μ IRE.

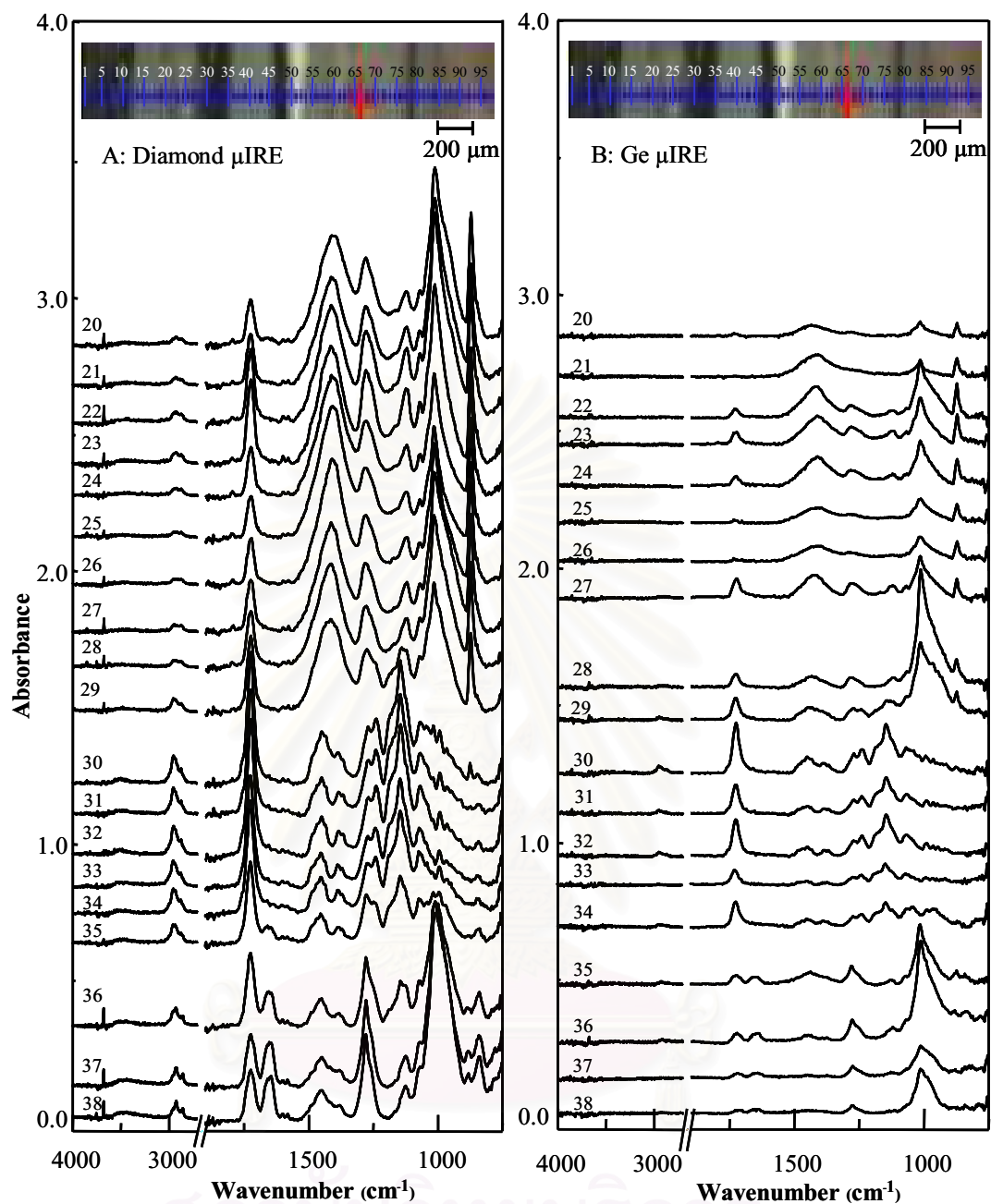


Figure 4.22 (continued) ATR spectra of a thirteen-layered paint chip from a door of blue car acquired by (A) the slide-on diamond μIRE and (B) the slide-on Ge μIRE .

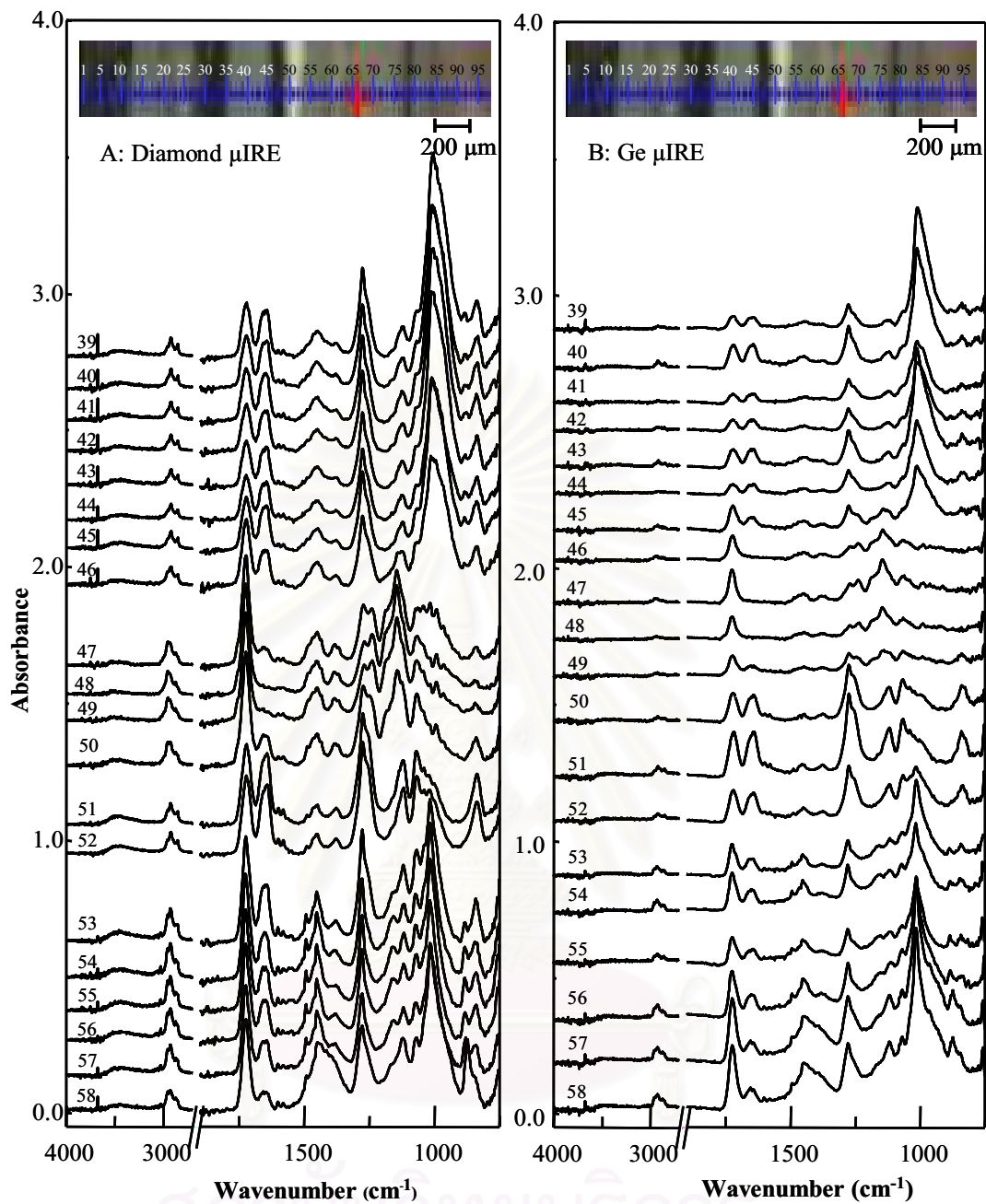


Figure 4.22 (continued) ATR spectra of a thirteen-layered paint chip from a door of blue car acquired by (A) the slide-on diamond μ IRE and (B) the slide-on Ge μ IRE.

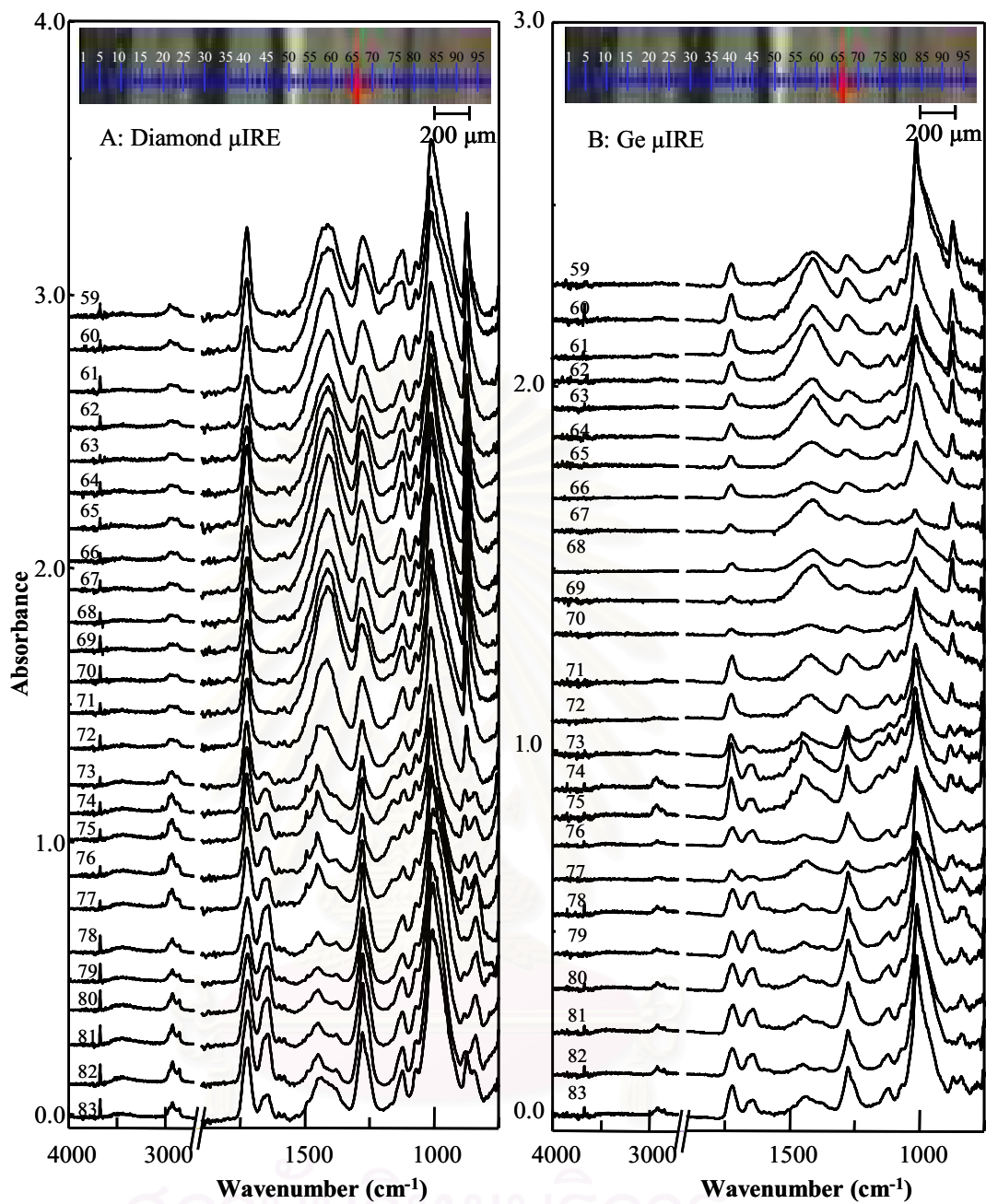


Figure 4.22 (continued) ATR spectra of a thirteen-layered paint chip from a door of blue car acquired by (A) the slide-on diamond μIRE and (B) the slide-on Ge μIRE .

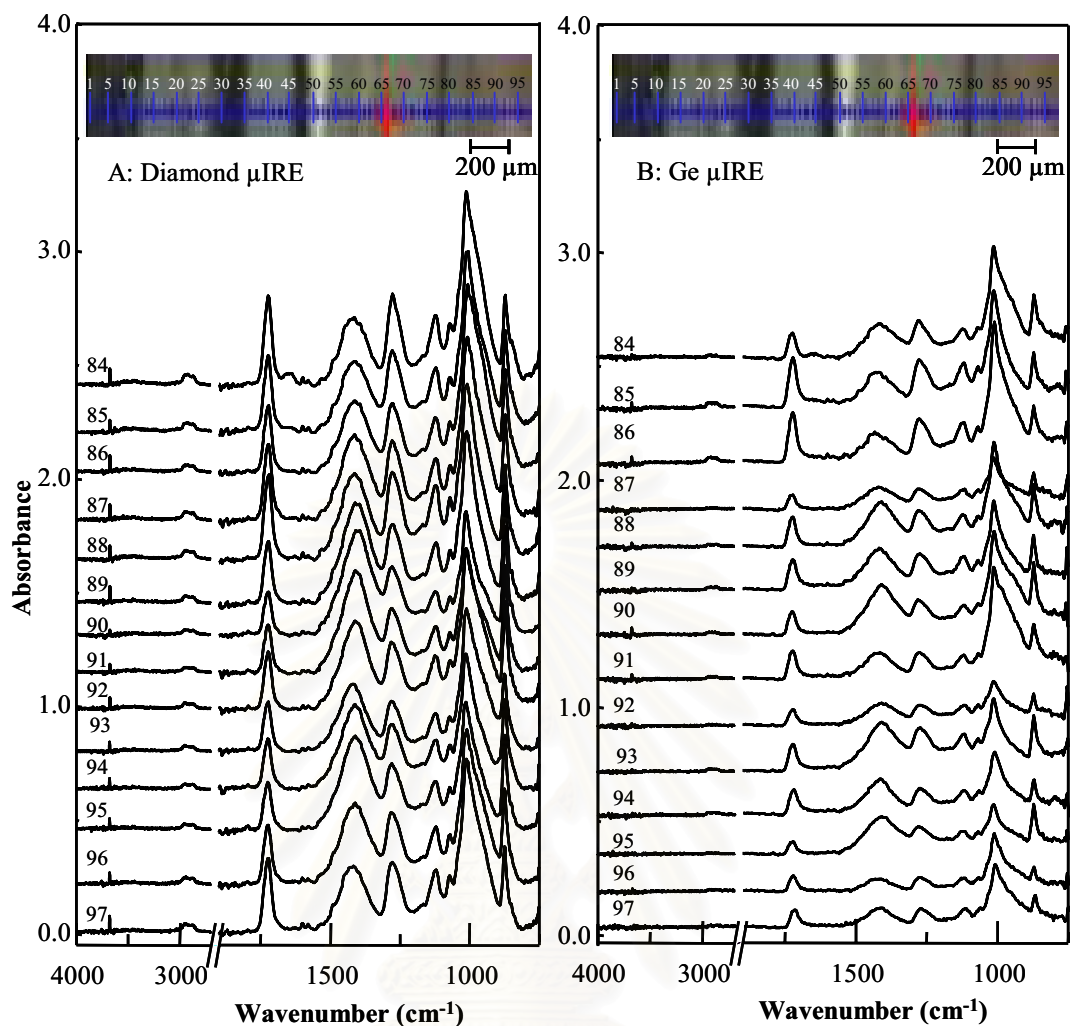


Figure 4.22 (continued) ATR spectra of a thirteen-layered paint chip from a door of blue car acquired by (A) the slide-on diamond μ IRE and (B) the slide-on Ge μ IRE.

Figure 4.23 (A) and (B) showed ATR spectra of a three-layered paint chip from a bumper of a black Toyota Fortuner car acquired by the slide-on diamond μ IRE and the slide-on Ge μ IRE, respectively. The line map was drawn along the thickness from the first layer (i.e., the air-contact surface) shown in the insert of Figure. The obtained spectra change from the first layer to third layer. The paint chip consisting of acrylic urethane enamel (spectra No. 1-4), acrylic urethane enamel (spectra No. 5-6) and polypropylene with heavy talc (spectra No. 7-10) was agreed with the spectra acquired from an individual layer analysis shown in Figure 4.17. The spectra acquired by the slide-on diamond μ IRE and slide-on Ge μ IRE were slightly different due to the inherently differences between both IREs. The major problem of the slide-on Ge μ IRE was the requirement of a relatively smooth surface. A rough surface did not

allow a good contact between the Ge IRE and the solid surface. In a worse case, an ATR FT-IR spectrum of a paint layer cannot be observed, (spectra No. 8-10). On the other hand, the slide-on diamond μ IRE did not have any problem associated with the sample contact. This is the major advantage of the sharp-tip configuration and the inherent hardness of diamond.

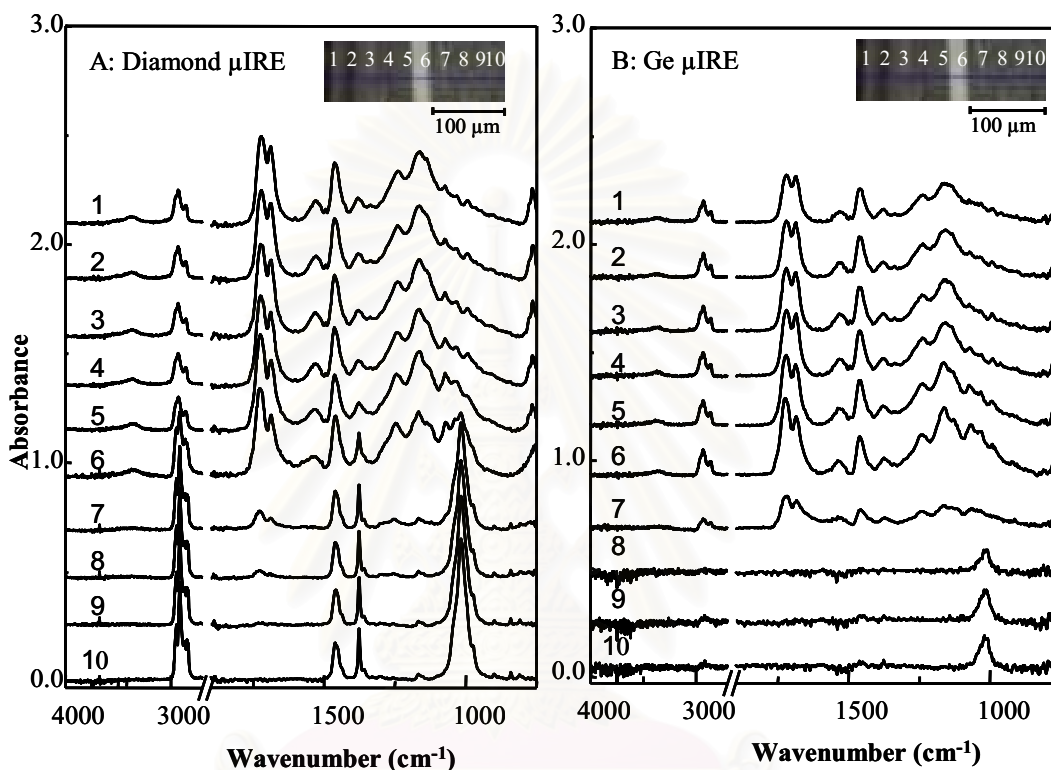


Figure 4.23 ATR spectra of a three-layered paint chip from a bumper of black Toyota Fortuner car acquired by (A) the slide-on diamond μ IRE and (B) the slide-on Ge μ IRE.

ATR spectra of multilayer automotive paints acquired by the slide-on diamond μ IRE and the slide-on Ge μ IRE were shown in Figure 4.24 (A) and (B), respectively. The paint fragment was obtained from a fender of a white Mitsubishi car. From optical image, the paint fragment has three layers, gray layer, white layer and brown layer. The first gray layer, from the observed spectra No.1-5 was indicated that they are acrylic-urethane enamel topcoat. Considering in the second white layer from the observed spectra No.6-17, there were found four paint layers within the white layer. The white paint layer consisted of the following components: acrylic-alkyd enamel (spectra No.6, 7), alkyd nitrocellulose (spectra No.8), acrylic urethane enamel (spectra

No.9-15) and alkyd nitrocellulose (spectra No.16-17). The third brown layer from the observed spectra No.18-20 was indicated that they are alkyd primer with high concentration of talc and calcium carbonate. According to the chemical information from the observed spectra of surface line mapping, they can be characterized white layer that cannot be distinguished by optical image. The spectra acquired by the slide-on diamond μ IRE and slide-on Ge μ IRE were slightly different due to the inherently differences between both IREs. In addition, some spectra of a paint layer from slide-on Ge μ IRE cannot be observed due to a rough surface do not have a good contact with the Ge μ IRE.

Since the slide-on diamond μ IRE and the slide-on Ge μ IRE have a small contact area, analysis by surface line mapping show the difference in chemical information at each small contact point that does not show by conventional ATR. Line map analysis showed chemical information changing from one layer to another layer. In addition, these techniques can be applied to analyze depth profiling on cross-section surface. The slide-on Ge μ IRE cannot be observed a rough cross-sectioned surface while the slide-on diamond μ IRE can identify hard and rough paint sample.

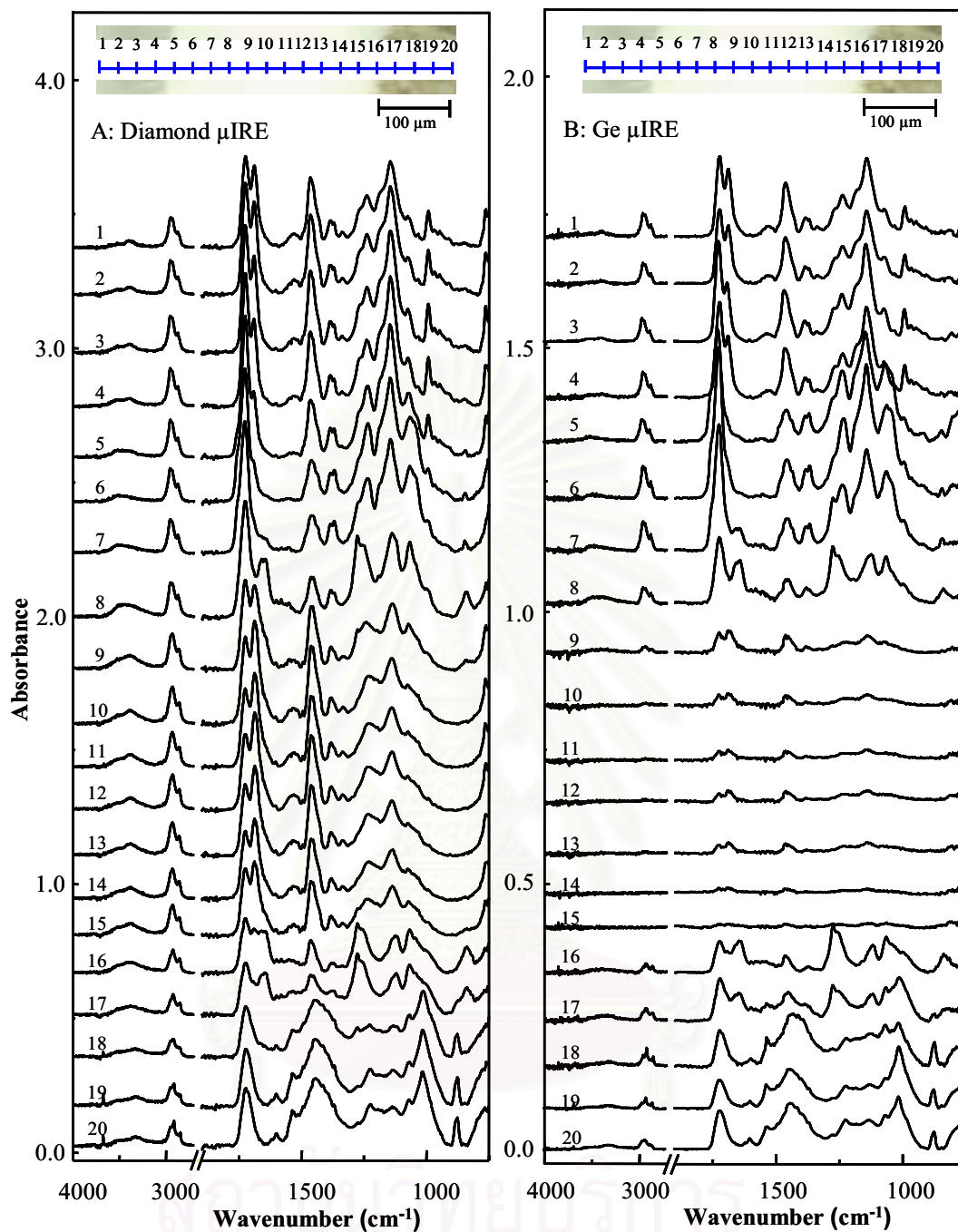


Figure 4.24 ATR spectra of a three-layered paint chip from a fender of white Mitsubishi car acquired by (A) the slide-on diamond μIRE and (B) the slide-on Ge μIRE .

4.2.4 Specular Reflection Measurement of Cross-section of Multilayer Automotive Paints

Specular reflection is one of the sampling techniques that providing surface molecular information. Specular reflection technique was analyzed automotive paint, since this technique is non-destructive and does not requiring sample preparation. Principle of Specular reflection was different from ATR technique. The incident radiations were incident on the sample which the angle of incidence is equal to the angle of reflection. The multilayer automotive paints were analyzed by specular reflectance technique. The paint chip was razorblade cut with an oblique angle (30 degree) in order to increase the length along the cross-section surface. An individual paint layer in the multilayer paint chip was analyzed along the cross-section surface. The illuminating apertures for a specular reflection measurement was controlled and limited to one single layer.

A two-layered paint chip from a silver gray car bumper was examined via the specular reflectance technique. In case of specular reflectance, the observed spectra showed derivative-type peak shape, as shown in Figure 4.25. The derivative-type peak shape was difficult to interpret. The Kramers-Kronig (KK) transformation was employed for converting the specular reflectance spectrum to absorption-like spectrum. Figure 4.26 showed the KK-transformed spectra of paint chip. The transformed spectrum was easier to interpret. The KK-transformed spectra showed differential type peak shape due to the KK transformation was work well with purely reflection. From theory, the total of incident light is the sum of reflected, scattered, transmitted, and absorbed light. Since paint chip is an opaque material, the incident radiation cannot be transmitted, most of the coupled radiations are absorbed by the material and the remaining will be reflected or scattered. In this experiment, infrared microscope was set in reflection mode. Thus, only pure reflected radiation can be observed. However, a cross-section surface of multilayer paint chip has rough surface when an infrared radiation is directed onto it undergoes specular reflection with diffuse reflective and scatter. The KK-transformed spectra (Figure 4.26) are compared with the ATR spectra acquired by the slide-on diamond μ IRE and the slide-on Ge μ IRE (Figure 4.13). The KK derived spectra are difficult to assign absorption bands

and peak position that directly relative with chemical composition since the spectra still showing the differential type peak shape.

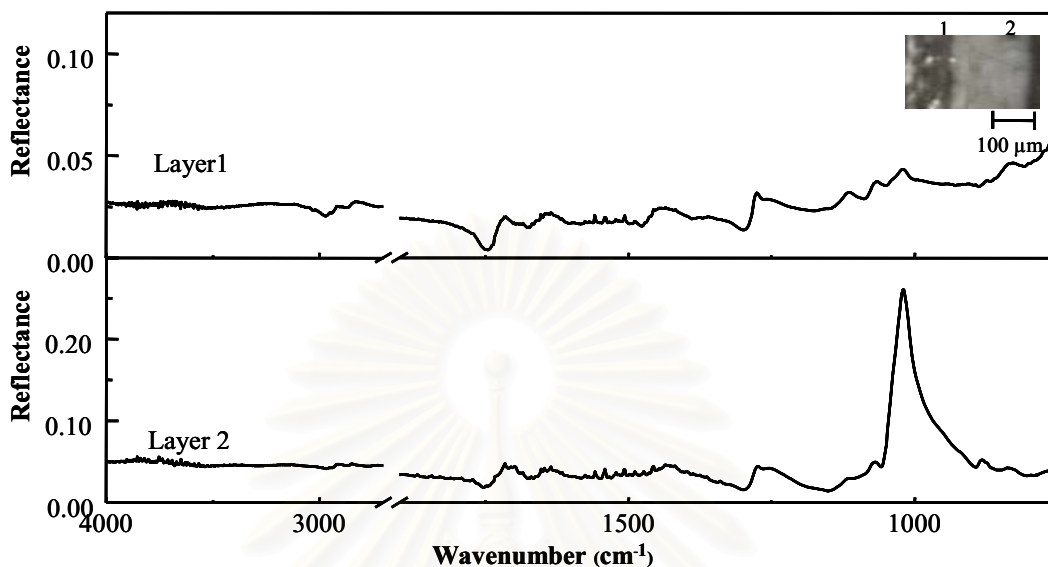


Figure 4.25 Specular reflectance spectra of a two-layered paint chip from a silver gray car bumper; layer 1 and layer 2.

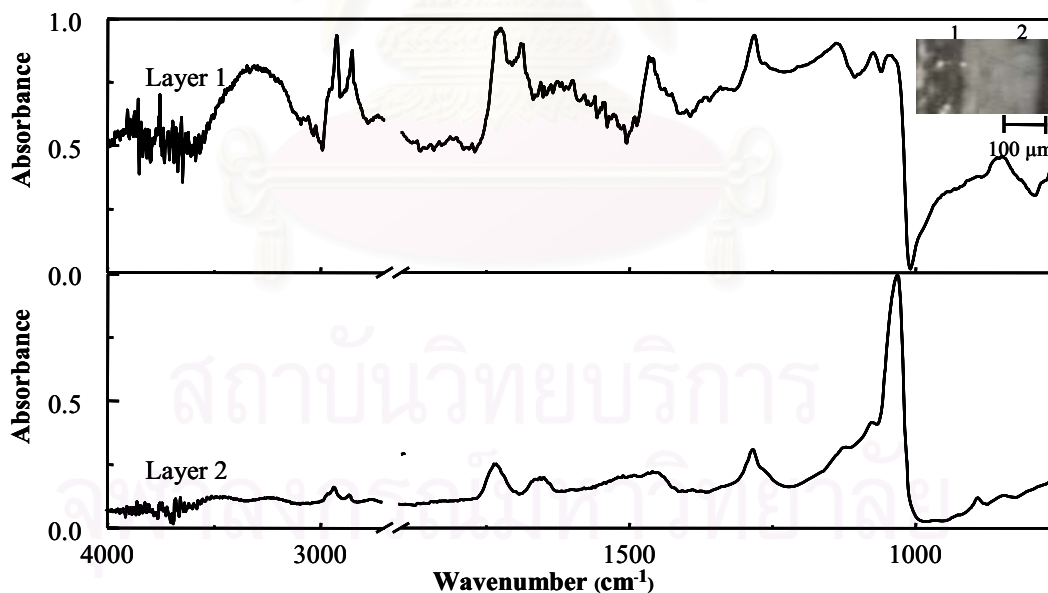


Figure 4.26 The KK-transformed spectra of those shown in Figure 4.25 of a two-layered paint chip from a silver gray car bumper; layer 1 and layer 2.

Figure 4.27 showed infrared spectra of a three-layered paint chip from black Toyota Fortuner bumper acquired via specular reflection technique which is difficult to interpret. The typical results of KK transformation are shown in Figure 4.28. The KK-transformed spectra showed differential type peak shape. The KK-transformed spectra (Figure 4.28) were slightly similar to the ATR spectra acquired by the diamond μ IRE and the Ge μ IRE (Figure 4.17) due to this paint chip having a slight smooth surface. Due to the second layer has a small thickness $\sim 25 \mu\text{m}$, the obtained spectrum implied that two homemade μ IREs can be analyzed small area like the specular reflection technique. However, specular reflectance spectra of cross-section surface of multilayer paint chip showed non-reproducible since the radiation reflected from different position of rough surface are not the same. Comparison of two spectra of paint evidence requires a high reproducibility. Additionally, decreasing of aperture size to limit in one thin layer is reduced energy throughput. Disadvantage of reducing energy throughput is a poor signal-to-noise ratio.

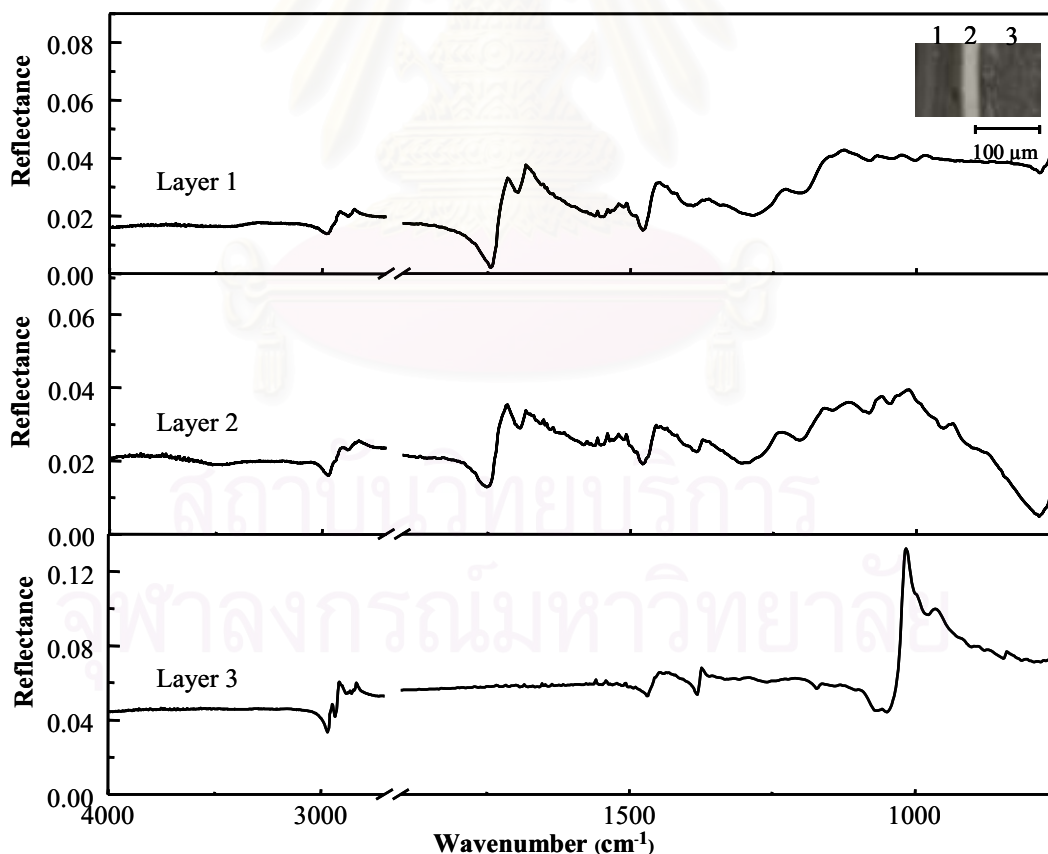


Figure 4.27 Specular reflectance spectra of a three-layered paint from black Toyota Fortuner bumper; layer 1, layer 2 and layer 3.

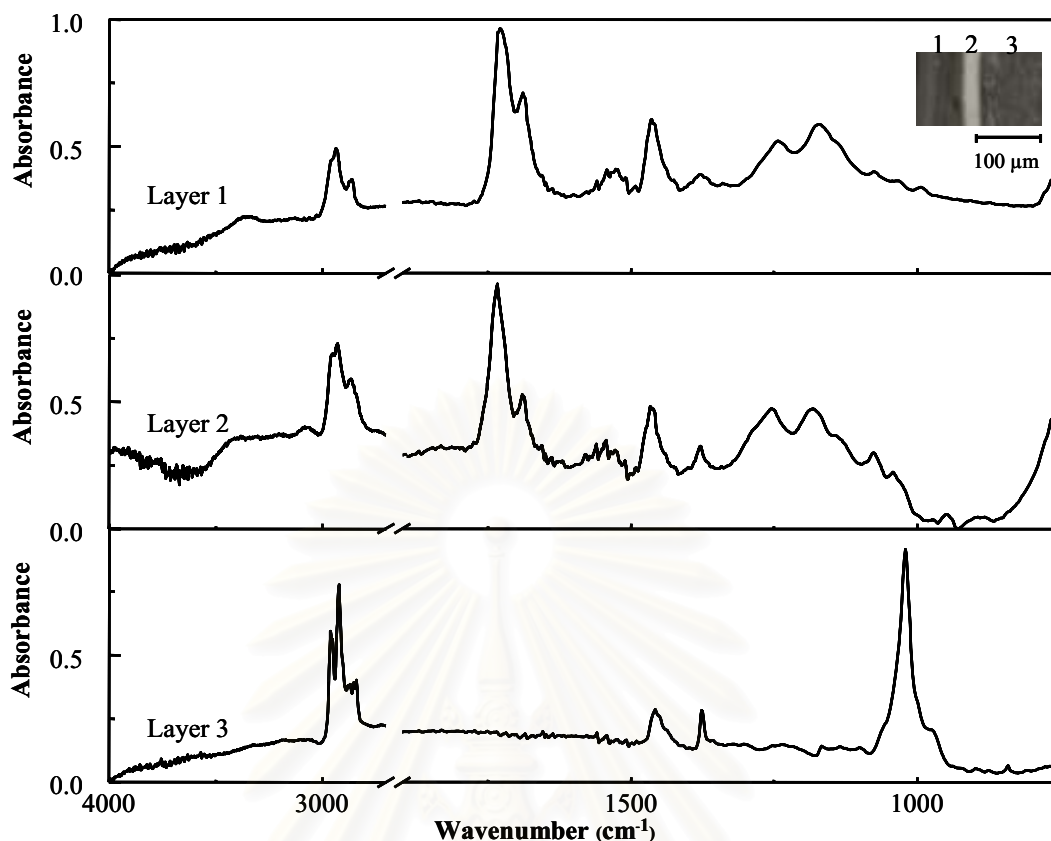


Figure 4.28 The KK-transformed spectra of those shown in Figure 4.27 of a three-layered paint chip from a black Toyota Fortuner bumper; layer 1, layer 2 and layer 3.

Figure 4.29 showed infrared spectra of a three-layered paint chip from white Mitsubishi fender acquired via specular reflection technique. The observed spectra show derivative-type peak shape that are difficult to interpret. Figure 4.30 showed the KK derived spectra of three-layered paint chip. The KK-transformed spectra of layer one and two (Figure 4.30) were similar to the ATR spectra acquired by both homemade μ IRES (Figure 4.18) but the spectra of the third layer was different. This is due to the fact that the third layer of this paint has very rough surface.

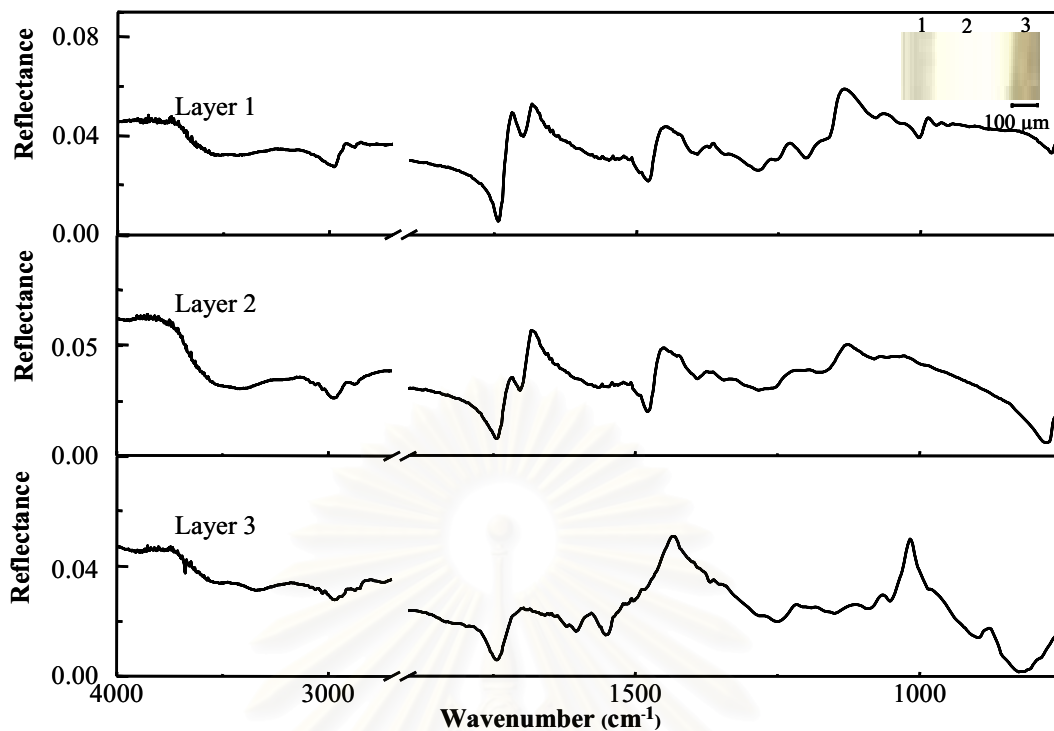


Figure 4.29 Specular reflectance spectra of a three-layered paint from white Mitsubishi fender; layer 1, layer 2 and layer 3.

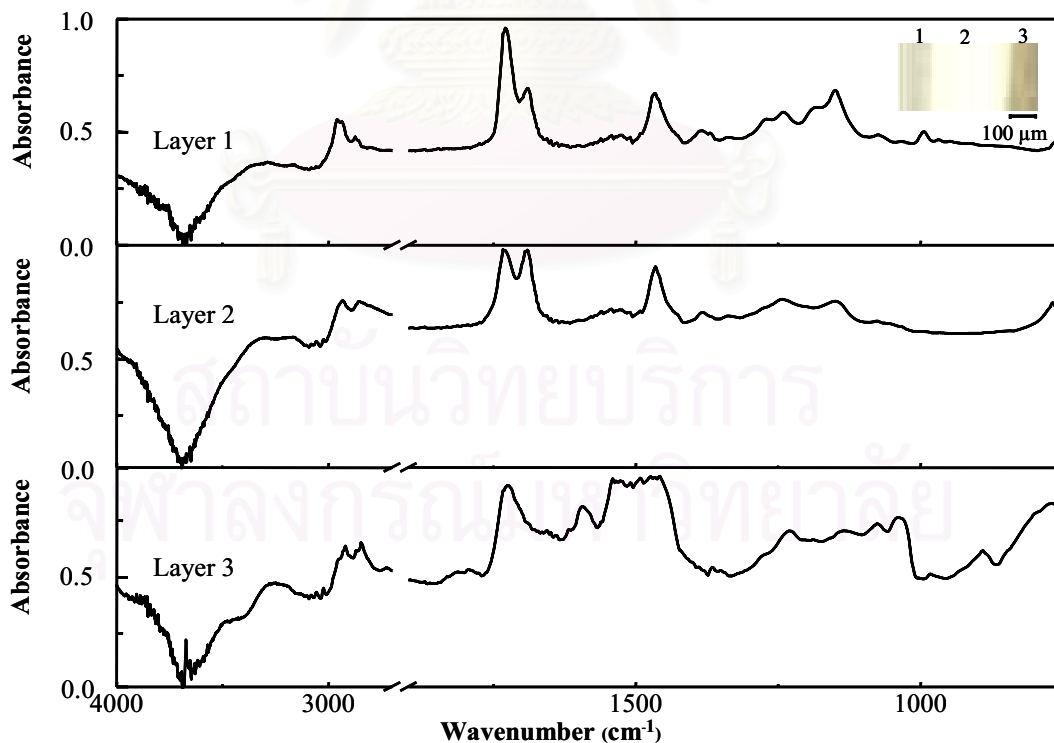


Figure 4.30 The KK-transformed spectra of the spectra shown in Figure 4.29 of a three-layered paint chip from a white Mitsubishi fender; layer 1, layer 2 and layer 3.

From the results of specular reflection technique, the good spectra were obtained from smooth and flat surface, and good reflected sample. The cross-section surface of multilayer paint chip have rough surface is not suitable for analysis. The advantages of specular reflection are provide surface molecular information, rapid analysis, non-destructive techniques, having small sampling area, and without sample preparation. Disadvantages are non-reproducibility technique and not suitable for analyzing rough surface while the observed ATR spectra are reproducibility and the slide-on μ IREs can be analyzed rough cross-section surface.

4.3 Characterization of Thin Trace Smears on Automotive Paint Support

In most of the car accident cases, the evidences were in the form of thin trace abrasive smear on automotive paint support. Sometimes it is impossible to isolate the thin trace smear from the paint support. In real accident case, an evident sample was examined by the slide-on diamond μ IRE and the slide-on Ge μ IRE. The blue BMW car was collided with the other unknown vehicle. Unknown black trace smear on a blue paint fragment was taken from the damaged blue BMW. The paint fragment was analyzed to determine the chemical information by the slide-on Ge μ IRE and the slide-on diamond μ IRE, as shown in Figure 4.31. Figure 4.31 showed (a) the spectrum of blue paint support from BMW car referring to known sample and (b) the spectrum of black trace smear referred to unknown sample. The ATR spectrum of blue paint support indicated that it was acrylic urethane clear coat and the same with first layer from analyzing of each paint layer on cross-section of multilayer paint from same BMW (Figure 4.19). The ATR spectrum of black trace smear indicated that it consisted of polypropylene and talc that were often used in new pickup truck bumper, the same type as the bumper of Toyota Fortuner (Figure 4.31 (c)). Car bumpers are made from a variety of materials, such as steel, aluminum, rubber, composite fiberglass, and plastic with a plastic cover to absorb energy during collisions depending on model, year and producer. The chemical information from paint evidence can narrow the possible suspected car.

The spectra of black trace smear acquired by the slide-on diamond μ IRE and the slide-on Ge μ IRE were slightly different. In case of the slide-on diamond μ IRE, peak

at 1727 and 1685 cm^{-1} from blue paint support were due to the sharp tip of diamond pieced through the thin trace smear and contact the lower paint support. While the slide-on Ge μIRE can identify thin trace smear without substrates interference.

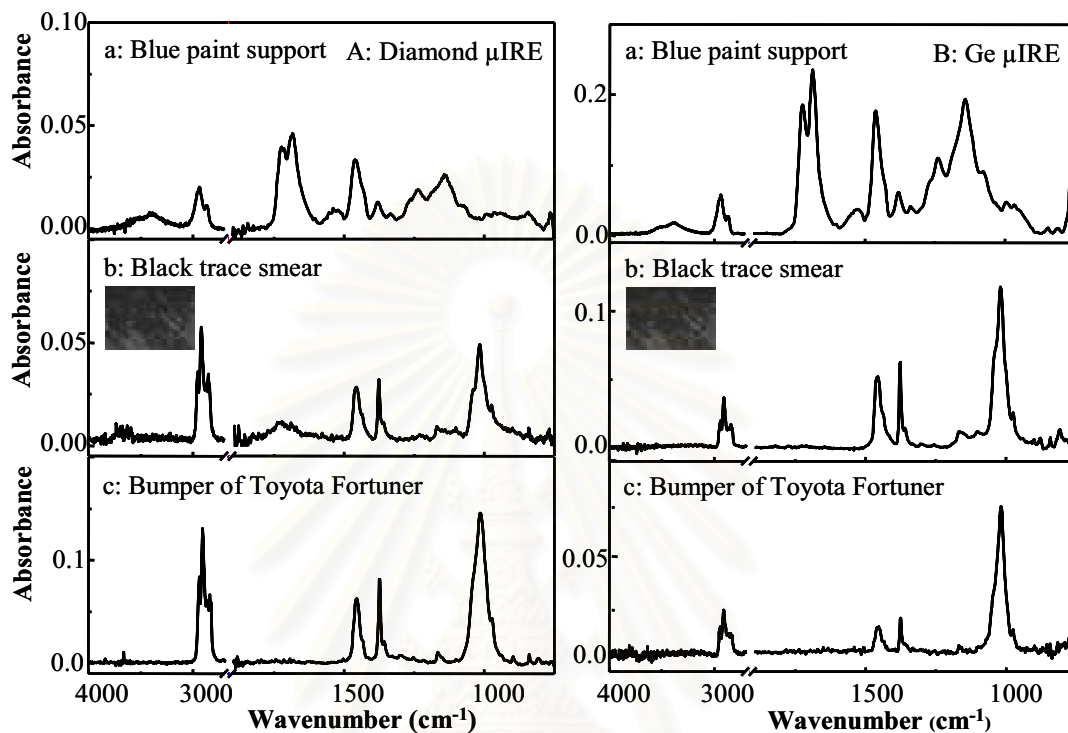


Figure 4.31 The spectra were acquired by (A) the slide-on diamond μIRE and (B) the slide-on Ge μIRE . Comparison of the ATR spectra of (a) the blue paint support of damaged BMW car referred to known sample, (b) the black trace smear on the damaged car referred to unknown sample and (c) the bumper of Toyota Fortuner.

สถาบันวิทยบริการ
จุฬาลงกรณ์มหาวิทยาลัย

CHAPTER V

CONCLUSIONS

ATR FT-IR microspectroscopy can distinguish most of the automotive paints with different colors and shades. The different paints have unique chemical composition. The spectra obtained from the slide-on diamond μ IRE and the slide-on Ge μ IRE are similar to those obtained from the conventional ATR. However, the intensity of ATR spectra acquired by both slide-on μ IREs are greater than that of conventional ATR. The advantage of both homemade slide-on μ IREs are small sampling areas and can be analyzed paint coated on metal without sample preparation. The analysis takes only a short time while the result is accurate and reliable.

The diamond μ IRE was employed for depth profiling of multilayer paint chips by increasing penetration diamond in to the paint chip. For rubbery or tough paint chip, the depth profiling of multilayer paint chip cannot be performed. Providing this problem, the slide-on diamond μ IRE and the slide-on Ge μ IRE were employed for directly analyzed individual layer on cross-section of paint fragment. Since the slide-on diamond μ IRE and the slide-on Ge μ IRE have small tip and small sampling area, these techniques do not require complicated sample preparation but only additional razorblade cut. The analysis gives chemical information about binder, main pigment, and additive present in individual layer of paint chip. The spectra acquired by the slide-on diamond μ IRE were slightly different from those acquired by the slide-on Ge μ IRE due to the inherent differences between both μ IREs.

Since the slide-on diamond μ IRE and the slide-on Ge μ IRE have small sampling area, non-destructive sample, and easy operation of the infrared microscope, the surface line mapping can reveal the changing in chemical composition in each small sampling position and can distinguish paint that has the same color. In real accident, paint evidence was found interfering from adjacent layer. Line map analysis showed chemical information changing from one layer to another layer. In addition, these techniques can be applied to analyze depth profiling on cross-section surface.

The specular reflection is not applicable to analyze cross-section surface of multilayer automotive paint chip due to that having a rough surface. The acquired spectra were difficult to interpret. The KK-transformed spectra showed differential type peak shape.

The paint evidences in the form of the thin trace smear were identified by both μ IREs. The slide-on Ge μ IRE is suitable to directly analyze paint trace smear without interference from paint support while the slide-on diamond μ IRE present the interference from paint support due to the sharp tip of diamond can penetrate the thin trace smear. The unique chemical information from paint traces help to investigate the car accident.

The homemade μ ATR accessories, the slide-on diamond μ IRE and the slide-on Ge μ IRE, are suitable for forensic analysis of automotive paints since they have small tip configuration, small sampling area, rapid, and non-destructive without a sample preparation. The advantage of the slide-on diamond μ IRE is the hardest material and having sharp tip, thus a good spectra can be obtained due to a good contact between hard and rough sample/diamond while the slide-on Ge μ IRE was suitable for thin film with smooth surface.

REFERENCES

- [1] Humecki, H. J. Practical Guide to Infrared Microspectroscopy. New York: Marcel Dekker, 1995.
- [2] ASTM E 1610-02. Annual Book of ASTM Standards. Vol. 14.02, West Conshohocken: ASTM international, 1995.
- [3] Govaerta, F.; and Bernard, M. Discriminated red spray paints by optical microscopy, Fourier transform infrared spectroscopy and X-ray fluorescence. Forensic Sci. Int. 140 (2004): 61-71.
- [4] Zieba-Palus, J.; and Borusiewicz, R. Examination of multilayer paint coats by the use of infrared, Raman and XRF spectroscopy for forensic purposes. J. Mol. Struct. 792-793 (2006): 286-292.
- [5] Suzuki, E. M. Infrared spectra of U.S. automobile original finishes: VII. Extended range FT-IR and XRF analyses of inorganic pigments in situ-Nickel Titanate and Chrome Titanate. J. Forensic Sci. 51 (2006): 532-547.
- [6] Zieba-Palus, J. Application of micro-Fourier transform infrared spectroscopy to the examination of paint samples. J. Mol. Struct. 511-512 (1999): 327-335.
- [7] Wampler, T. P.; Bishea, G. A.; and Simonsick, W. J. Recent change in automotive paint formulation using pyrolysis-gas chromatography/mass spectrometry for identification. J. Anal. Appl. Prrolysis 40-41 (1997): 79-89.
- [8] Bruns, T. D.; and Doolan, K. P. A comparison of pyrolysis-gas chromatography-mass spectrometry and Fourier transform infrared spectroscopy for the analysis of a series of modified alkyd paint resins. Anal. Chim. Acta 422 (2000): 217-230.
- [9] Bruns, T. D.; and Doolan, K. P. The discrimination of automotive clear coat paints indistinguishable by Fourier transform infrared spectroscopy via pyrolysis-gas chromatography-mass spectrometry. Anal. Chim. Acta 539 (2005): 157-164.

- [10] Bruns, T. D.; and Doolan, K. P. A comparison of pyrolysis-gas chromatography-mass spectrometry and Fourier transform infrared spectroscopy for the characterization of automotive paint samples. Anal. Chim. Acta 539 (2005): 145-155.
- [11] Edward, G. B. Handbook of Vibrational Spectroscopy Chichester: John Wiley & Sons Ltd, 2002.
- [12] Gelder, J. D.; Vandenabeele, P.; Govaert, F.; and Moens, L. Forensic analysis of automotive paints by Raman spectroscopy. J. Raman Spectrosc. 36 (2005): 1059-1067.
- [13] Buzzini, P.; Massonnet, G.; and Sermier, F. M. The micro Raman analysis of paint evidence in criminalistics. J. Raman spectrosc. 37 (2006): 922-931.
- [14] Suzuki, E. M. In situ identification and analysis of automotive paint pigments using line segment excitation Raman spectroscopy: I. Inorganic topcoat pigments. J. Forensic Sci. 46 (2001): 1053-1069.
- [15] Adamsons, K. Chemical depth profiling of multi-layer automotive coating systems. Prog. Org. Coat. 45 (2002) 69-81.
- [16] Flynn, K.; O'Leary, R.; Lennard, C.; Roux, C.; and Reedy, B. J. Forensic applications of infrared chemical imaging: Multi-layered paint chips. J. Forensic Sci. 50 (2005): 832-841.
- [17] Chang, W. T.; Chen, T. H.; Yu, C. C.; and Kau, J. Y. A critical evaluation of spectral library searching for the application of automotive paint database. J. Forensic Sci. 2 (2003): 47-58.
- [18] Giang, Y. S.; Wang, S. M.; Cho, L. L.; Yang, C. K.; and Lu, C. C. Identification of tiny and thin smear of automotive paint following a traffic accident. J. Forensic Sci. 47 (2002): 625-629.
- [19] Giang, Y. S.; Cho, L. L.; Wang, S. M.; and Chiu L. Y. Identification of tiny, thin and smeared dot of red paint in fatal traffic accident case by Fourier transform-infrared microspectroscopy. J. Forensic Sci. 4 (2005): 47-54.
- [20] Wernstahl, K. M. Survive life prediction of automotive coatings, correlating infrared measurements and gloss retention. Polym. Degrad. Stab. 54 (1996): 57-65.

- [21] Chang, W. T.; Chen, T. H.; Yu, C. C.; and Kau, J. Y. Comparison of embedding methods used in examining cross-section of automotive paints with micro-Fourier transform infrared spectroscopy. J. Forensic Sci. 1 (2002): 55-60.
- [22] Ryland, S.; and others. Discrimination of 1990s original automotive paint systems a collaborative study of black nonmetallic base coat/clear coat finishes using infrared spectroscopy. J. Forensic Sci. 46 (2001): 31-45.
- [23] Suzuki, E. M. Infrared spectra of U.S. automobile original topcoats (1974-1989) I. Differentiation and identification based on acrylonitrile and ferrocyanide $C\equiv N$ stretching absorptions. J. Forensic Sci. 41 (1996): 376-392.
- [24] Suzuki, E. M. Infrared spectra of U.S. automobile original topcoats (1974-1989) II. Identification of some topcoat inorganic pigments using an extended range ($4000-220\text{ cm}^{-1}$) Fourier transform spectrometer. J. Forensic Sci. 41 (1996): 393-406.
- [25] Suzuki, E. M.; and Marshall, W. P. Infrared spectra of U.S. automobile original topcoats (1974-1989) III. In situ identification of some organic pigments used in yellow, orange, red, and brown nonmetallic and brown metallic finishes-Benzimidazolones. J. Forensic Sci. 42 (1997): 619-648.
- [26] Suzuki, E. M.; and Marshall, W. P. Infrared spectra of U.S. automobile original topcoats (1974-1989) IV. Identification of some organic pigments used in red and brown nonmetallic and metallic monocoats-Quinacridones. J. Forensic Sci. 43 (1998): 514-542.
- [27] Suzuki, E. M. Infrared spectra of U.S. automobile original topcoats (1974-1989) V. Identification of organic pigments used in red nonmetallic and brown nonmetallic and metallic monocoats. J. Forensic Sci. 44 (1999): 297-313.
- [28] Suzuki, E. M. Infrared spectra of U.S. automobile original topcoats (1974-1989) VI. Identification and analysis of yellow organic automotive paint pigments-isoindolinone yellow, isoindoline yellow, anthrapyrimidine yellow, and miscellaneous yellows. J. Forensic Sci. 44 (1999): 1151-1175.

- [29] Urban, M. W. Attenuated Total Reflectance Spectroscopy of Polymer: Theory and Practice. Washington: American Chemical Society, 1996.
- [30] Calmers, J. M. and Griffiths, P. R. (Eds). Hand Book of Vibrational Spectroscopy Volume 2. UK: John Wiley & Sons Ltd, 2002.
- [31] Harrick, N. J. (Ed.). Internal Reflection Spectroscopy. New York: Harrick Scientific Corporation, 1979.
- [32] Ekgasit, S.; and Padermshoke, A. Optical contact in ATR FT-IR Spectroscopy. Appl. Spectrosc. 55 (2001): 1352-1259.
- [33] Katon, J. E. Infrared Microspectroscopy. A Review of Fundamentals and Applications. Micron 27 (1996): 303-314.
- [34] Ekgasit, S.; and Thongnopkun, P. Transflectance Spectra of Faceted Diamonds Acquired by Infrared Microscopy. Appl. Spectrosc. 59 (2005): 1160-1165.
- [35] Ekgasit, S.; and Thongnopkun, P. Novel ATR FT-IR Microscopy Using a Gem Quality Diamond as an Internal Reflection Element. Appl. Spectrosc. 59 (2005): 1236-1241.
- [36] Smith, B. C. Fundamentals of Fourier Transform Infrared Spectroscopy. New York: CRC Press, 1996.
- [37] Coleman, P. B. Practical Sampling Techniques for Infrared Analysis. London: CRC Press, 1993.



APPENDICES

สถาบันวิทยบริการ
จุฬาลงกรณ์มหาวิทยาลัย

APPEN

1. Conventional ATR Instruments a

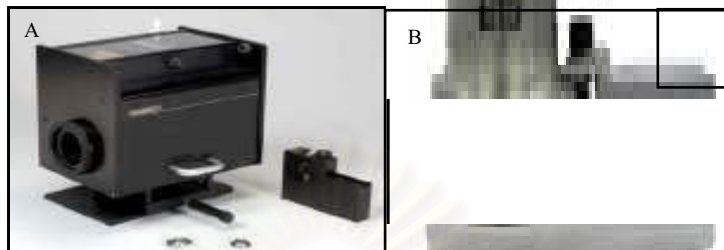


Figure 1. (A) Single reflection attenuated total reflection accessory (the Seagull™, Harrick Scientific, USA) and (B) a hemispherical Ge.

2. The Diamomd μIRE

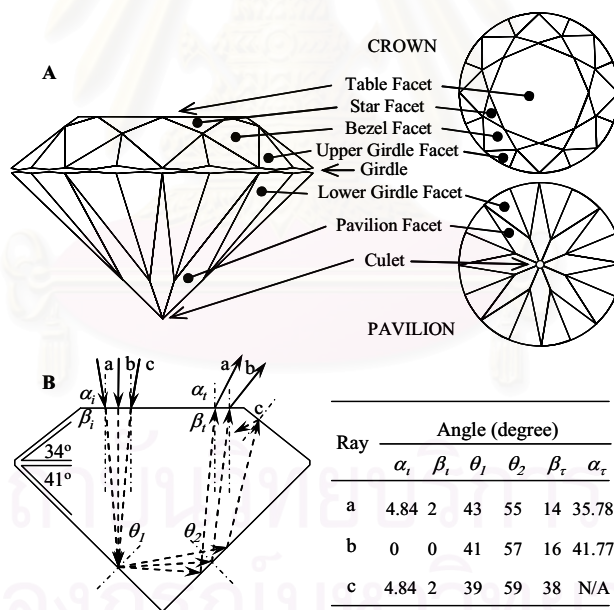


Figure 2. (A) A schematic drawing of a round brilliant cut diamond. (B) Ray tracing of different radiations inside a round brilliant cut diamond. A summary of angles at diamond/air interface are shown.

3. Reference Spectra of Resins and Pigments Used for Automotive Paints

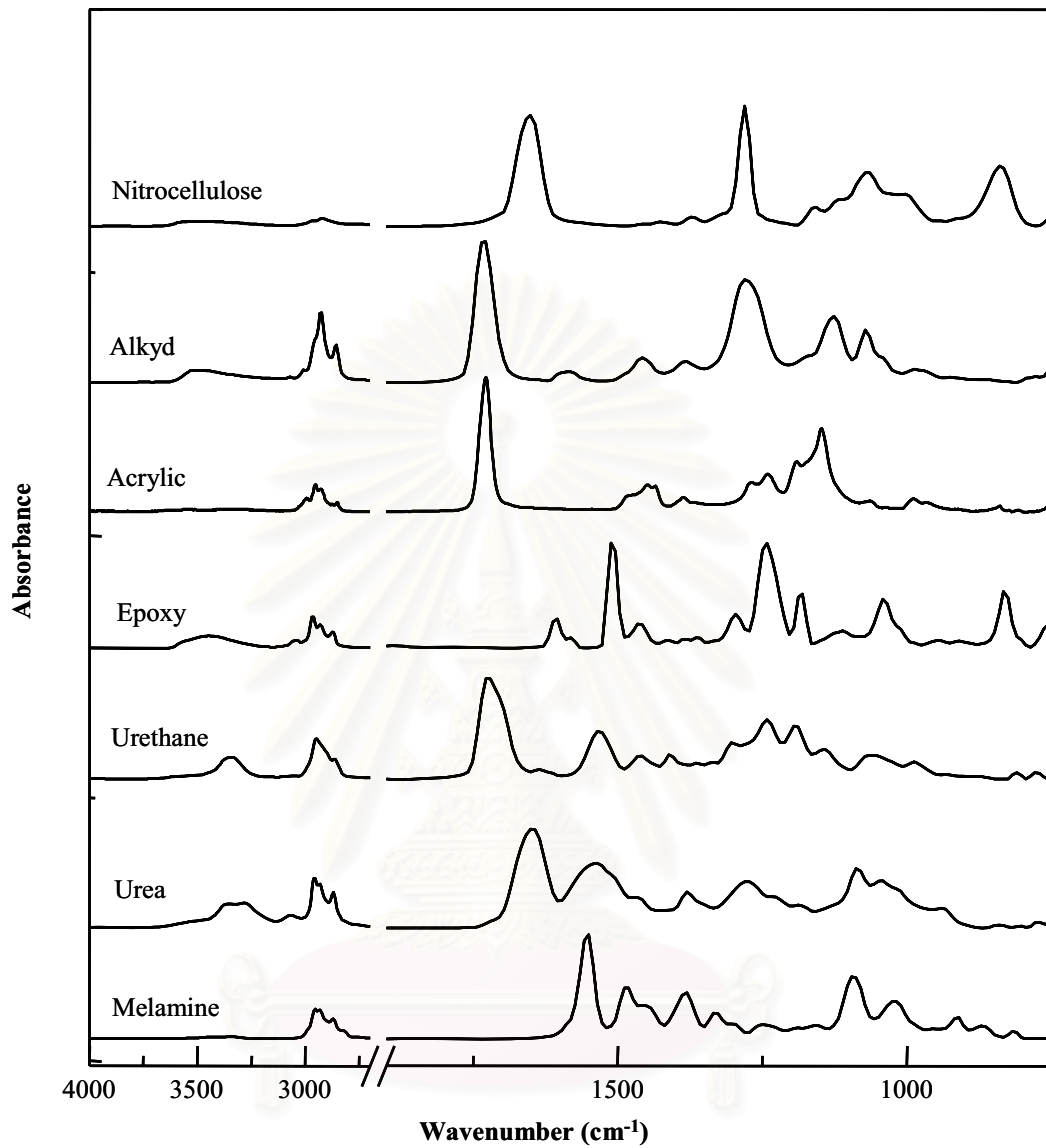


Figure 3. Reference spectra of resin used for automotive binders.

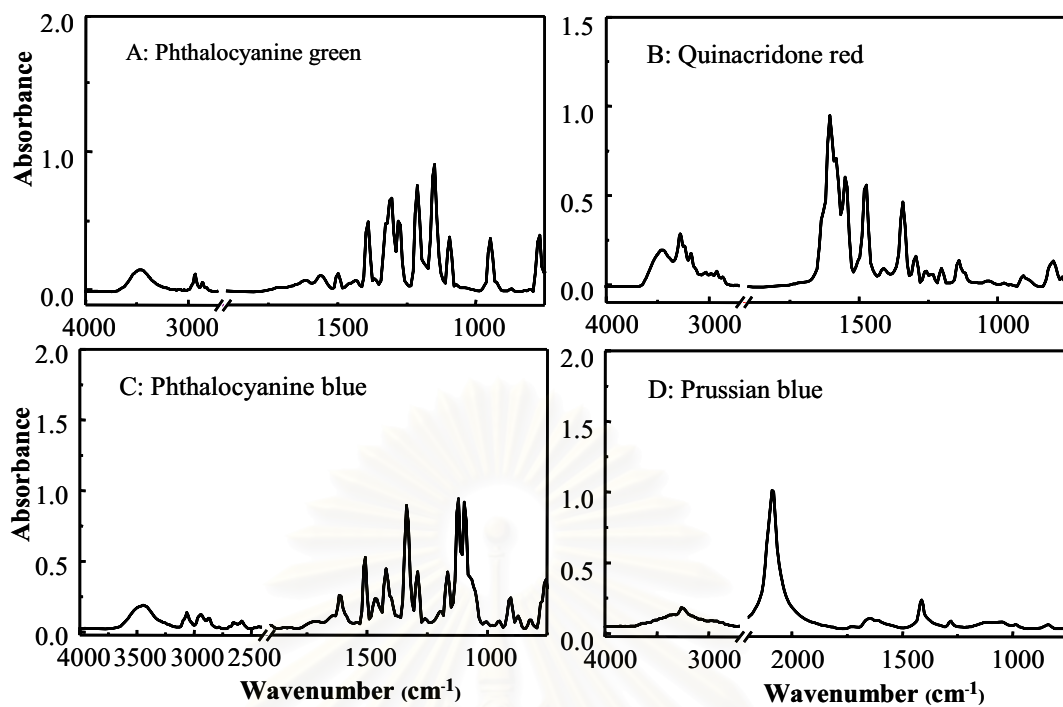


Figure 4. Reference spectra of pigment used for automotive paints.

สถาบันวิทยบริการ
จุฬาลงกรณ์มหาวิทยาลัย

4. Peak Assignments

Table 1 Peak assignments of polypropylene and talc.

Sample	Wavenumber (cm ⁻¹)	Peak assignments
Polypropylene	2949	Asymmetric C-H stretching of -CH ₃
	2918	Asymmetric C-H stretching of -CH ₂
	2867	Symmetric C-H stretching of -CH ₃
	2838	Symmetric C-H stretching of -CH ₂
	1459	CH ₃ bending
	1376	CH ₃ bending
	1166	C-C stretching
	974	CH ₃ rocking
Talc	1017	Si-O-Si stretching

5. Chemical Structures

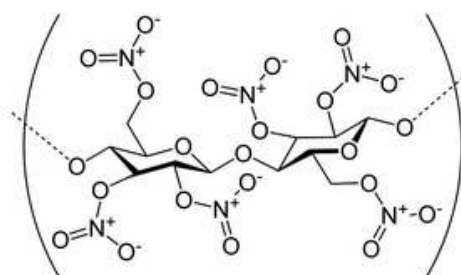


Figure 5. Chemical structure of nitrocellulose.

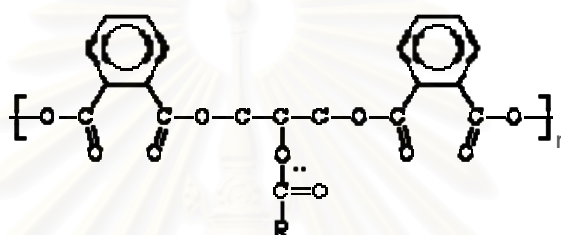


Figure 6. Chemical structure of alkyd resin.

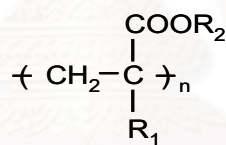


Figure 7. Chemical structure of acrylic resin.

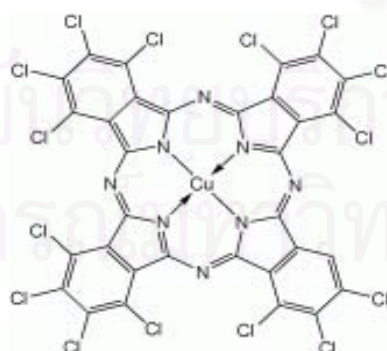


Figure 8. Chemical structure of Pththalocyanine green.

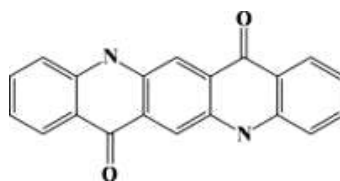


Figure 9. Chemical structure of Quinacridone red.

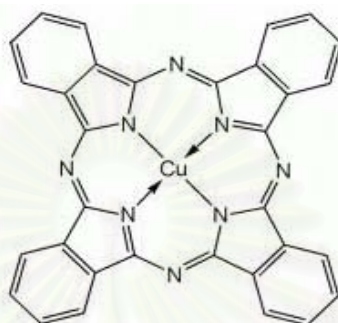


Figure 10. Chemical structure of Pthphalocyanine blue.

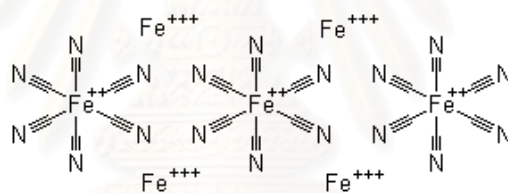


Figure 11. Chemical structure of Prussian blue.

สถาบันวิทยบริการ
จุฬาลงกรณ์มหาวิทยาลัย

6. Flowchart for Infrared Classification of Automotive Paint Binder

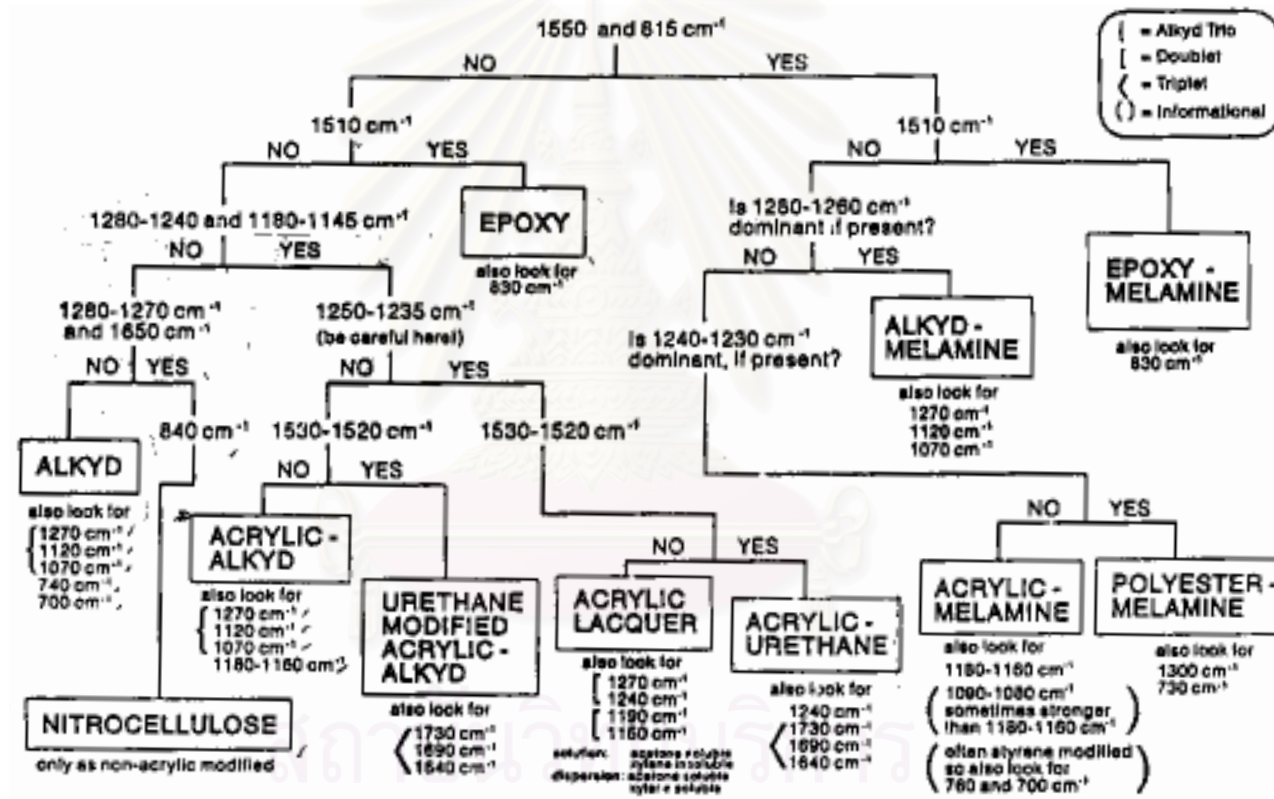


Figure 11. Flowchart for infrared classification of automotive paint binder [1].

CURRICULUM VITAE

Miss Pornpan Watcharasanyakorn

- 1983 Born : September, 12th, Bangkok, Thailand
 Father : Perapong Watcharasanyakorn
 Mather : Supattra Watcharasanyakorn
- 1989 Elementary School (Sitwathana School, Bangkok)
- 1998 Secondary School (Bencharachalai School, Bangkok)
- 2000 High School (Satriwithaya School, Bangkok)
- 2004 Bachelor of Engineering (Petrochemicals and Polymeric
 Materials), Silpakorn University, Nakornpathom, Thailand
- 2006 Master of Science (Petrochemistry and Polymer Science),
 Chulalongkorn University, Bangkok, Thailand

สถาบันวิทยบริการ
จุฬาลงกรณ์มหาวิทยาลัย